Magnetic Resonance Imaging of Intraspinal Stem Cell Grafts: Tracking and Targeted Transplantation

A Dissertation
Presented to
The Academic Faculty

by

Jason J. Lamanna

In Partial Fulfillment
of the Requirements for the Degree
Doctor of Philosophy in the
Department of Biomedical Engineering

Georgia Institute of Technology & Emory University
August 2015

Magnetic Resonance Imaging of Intraspinal Stem Cell Grafts:
Tracking and Targeted Transplantation

Approved by:

Dr. Nicholas M. Boulis, Advisor
Department of Neurosurgery, School of Medicine
Emory University
Department of Biomedical Engineering
Georgia Institute of Technology & Emory University

Dr. John N. Oshinski, Advisor
Department of Radiology, School of Medicine
Emory University
Department of Biomedical Engineering
Georgia Institute of Technology & Emory University

Dr. Jacques Galipeau
Departments of Hematology and Medical Oncology, Pediatrics, and Medicine
School of Medicine
Emory University

Dr. Shawn Hochman
Department of Physiology, School of Medicine
Emory University
Department of Biomedical Engineering
Georgia Institute of Technology & Emory University

Dr. Shella Keilholz
Department of Biomedical Engineering
Georgia Institute of Technology & Emory University

Date Approved: May 11th, 2015

To my family and friends

ACKNOWLEDGEMENTS

I would first like to acknowledge and specifically thank my mentors, Dr. John Oshinski and Dr. Nicholas Boulis. Thank you for having me in the lab, developing ideas and experiments that formed this thesis, and for the flexibility to independently explore the questions addressed in this thesis. I don't think I could have imagined a better scenario for my dissertation studies and I have learned so much from you both.

I also must express great appreciation for my committee members, Dr. Jacques Galipeau, Dr. Shawn Hochman, and Dr. Shella Keilholz. Thank you for all of the guidance and time put into guiding me on this journey. I also thank you for your flexibility. I would specifically like to thank Dr. Hochman for his guidance and enormously helpful review of my work.

Without the support of my colleagues in the lab, this thesis would not have been possible. I would like to especially thank Dr. Juanmarco Gutierrez and Lindsey Urquia. Words cannot express how much time and effort they put into these projects. Juanmarco contributed incalculable amounts of insight and kept me sane during the process. Lindsey spent at least a thousand hours working on the histology for this project. We're the three best friends that anyone could have… I would also like to thank the others who devoted a lot of time and worked on these projects, including Dr. Thais Federici, Victor Hurtig, Dr. Jon Riley, Cheryl Moreton, and Elman Amador.

I am very grateful of my lab mates. Thank you to Eleanor Donnelly, Deirdre O'Connor, Anthony Dosante, Jeff Mader, Jessica Emery, Annie McDonough, Luke Timmins, Lizz Iffrig, and Adrian Lam who all contributed to this work.

I would also like to thank my collaborators, including Dr. Allan Kirk, Jaclyn Espinosa, Michael Larche, Cody Anderson, Pete Piferi, Eric Jablonoski and Andrey Krasnopeyev for all of their contributions.

I appreciate the support of all the students, faculty, and administrators at Emory University and Georgia Institute of Technology in the MD/PhD program and the Biomedical Engineering Program, specifically Mary Horton. Special thank you to Neal Laxpati for all of his supervision and insight.

Thank you to my friends and colleagues from medical school who supported me in medical school and in my transition to graduate school. Thank you Jimmy Daruwalla, Emily Ferrell, Phil Mitchell, Tarik Madni, Dina Itum, Max Weiss, Karl Langberg, and Emily Ebert for all of the good times.

Thank you to my friends Zach Shader, Zach Levine, Dan Ludin, Jordan Rosenbalm, Max Tyroler, Mat Shorstein, Lina Gugucheva, Daniel Liss, Chris Akers, and Leslie Stockton for motivating me in this long, difficult journey. I truly feel lucky to have such great friends and support.

Most importantly, I would like to especially thank my Mom, Dad, and Sister Kelly for always being there for me throughout the years. I love you all very much and this would not have been possible without your love and support. This work is dedicated to you.

This work was supported by the Amyotrophic Lateral Sclerosis Association and the Emory University/Georgia Institute of Technology Center for Regenerative Medicine and Engineering.

TABLE OF CONTENTS

LIST OF TABLES

LIST OF FIGURES

LIST OF ABREVIATIONS

ALS	Amyotrophic Lateral Sclerosis
ANOVA	Analysis of Varience
βTIII	Beta-tubulin III
CNS	Central Nervous System
CD	Cluster of Differentiation
DBS	Deep Brain Stimulation
fALS	Familial Amyotrophic Lateral Sclerosis
FDA	Food and Drug Administration
GFAP	Glial Fibrillary Acidic Protein
GRE	Gradient Echo
Hep	Heparin
hNPC	Human Neural Progenitor Cell
hNPC-F^{High}	High dose ferumoxytol labeled human neural progenitor cell
hNPC-F^{Low}	Low dose ferumoxytol labeled human neural progenitor cell
HuNu	Human Nucleus
MRI	Magnetic Resonance Imaging
MHC	Major Histocompatibility Complex
MS	Multiple Sclerosis
NPC	Neural Progenitor Cell
PFA	Paraformaldehyde
PBS	Phosphate Buffered Saline
pNPC	Pig Neural Progenitor Cell
PLO	Poly-L-Ornithine

PS	Protamine Sulfate
PB	Prussian Blue
SCI	Spinal Cord Injury
SMA	Spinal Muscular Atrophy
SPION	Superparamagnetic Iron Oxide Nanoparticle
T	Tesla
TE	Echo Time
TEM	Transmission Electron Microscopy
TR	Repetition Time
TSE	Turbo Spin Echo

SUMMARY

Transplantation of cellular therapeutics into the spinal cord has been explored as treatment for a range of degenerative and traumatic diseases. The post-transplantation fate of cellular therapeutics is poorly understood in both large animal models and in human studies because of limitations in cell graft detection. A minimally invasive technology for cellular graft tracking to visualize grafts *in vivo* is needed. However, it is important that the diagnostic marker does not impact the engraftment or efficacy of transplanted cells. We developed a straightforward, rapidly translatable method to label human neural progenitor/stem cells with magnetic ferumoxytol nanoparticles. We investigated the potential effect of ferumoxytol labeling on biological properties of the cells and transplanted them into a large animal (porcine) spinal cord. We assessed the feasibility and safety of *in vivo* diagnostic cell graft tracking using Magnetic Resonance Imaging and post-mortem histological identification in a clinically relevant model. Furthermore, we leveraged this tracking approach to develop and assess a minimally invasive, Magnetic Resonance Imaging-guided technique for targeted intraspinal stem cell graft transplantation in a large animal model.

CHAPTER 1

INTRODUCTION

The purpose of Chapter 1 is to briefly introduce the problem and setup the motivation for the thesis.

1.1 Spinal Cord Disease and Amyotrophic Lateral Sclerosis

Diseases of the spinal cord can arise from very diverse pathological disease processes, including tumorigenic, traumatic and neurodegenerative etiologies. Consequences include significant impairment of motor, sensory, and/or autonomic functions. Furthermore, the spinal cord and surrounding structures have a complex, delicate organization with limited capability for self-repair. Diseases such as traumatic Spinal Cord Injury (SCI) and non-traumatic conditions such as Multiple Sclerosis (MS), Amyotrophic Lateral Sclerosis (ALS) and Spinal Muscular Atrophy (SMA) push the self-renewing capacity of the spinal cord beyond what is feasible resulting in chronic impairment and a poor prognosis. This poor prognosis is not exclusively due to the pathophysiology and limited capacity for repair, but also to the challenge of developing and delivering therapeutics to the spinal cord.

Amyotrophic Lateral Sclerosis (ALS) is a fatal and relentlessly progressive neurodegenerative disease that involves death of upper motor neurons in the cerebral cortex/brain stem and lower motor neurons in the spinal cord. ALS has a reported incidence of between 1.5 and 2.6 per 100,000 person/years among Caucasian populations

in Europe and North America[86]. ALS constitutes a disease with highly variable clinical features and poor ability to predict prognosis. Median survival after diagnosis ranges from 3 to 5 years[40,156]. Riluzole, the only Food and Drug Administration (FDA) approved pharmacological treatment for ALS, has shown limited efficacy, prolonging the median survival of patients by only 2 to 3 months. The disease is characterized by a progressive degeneration of the MNs that supply voluntary muscles, including UMNs in the cerebral cortex and LMNs in the spinal cord[4]. The clinical presentation is heterogeneous, but the degeneration universally presents clinically as progressive motor weakness that leads to paralysis and ultimately to death, usually from respiratory failure. ALS is considered to be sporadic in most cases with mutations in certain genes accounting for over half of familial ALS (fALS) cases[29,106,119,122]. Some of these genes are known to alter the onset, severity or progression of the disease[157]. Discovery of ALS causing genetic mutations has not led to a breakthrough in understanding the pathogenesis of the disease. The search for a common pathway for all mutations leading to degeneration is tantamount in developing therapeutic targets[121]. Accumulation of disease causing mutant proteins and the neuroinflammatory reaction caused by activated glial cells are two common characteristics of many neurodegenerative diseases, such as ALS, Alzheimer's and Parkinson's. The discovery of these underlying mechanisms of pathogenesis and the lack of an effective therapy for ALS provides a unique atmosphere for the discovery of new pharmacological and non- pharmacological therapeutics.

1.2 Stem Cell Therapy

"Stem cell" is a term used to describe a specific cell type that has two key

characteristics: the capacity to differentiate to multiple cell types and the ability to replicate or self-renew its population. There are many different classes of stem cells based on their source and differentiation capabilities. Embryonic stem cells are termed *pluripotent* owing to their ability to differentiate into cells of all three germ layers. Other stem cells, such as neuronal progenitor cells, have more limited differentiation capabilities and are termed *multipotent*. Multipotent stem cells are innately limited to differentiate only into cells from the lineages from which they were derived. Neural progenitor cells are limited to differentiate to either neuronal or glial cells, including astrocytes and oligodendrocytes.

Stem cells, or stem cell-derived cells, can most simply be used to replace lost cells such as oligodendrocytes, neurons, motor neurons, and astrocytes. These cells may also provide an additional therapeutic effect by secreting trophic factors that are neuroprotective or that promote neuroregeneration, such as cytokines and growth factors. The modification of stem cells via gene therapy to produce or reduce specific factors is an additional level of specificity, which allows the therapeutic to target specific aspects of the disease under investigation.

Restoration of motor neuron function through cellular replacement has been studied as a therapeutic strategy in rodent models of ALS and spinal cord injury. Although transplantation of neurons derived from human embryonic stem cells and neural stem cells has been examined in rodents,[12,142,162,164] practical issues might limit the clinical translation of direct motor neuron replacement to humans.

Axonal defects, including degeneration of the neuromuscular junction and distal axon, are some of the earliest hallmarks of ALS, occurring before symptom onset and the ultimate loss of motor neurons.[35] Consequences of these early defects include a loss of trophic support, suggesting that intraspinal transplantation of stem cells that secrete neurotrophic factors could be a strategy that provides a bystander mechanism of neuroprotection for diseased motor neurons. Neuroprotection by growth factors has been studied extensively for the treatment of ALS, and vascular endothelial growth factor and insulin-like growth factor I (IGF-I) have been shown to provide neuroprotection in both *in vitro* and *in vivo* models of ALS and motor neuron degeneration.[135,136] Transplantation of stem cells that secrete growth factors provides support for endogenous cells in the spinal cord microenvironment. Cortical human neural progenitor cells engineered to secrete glial cell-derived neurotrophic factor (GDNF) confer motor neuron protection after transplantation into the spinal cords of $SOD1_{G93A}$ transgenic rats.[148] Similarly, transplantation of neural progenitor cells producing either GDNF or IGF-I into $SOD1_{G93A}$ mice attenuates motor neuron loss.[110] Cellular therapies might, therefore, represent a source of neurotrophic support for diseased motor neurons in ALS.

1.3 Stem Cell Transplantation for ALS: The Emory Experience

In September 2009, the US FDA approved the first clinical trial of human spinal cord stem cell (HSSC) injections into the spinal cord for the treatment of ALS (ClinicalTrials.gov identifier NCT01348451). In the trial, which involved 15 patients with ALS, HSSCs were delivered into lumbar and/or cervical segments of the spinal cord using the stabilization device developed by our group (**Figure 1**). In 2012, enrollment

was completed and surgical transplantation of all patients occurred without neurological complications of the procedure[33,38,127,128]. The primary objective of the trial was to determine the feasibility, safety and toxicity of direct spinal cord transplantation of HSSCs into patients with ALS. The study was designed to balance risk to participants with the acquisition of new knowledge regarding direct spinal cord transplantation, and included a sequential series of patient cohorts that fall under a 'risk escalation' paradigm. Under this paradigm, risk to patients receiving HSSC transplants escalated across the different cohorts according to disease severity and the number and placement of injections. In 2013, the FDA approved the Phase 2 dose escalation and safety trial, which is currently in progress with enrollment completed (ClinicalTrials.gov identifier NCT01730716).

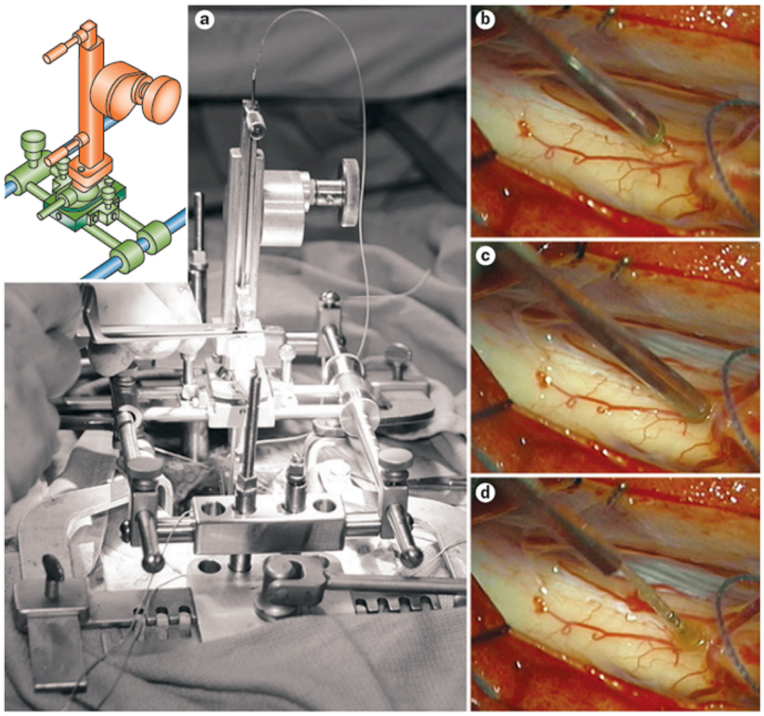

Figure 1. Spinal cord stabilization and injection system for intraspinal stem cell transplantation. A) Platform anchored to patient's spine allows the platform to move with the patient during ventilation and inadvertent patient movement preventing spinal cord shearing. The two bridge rails (blue), one of which is scored at 2-mm intervals to aid regular positioning of injections are fixed to percutaneous spine mounted posts. Gondola (green) allows for adjustment in the x and y planes and correction of the sagittal and coronal angles of the cannula trajectory. Mechanical Z drive (orange) allows precise raising and lowering of a floating cannula. **B)** Cannula tip is position 1 – 2 mm medial to the dorsal root entry zone. **C)** Needle penetrates a fixed depth into spinal cord. 4, 5, or 6 mm tips are used depending on preoperative measurements of cord thickness. **D)** Once needle tip is positioned at the target, metal outer sleeve is pulled up leaving flexible tubing exposed. This flexibility adds further safety.

1.4 Survival and Identification of Transplanted Cell Grafts

The current ALS trial lacks a method for identifying transplanted stem cells. The barriers to identifying the transplanted cells include the relatively small number of cells compared to the volume of the spinal cord, the typical long delay between transplantation and autopsy, and the inability to mark the cells by immunohistochemistry specific for human proteins. We have developed the technique of matching the "fingerprint" pattern of spinal cord vasculature imaged live during surgery to the *post-mortem* tissue (**Figure 2**). Ongoing work at Emory by Dr. Jonathan Glass' group[150] has used rtPCR targeting donor specific Human Leukocyte Antigen (HLA) genes, as well as FISH and anti-RBMY1A1 RNA binding protein immunohistochemistry (IHC) for Y chromosome markers (**Figure 3**). However, the former method provides little data on the percentage of transplanted cells to engraft and no data on the fate of the cells. Similarly, Y chromosome probe staining can only be employed in female patients. Therefore, it has

proven difficult to identify the cell graft with *post-mortem* tissue histology, difficult to confirm that the graft was delivered to the appropriate location in the spinal cord, and difficult to track the cell graft while the patient is still alive to fully understand long-term effects and/or to be able to optimize protocol regimens. These methodological gaps create a vulnerability to failure in ongoing and upcoming clinical trials. The need for a diagnostic marker of transplanted cell grafts is apparent from our experience[100].

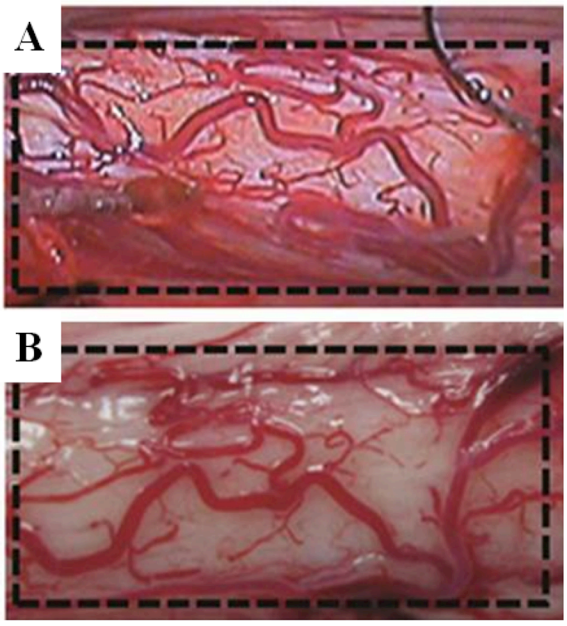

Figure 2. Gross analysis of male ALS spinal cord. Gross image of the spinal cord shows the cord surface at the site of Human Spinal Stem Cell transplant. The vascular anatomy between intraoperative videos **(A)** corresponds to the post-mortem tissue **(B)**.

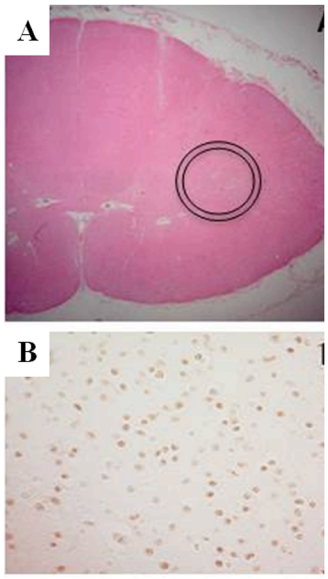

Figure 3. Histology and Immunohistochemistry in patient tissue. A lower power view of the spinal cord. Nest of cells located in circled region. High power image of immunohistochemical staining with antibody RBMYAL, an RNA binding protein voded on the Y chromosome, and seen only in male cells.

1.5 Thesis Organization

The remainder of the thesis is as follows:

CHAPTER 2: *Objectives and specific aims.* Reviews the overall objective of the thesis in three specific aims. Specific Aim 1 covers *in vitro* labeling of human neural progenitor cells with ferumoxytol nanoparticles (Chapter 4). Specific Aim 2 assesses the ability to use the labeling approach from Specific Aim 1 in a large animal (porcine) model of spinal cord transplantation (Chapter 5). Specific Aim 3 leverages the methods developed in Specific Aims 1 and 2 to develop and test a novel MRI-guided spinal cord transplantation device (Chapters 6 and 7).

CHAPTER 3: *Cellular Therapeutics Delivery To The Spinal Cord: Technical Considerations For Clinical Application.* Dr. Miller, Dr. Riley, Victor Hurtig, Dr. Boulis, and I review the current state of clinical trials and techniques available for transplantation of cellular therapeutics into the spinal cord. We also discuss advances in cellular graft tracking and image guided-delivery that will improve stem cell transplantation in the spinal cord.

CHAPTER 4: *Magnetic Nanoparticle Labeling of Human Cortical Neurospheres with Ferumoxytol for Diagnostic Cellular Tracking* discusses the approach used to label clinical grade human neural progenitor cells with ferumoxytol nanoparticles for cellular graft tracking with MRI and assess the hypothesis that these cells can be labeled with ferumoxytol. The potential *in vitro* adverse effects on biological function of the cells are analyzed.

CHAPTER 5: *Long-Term MR Tracking And Stereological Quantification Of Ferumoxytol Labeled Human Neural Progenitor Cells Transplanted Into The Porcine Spinal Cord* applies the ferumoxytol-labeled human neural progenitor cells to a large animal model of spinal cord cell transplantation and assesses the hypothesis that ferumoxytol can be used as a diagnostic cellular marker. The potential *in vivo* adverse effects on biological function and safety in the animal model are analyzed.

CHAPTER 6: *Development Of A Magnetic Resonance Imaging Compatible Spinal Injection System* overviews development of a MRI-compatible injection platform and development of a system capable of conducting MRI-guided transplantation of cellular therapeutics into the spinal cord.

CHAPTER 7: *Minimally Invasive Magnetic Resonance Imaging-Guided Transplantation Of Human Neural Stem Cells Into The Porcine Spinal Cord*. Lindsey Urquia, Victor Hurtig, Dr. Gutierrez, Cody Anderson, Pete Piferi, Dr. Federici, Dr. Oshinski, Dr. Boulis, and I test the hypothesis that cellular therapeutics can be transplanted into the spinal cord of a large animal under the guidance of MRI.

CHAPTER 8: *Conclusions.* I conclude the thesis by discussing the implications of this work, possible clinical translation, and future directions.

CHAPTER 2

OBJECTIVES AND SPECIFIC AIMS

Transplantation of cellular therapeutics to the spinal cord is a promising treatment option for patients with neurodegenerative and traumatic diseases of the spinal cord. However, ongoing clinical trials have limited evidence confirming successful graft delivery and no histopathological evidence of graft survival. These limitations complicate the assessment of clinical outcomes and determination of therapeutic efficacy. The aim of this thesis is to develop and validate a methodology to address these key limitations. We will label human neural progenitor cells *in vitro* with the Super-Paramagnetic Iron Oxide Nanoparticle (SPION) ferumoxytol. This method will allow non-invasive cell graft tracking *in vivo* with Magnetic Resonance Imaging (MRI) and post-mortem histological identification in our large animal (porcine) model. This approach will aim to allow clinicians to better understand the fate of transplanted cell grafts. ***The overall goals of this proposal are (1) to label human neural progenitor cells with the MR contrast agent ferumoxytol, (2) to evaluate the effects of ferumoxytol labeling, and (3) to assess the clinical utility in a large animal spinal cord. Successful completion of this would enable MR-guided approaches to spinal cord cell transplantation.*** In order to do so, we propose the following specific aims:

1. **Develop and evaluate a method to label human neural progenitor cells cultured as free-floating neurospheres with ferumoxytol nanoparticles.** This aim consists of the following sub-aims:

    a. **Develop a protocol to enable stem cells grown in cortical neurospheres to internalize ferumoxytol**
    b. **Quantify the efficiency of ferumoxytol internalization and MRI contrast produced**
    c. **Evaluate the effects of ferumoxytol labeling on cell viability and functionality**

2. **Assess the ability to visualize ferumoxytol-labeled cells in a large animal (porcine) spinal cord model of cell transplantation using MRI.** To evaluate the clinical utility of employing ferumoxytol-labeled cell grafts for visualization and tracking, we must transplant cells in to a large animal spinal cord. We propose three sub-aims.

    a. **Identify the location and quantify the size of transplanted ferumoxytol-labeled cell grafts *in vivo*, over time using MRI**
    b. **Correlate MR images of ferumoxytol-labeled grafts to histological quantification of cell engraftment and iron deposition**
    c. **Evaluate the effects of ferumoxytol labeling on *in vivo* cell graft dynamics**

3. **Develop a minimally invasive, MR-guided method for intraspinal cell transplantation.** This aim consists of the following sub-aims:

    a. **Develop an MR-compatible spine-mounted device capable of MR-guided intraspinal cell graft transplantation**
    b. **Test the MR-guided intraspinal transplantation device *in vitro* using a spinal cord phantom model**
    c. **Assess *in vivo* feasibility of the MR-guided transplantation system in a large animal (porcine) spinal cord using ferumoxytol-labeled cells**

CHAPTER 3

CELLULAR THERAPEUTICS DELIVERY TO THE SPINAL CORD: TECHNICAL CONSIDERATIONS FOR CLINICAL APPLICATION*

Current literature demonstrates the efficacy of cell-based therapeutics in small animal models of varied spinal cord diseases. However, logistic challenges remain towards development of an optimized delivery approach to the human spinal cord. Clinical trials utilize a variety of methods to achieve this aim. In this chapter, I review currently employed delivery methods, compare the merits of alternate delivery paradigms, introduce their implementation in completed and ongoing clinical trials, and discuss promising near-term advances in image-guided delivery and *in vivo* graft tracking.

* **Lamanna JJ**, Miller JH, Riley JP, Hurtig CV, Boulis NM. Cellular Therapeutics Delivery to the Spinal Cord: Technical Considerations for Clinical Application. *Therapeutic Delivery*. 2013;4(11*)*. 1397- 410.

3.1 INTRODUCTION

The human spinal cord is complex and has a limited capacity for self-repair. This holds true for both spinal cord injury (SCI) and non-traumatic conditions such as Multiple Sclerosis (MS), Amyotrophic Lateral Sclerosis (ALS) and Spinal Muscular Atrophy (SMA). There remain no clinically proven effective treatment options for patients with SCI aside from stabilization and supportive measures [49,124,131]. The most recent traumatic SCI guidelines provide only Class III evidence for hemodynamic support to an elevated mean arterial pressure of 85-90 mmHg [131]. Further, ALS and SMA remain as insidious and fatal neurodegenerative diseases without adequate pharmacologic treatments. Recent literature supports a considerable interest in clinical translation of cellular therapeutics as possible disease modifying agents given preclinical efficacy data[69]. To this end, multiple putative cellular therapeutics have undergone clinical investigation, as illustrated in **Table 1** and **Table 2**. However, an understanding of the factors necessary to achieve optimal graft delivery and the technology necessary to achieve this goal continue to undergo evolutionary advancements.

Current strategies to deliver cellular therapeutics to the spinal cord include local and intravascular delivery approaches. Local administration may be achieved through either direct cellular injection into the spinal cord parenchyma or through intrathecal delivery into the subarachnoid space. Each approach is associated with advantages and drawbacks. The pathology being treated, constraints inherent to the delivery approach, and limitations of current technology must be considered. The broadened future translation of cellular therapeutics will be hastened by continued evolutionary improvements to current delivery methods and associated technologies. This manuscript

will review the above mentioned delivery methods with an emphasis on advantages and limitations, introduce recently completed and ongoing clinical trials in the context of the delivery approaches employed, and describe near term advancements that promise to improve current generation cell graft delivery methods.

3.2 DELIVERY METHODS

Two primary routes may be considered for delivery of cellular therapeutics to the spinal cord: local or intravascular administration. When broadening a discussion to gene-based therapeutic approaches, peripheral delivery with retrograde axonal transport is an additional option. Retrograde axonal transport is not suitable for delivery of cellular therapeutics. Intravascular approaches may include both intra-arterial and intravenous routes while local administration may be achieved by either intraparenchymal or intrathecal injection. Each delivery strategy has inherent benefits and limitations which must be considered in the context of both the pathology being treated and the specific therapeutic goals. Route-specific factors to consider include: 1) obtainable anatomic specificity, 2) desired graft distribution, 3) tolerable degree of invasiveness to deliver therapy, and 4) implications for immunologic sensitization.

Previous groups have directly compared intravenous, intrathecal, and intraparenchymal methodologies for transplanting cells to the spinal cord in rodents [5,6,77,105,112,141,158]. In a rodent model of SCI, the engraftment efficiency of Mesenchymal Stem Cells (MSCs) transplanted with direct intraparenchymal injection to the lesion site (6.1%) was greater than both intrathecal (3.4%) and intravenous approaches (1.6%) 21 days after transplantation[112]. However, the results from this study are difficult to interpret

as the delivered dose was not consistent between transplantation methods, with more cells delivered with the intrathecal and intravascular approaches. Takahashi and colleagues compared different methods of administering neural stem/progenitor cells to treat SCI in mice and tracked the cell grafts for 42 days *in vivo* using a bioluminescence imaging reporter gene strategy [152]. The same delivered dose (5×10^5 cells / 2 μL) was maintained for all groups undergoing transplantation via the intravenous, intrathecal, or intraparenchymal route. The intraparenchymal approach had the greatest engraftment efficiency with numerous differentiated cells within the injured parenchyma. With the intrathecal approach, few grafted cells were located on the surface of the lesion site and on other areas of uninjured spinal cord. The engrafted cells differentiated into neurons, astrocytes, and oligodendrocytes as well. With both of these approaches, cells were not found engrafted at off-target sites, outside of the spinal cord. In the intravenous transplant group, cells were not engrafted at the injury site or spinal cord, but rather located in the lung, spleen, and kidney. Furthermore, several mice in the intravenous group died shortly after transplantation due to likely pulmonary embolism. The longitudinal bioluminescence imaging results showed a similar pattern of graft survival, with the most signal loss or cell death occurring in the first week after transplantation. These results do not account for possible improved homing of alternate cell types. However, with the given cell type, the intraparenchymal approach improved engraftment efficiency, targeting to the injured site, and reduced procedural-associated complications, when the delivered dose is held constant[152]. The utility of *in vivo* graft tracking methods is also apparent in this study.

Below, preclinical and clinical data separately exploring the utility of each approach is discussed. An exhaustive discussion of the homing capacity of different cell types for intravascular and intrathecal delivery approaches is outside the scope of this manuscript and is not discussed in detail. Clinical data for technical considerations of transplantation in select ongoing and completed clinical trials are provided **Table 1**. Greater detail is given to intraparenchymal delivery due to the wide variety of inherent technical considerations associated with this approach. An expanded list of published clinical trials and associated adverse events are provided **Table 2**. A direct comparison between adverse events of individual trials and cell delivery approaches is confounded by inherent differences in: 1) expected adverse events, 2) trial design methodologies, 3) patient populations, 4) regulatory oversight, 5) data collection, and 6) quality assurance.

Table 1: Review of technical aspects in select clinical trials transplanting cells to the spinal cord. Abbreviations: Spinal Cord Injury (SCI), Amyotrophic Lateral Sclerosis (ALS), Multiple Sclerosis (MS), and Mesenchymal Stem Cell (MSC)

Delivery Method	Location (Sponsor)	Year (Status)	Indication	Cell Line	Target	Dose	Cannula / Rate
Intraparenchymal	Multicenter, USA and Israel (Proneuron Biotech) [53,65,71]	2000 - 2011 (Phase 2 Complete)	SCI	"Alternatively activated" autologous macrophages	Caudal contusion boundary (posterior columns, corticospinal, spinothalamic)	Six injections 20 uL / injection 1.25E4 cells/uL	30 gauge reflux prevention: 20 - 30 s
	Multicenter, USA (Geron Corp.) [NCT01217008]	2009 – 2012 (Phase 1 Terminated)	SCI	Embryonic-derived oligodendrocyte progenitor cells	Intralesional	Single injection 50 uL / injection 4E4 cells/uL	Not described
	Novara, Italy (Maggiore della Carità Hospital) [89-92]	2001 - 2009 (Two Phase 1 Complete)	ALS	Autologous human bone marrow-derived MSCs	Bilateral upper thoracic central cord region, toward ventral horns	Two - five injections Patient specific 25 uL / injection 6E5 cells/uL	18 gauge 2 uL / min no reflux prevention
	Emory University, Atlanta, GA, USA (Neuralstem, Inc.) [38,127]	2009 - (Phase 1 recruiting complete)	ALS	Fetal spinal cord-derived neural stem cells	Unilateral or bilateral thoracolumbar and/or unilateral cervical ventral horn	Up to 10 thoracolumbar and 5 cervical injections in separate procedures 10 uL / injection 1E4 cells / uL	29 gauge 5 uL / min reflux prevention: 60s

Table 1 Continued…

Delivery Method	Location (Sponsor)	Year (Status)	Indication	Cell Line	Target	Dose	Cannula / Rate
Intrathecal	Multicenter, Israel (Hadassah Medical Organization) [62]	2006 - 2009 (Phase 1/2 Complete)	MS / ALS	Autologous MSCs	Spinal cord pathology via intrathecal lumbar puncture (all patients) and intravascular (subset) infusion	Single infusion Mean intrathecal dose: 63E6 (MS) 54E6 cells (ALS) Mean intravascular dose: 24E6 (MS) 23E6 cells (ALS) 2 mL saline / infusion.	Not described
	Rochester, MN (Mayo Clinic) [NCT01609283]	2012 - (Phase 1 Recruiting)	ALS	Autologous adipose-derived MSCs	Spinal cord pathology via intrathecal infusion	Up to two infusions in separate procedures 1E8 cells/infusion	Not described
Intravascular	Houston, Texas, USA (Memorial Hermann Healthcare) [NCT01328860]	2011 - (Phase 1 Ongoing; Recruiting)	SCI	Autologous human bone marrow-derived progenitor cells	Spinal cord lesion via intravascular infusion	Single Infusion	Not described
	Seoul, Korea (Seoul National University Hospital) [118]	2009 - 2010 (Phase 1 Complete)	SCI	Autologous adipose tissue-derived MSCs	Spinal cord lesion via cephalic vein infusion	Four infusions 4E8 cells/infusion 100 mL saline / infusion	3 - 4 hour infusion

Table 2: Review of published clinical trials transplanting cells to the spinal cord. Abbreviations: Amyotrophic Lateral Sclerosis (ALS), Spinal Cord Injury (SCI), Multiple Sclerosis (MS), Mesenchymal Stem Cell (MSC), Mononuclear Cell (MNC), Bone Marrow (BM), and Cerebrospinal Fluid (CSF)

Delivery Method	Year	Location	Indication (# Patients)	Cell Line	Observed Adverse Events (# Patients)
Intraparenchymal	2012	Atlanta, GA, USA[38,127]	ALS (12)	Fetal spinal cord-derived stem cells	Transient radicular-type pain and/or sensory abnormalities (several); repaired CSF leak (1); wound dehiscence (1)
	2012	Multicenter, USA and Israel[53,65,71]	SCI (26)	Autologous macrophages	Surgery for late spinal instability (1); post-op subsegmental atelectasis (1); resolved bacterial meningitis (1); pseudomeningocele (1)
	2012	Murcia, Spain[10]	ALS (11)	Autologous BM MNCs	Transient wound pain (7), intercostal pain (5), hypoesthesia (7), paresthesia (4), dysesthesia (2), headache (2) and/or intracranial hypotension (3); persistent hypoesthesia (2)
	2012 2008	Novara, Italy[89-92]	ALS (9 and 10)	Autologous BM MSCs	Transient pain (7), dysesthesia (6), light-touch impairment in one leg (4) or sacral region (1), and/or tingling sensation in one leg (6)
	2011	Ankara, Turkey[3]	SCI (4)	Autologous BM MNCs	None observed
	2010	Lisbon, Portugal[80,81]	SCI (20)	Autologous olfactory mucosal cells	Sensory deficit secondary to resolved aseptic meningitis (1); minor resolved subcutaneous CSF collection (3); transient irritable bowel syndrome (1)
	2009	Ankara, Turkey[28]	ALS (13)	Autologous BM MNCs	None observed
	2008	Brisbane, Australia[34,87]	SCI (6)	Autologous olfactory ensheating cells	None observed after 1 year of follow-up
	2007	Tehran, Iran[132]	SCI (33)	Autologous schwann cells	Transient sensory-motor decline (2)
	2007	Incheon, Korea[165]	SCI (35)	Autologous BM cells	Fever (22); transient neurological deterioration (1), spasticity (1), rigidity (3), headache (3), numbness or tingling sensation (6), rash (5); neuropathic pain (7)

Table 2 Continued…

Delivery Method	Year	Location	Indication (# Patients)	Cell Line	Observed Adverse Events (# Patients)
Intrathecal	2012	Mumbai, India[139]	Multiple (Unknown)	Autologous BM MNCs	Unknown
	2012	Moscow, Russia[36]	SCI (20)	Autologous hematopoietic stem cells	None observed
	2012	Kerman, Iran[61]	SCI (11)	Autologous BM MSCs	None observed
	2012	Osaka, Japan[133,134]	SCI (5)	Autologous BM stromal cells	None observed
	2010	Jerusalem, Israel[62]	MS/ALS (34)	Autologous MSCs	Fever (21); transient headache (15), rigidity (2), and leg pain (3); aseptic meningitis attributed to intrathecal injection (1)
	2009	Chennai, India[68]	SCI (297)	Autologous BM MNCs	Fever (95); transient headache (67), tingling sensation (68), spasm (1) and pain (17)
	2009	Bangalore, India[108]	SCI (30)	Autologous BM MSCs	None observed after 1 year of follow-up
Intravascular	2011	Seoul, Republic of Korea[118]	SCI (8)	Autologous adipose tissue-derived MSCs	None observed after 3 months of follow-up
	2010	Jerusalem, Israel[62]	MS/ALS (34)	Autologous MSCs	Fever (21); transient headache (15), rigidity (2), and leg pain (3); aseptic meningitis attributed to intrathecal injection (1)
	2011	Beijing, China[161]	MS (36)	Autologous peripheral blood stem cells	Adverse events were not measured or discussed
	2009	Sao Paulo, Brazil[25]	SCI (39)	Autologous peripheral blood stem cells	Pneumothorax associated with stem cell collection (1); local allergic reaction to contrast agent (3)
	2006	Buenos Aires, Argentina[102]	SCI (2)	Autologous BM MSCs	None observed

3.2.1 Intravascular Delivery

Vascular-mediated cellular therapeutics delivery has been trialed for a variety of non-neurologic treatment endpoints[48,113,160]. Cells delivered to the spinal cord through an intravenous or intra-arterial route must bypass the blood brain barrier (BBB). Therefore, vascular-mediated cellular delivery relies entirely upon the CNS-homing capabilities of an introduced cell type, with additional considerations including the dose and rate of delivery. Preclinical small animal studies have supported the capability of MSCs to support remyelination[2,50] with other unpublished reports of improvement following SCI in small animal models[118].

The primary advantage of intravascular delivery is the use of a minimally invasive approach. Disadvantages of this delivery method include the concern for tumorigenesis of a systemically delivered cell type and vascular complications associated with bulk cell delivery (e.g. pulmonary embolism). Pulmonary embolism has been observed in small animal studies with high rate delivery of elevated quantities of cellular grafts likely indicating bulk sequestration within the pulmonary vasculature[37]. This effect is reported to be absent with lower quantities of administered cells and when high doses are given at a lower rate of administration[118]. While methods of follow-up have varied widely, neither observation of tumorigenesis nor of vascular-related complications of cell administration have been reported to date in clinical trials[22,25,62,102,118]. Adverse events from published clinical trials are provided in **Table 2.** While small animal studies and initial clinical usage appear to demonstrate the achievable safety with this approach, detailed analysis of the results of intravascular cell delivery is complicated by multiple factors. These include: 1) a lack of data in large animal studies (e.g. biodistribution scaling studies or attempts to demonstrate

efficacy), 2) variability in the cell types administered between studies, 3) inconsistent attempts to document cellular homing in small animal and clinical studies, 4) the lack of a control arm in the performed clinical studies, and 5) significant variability in the manner of post-intervention follow-up.

3.2.2 Intrathecal Delivery

Intrathecal cell delivery to the spinal cord is accomplished through access to the subarachnoid space in an approach that is technically identical to a lumbar puncture. Protocols have described delivery in either a single session or fractionated over multiple injection procedures with some using concomitant intrathecal steroid injections to reduce the risk of aseptic meningitis. Advantages to an intrathecal approach include concentration of graft delivery adjacent to the neuraxis and the use of a minimally invasive approach. Possible disadvantages include the risk of developing meningitis from the injection procedure (aseptic or bacterial), immunologic activation, and a risk of disseminated tumorigenesis from injected cellular grafts. The actual risks of these outcomes will be forthcoming as additional trial results are published. However, adverse events from published clinical trials are provided in **Table 2**.

Similar to intravascular cellular therapeutics delivery, some preclinical data supports cellular 'homing' to the site of interest, as briefly discussed above. Support for a cellular homing capability through the subarachnoid space is best supported in small animal SCI studies. This homing capacity, although not seen in all preclinical small animal studies [152], has been observed to be restricted to the lesion site and adjacent tissue[6,21,77,137]. Cellular homing has also been explored in a large animal (canine) study.

Intrathecal delivery of autologous and allogeneic MSCs in an experimental model of SCI supported migration and engraftment of both to the injury site[54]. Despite a 'homing capability', the majority of injected cells have been documented to remain in the intrathecal space in preclinical studies of SCI[101] and ALS[47]. Thus, apart from safety considerations, it is unclear how to choose the dose (graft cell number) given the limited penetration of cord parenchyma. Furthermore, variability in observed penetration creates a significant hurdle for translation of these approaches.

While no domestic reports have yet been published on the clinical application of intrathecal delivery, the international literature indicates that cellular grafts have been delivered for the treatment of cerebral palsy[117,159], ALS[62,116], MS[62], and SCI[15,16,85]. While rigorous interpretation of these results is complicated by multiple factors, they provide pilot data as to the lack of tumorigenicity and overall safety profile that may be achieved with intrathecal cell-based administration. Additionally, two clinical studies have attempted to categorize radiographic biodistribution of labeled cells. Callera *et al*[15,16] attempted to provide radiographic support for cell delivery and engraftment at a site of SCI. The authors demonstrated a cohort-specific hypointensity at the lesion site in patients that received autologous CD34+ bone marrow cells labeled with magnetic nanoparticles. Karussis *et al* [62] labeled a subset of enrolled trial patients that had ALS and MS with ferumoxides, superparamagnetic iron oxide nanoparticles (SPIONP), visible on Magnetic Resonance Imaging (MRI). The authors reported diffuse radiographic evidence of cells within the parenchyma, meninges, and at the ventral/dorsal root entry zones. However, no histopathology was available, so the actual engraftment efficiency represented by this MRI signal is unclear. Continued development of radiographic

markers for cellular homing and an improved understanding for the mechanistic basis of cellular homing will be critical to the further clinical development of intrathecal cellular delivery. Ongoing and completed clinical protocols for intrathecal cellular graft delivery are summarized in **Table 1 & Table 2.**

3.2.3 Intraparenchymal Microinjection

Direct microinjection into the spinal cord represents the most conceptually straightforward but technically involved delivery paradigm. This process requires exposure of the spinal cord at the level of interest followed by targeting, cannulation, and graft injection. Advantages of a direct microinjection delivery paradigm include the ability to deliver cellular grafts with anatomic specificity as well as to precisely titrate the dose at the target site. However, this anatomic specificity constrains the utility of this approach when treating anatomically diffuse disorders (e.g. ALS, SMA). Potential disadvantages include the morbidity that may occur with: surgical exposure, spinal cord cannulation/infusion into the spinal cord, and tissue injury from immunologic rejection of cellular grafts in the spinal cord. Notable adverse events of trials published to date are summarized in **Table 2.** While several of the listed adverse events are expected of the surgical approach (e.g. incisional pain, pseudomeningocele), the possible sequelae of both the approach and intraparenchymal microinjection process appear to be mainly transient. Multiple factors must be considered when utilizing a direct microinjection approach, including: 1) cannula stabilization technique, 2) targeting methodology, 3) cannula type, and 4) infusion parameters.

3.2.3.1 Direct Microinjection Approach Considerations

Cannula stabilization techniques range from non-stabilized (freehand) to fully stabilized approaches. Stabilized techniques may further be divided into patient-stabilized and non-patient stabilized approaches. Much of the literature exploring the delivery of cellular therapeutics for various spinal cord afflictions in small animal disease models utilized a non-stabilized approach in which a microinjection needle was used to cannulate the spinal cord by hand with the volume and rate manually controlled by the surgeon or assistant. Stabilized approaches to cell delivery provide the ability to precisely target single or multiple sites within the spinal cord with a reduced concern for iatrogenic SCI. Further, stabilized approaches allow for the timed infusion of a graft while using a pre-programmed delivery pump. Patient-stabilized delivery approaches are anchored relative to the patient's anatomy (e.g. spinal elements) whereas non-patient stabilized approaches are held immobile relative to an alternate point of reference (e.g. operating room table). In our experience, patient stabilized approaches appear to reduce the risk of inadvertent movement of the spinal cord relative to the microinjection cannula that may occur from expected (e.g. cardioballistic, cardiorespiratory) or inadvertent (e.g. iatrogenic) spinal cord movement[129]. **Figure 4 A-D** demonstrates an example of a patient stabilized microinjection platform, the most recent iteration of the platform utilized by our group. It is respectively shown disassembled and assembled in **Figure 4 A, B**. **Figure 1C** demonstrates a thoracolumbar approach in a preclinical large animal (swine) with self-retaining retractor blades in place and stabilizing posts rostral and caudal to the incision. **Figure 4 D** shows the fully assembled platform with microinjector and microinjection cannula in place after completion of laminectomy and dural opening.

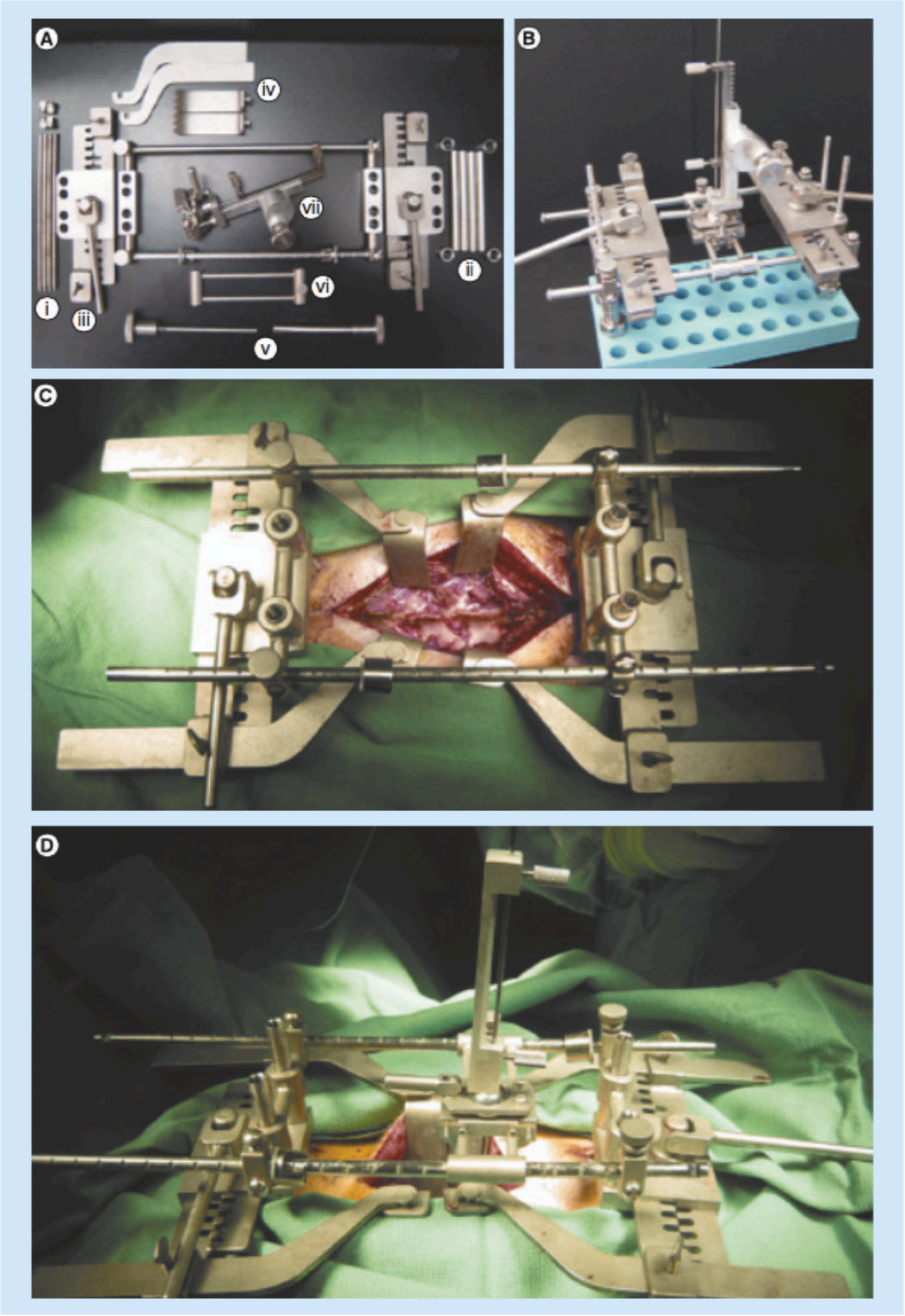

Figure 4: Gamma Microinjection Platform. A) (Far left) The laminar bone screws are shown with associated nuts. (Far right) sheaths and spacers for bone screws. (Right,

Left) Self-retaining retractors with four holes for alignment with translaminar screws/sheaths and platform rail system. (Top) Two of four required retractor arms and blades. (Far Bottom) Tunnelers to dock laminar screw sheaths on lamina prior to screw introduction. (Bottom) Gondola platform to mount microinjector platform on platform rail system. (Center) Platform rail system and microinjector. **B)** *In situ* demonstration of γ-platform without attached retractor arms/blades. **C)** *In vivo* demonstration of gamma platform prior to laminectomy and before attachment of gondola or microinjector platform. **D)** *In vivo* demonstration of fully assembled microinjection platform. * Reproduced with Permission from this reference[130].

Current methodologies for targeting cellular grafts to the spinal cord include freehand injection based upon knowledge of internal spinal cord anatomy, the use of microelectrode recording, and the use of anatomic (coordinate-based) microinjection. The use of intraoperative imaging-based graft delivery is a possible future targeting approach that is discussed later in this review. Freehand targeting has been used in both preclinical small animal studies and in international clinical settings. Concerns with this approach include inconsistently reproducible accuracy to the target and precision between injections when considering multiple targets. Our group has employed both microelectrode recording- and coordinate-based targeting strategies[125,126]. Both approaches utilize an understanding of the cross-sectional anatomy of the spinal cord. A schematic view of the spinal cord is shown in **Figure 5**. Microelectrode recording is used in a capacity similar to deep brain stimulation. As the microelectrode is passed into the spinal cord, the audible and visible waveform differs between white and grey matter. Disadvantages of this approach include a need to rigidly cannulate the spinal cord and the possible need to make multiple passes with the microelectrode. In our early preclinical

experiences, this resulted in an elevated early post-surgical morbidity profile. The coordinate-based technique utilizes external landmarks to interpolate the coordinates for intraspinal microinjection targets. Identification of the dorsal root entry zone (DREZ) has proven a reliable surface landmark by which to target sites of interest within the spinal cord. Following target cannulation, infusion is undertaken at predefined volume and rate infusion parameters. **Figure 5** provides a schematic representation of how our group utilizes this technique to target the ventral horn in both a preclinical and clinical setting. A reproducible depth is maintained by incorporation of a flange at a known distance from the needle tip, as shown in **Figure 6**. We have previously used a Z drive with a micrometer attached to measure the depth of penetration. However, the cord tends to be compressed by the needle passing through the pia, confounding depth measurements. This phenomenon generally results in an underestimate of penetration depth resulting in targeting deeper than the intended target.

In the experience of our group, the single greatest impact upon morbidity reduction in preclinical studies has been observed through advancements in cannula design. **Figure 6 A, B** illustrates a comparison between a rigid and floating cannula. The floating cannula has a beveled tip to ease penetration through the pia and a flange at a known distance from the microinjection needle tip. The latter allows accuracy to a desired depth, and depth precision when comparing serial individual injections. The floating cannula is introduced into the spinal cord in rigid confirmation. Once depth is reached and the flange is flush to cord surface, the rigid outer cannula is retracted. This is demonstrated in **Figure 6 C.** This allows the floating cannula to accommodate pronounced spinal cord excursion that occurs with patient ventilation, cardioballistic cord

pulsation, and inadvertent patient movement/injection hardware manipulation. In addition to stabilizing the floating cannula tip, the flange may also act to retard reflux by capping the penetration site. Cannula design-based efforts to minimize reflux in cranial cell delivery applications have attempted through the use of either a stepped cannula design [66] or the use of a curved 'steerable' cannula [115]. In cranial applications, the latter is reported to have significant reductions in infusate reflux compared to straight cannula administration. This may be both because the injection apparatus incorporates a stepped design and that the steerable needle prevents a line of site trajectory between the parenchymal surface and the target.

The set of chosen infusion parameters is also crucial towards optimizing both the delivered dose and engraftment efficiency. Number of injections, infusion rate, infusion volume, reflux prevention (cannula held in tissue for a time after cell infusion), and the quantity of cells delivered comprise the relevant factors. Manipulation of these factors can impact observed reflux, graft viability, and local tissue trauma associated with graft delivery. Elevated rate, volume, and delivered dose may overcome the capability of the graft site to accommodate the graft and may also result in local injury. Additionally, an elevated injection rate may compromise graft viability through both increased velocity and a shearing effect observed within the microinjection cannula [1,115,154]. Finally, a threshold effect may be observed in the local graft environment above which elevated graft density can result in diminished graft viability[143]. Infusion parameters implemented in current and recently completed clinical trials are in summarized in **Table 1**.

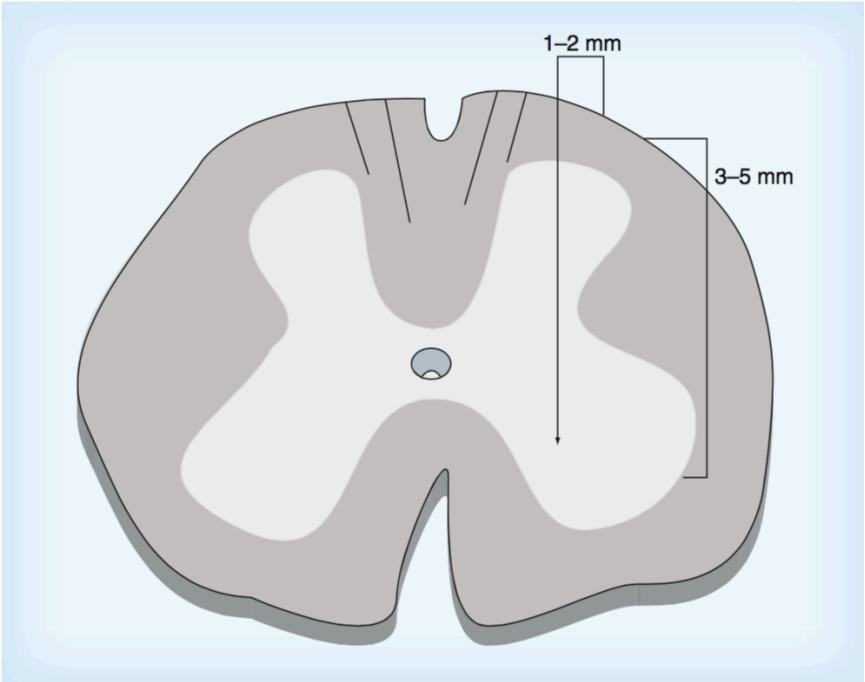

Figure 5: Anatomic Targeting. A schematic is provided demonstrating the use of the dorsal root entry zone as a targeting landmark. The microinjection needle is translated 1-2mm medially to accommodate for pial vascularity. * Reproduced with Permission from this reference[127].

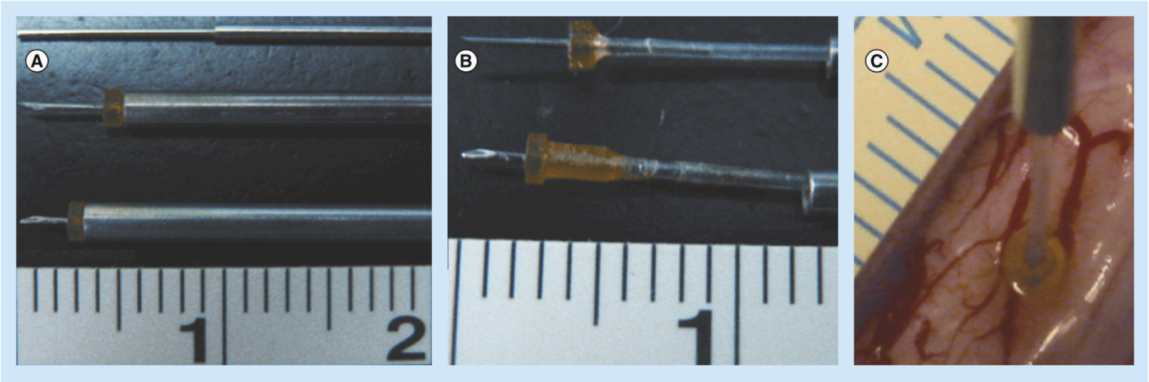

Figure 6: Cannula Type Comparison. A comparison of rigid and floating cannulas is provided. **A)** A 29-gauge stainless steel stepped rigid cannula (top) is shown adjacent to two floating cannulas (middle, bottom). The floating cannulas are shown in rigid conformation. Floating cannulas with 4mm (middle) and 3mm (bottom) fixed needle tips

are shown. **B)** In this panel, the outer rigid cannula has been retracted. Flexible silastic tubing is shown. The flange at the base of the needle prevents overpenetration. The longer proximal flange (bottom) aids in orthogonal spinal cord penetration while the more heavily tapered bevel (bottom) aids in pial penetration. **C)** The floating cannula is introduced into the spinal cord in rigid conformation. After pentration to the appropriate depth, using a preselected needle of desired length, the rigid outer cannula is retracted. The flexible silastic tubing is then capable of maintaining positional stability with cardioballistic and ventilation-associated spinal cord movement. * Reproduced with Permission from this reference[130]

3.2.3.2 Direct Microinjection Trial Summary & Future Directions

A selected review of completed and ongoing direct delivery clinical trials is provided in **Table 1** with additional completed trials listed in **Table 2**. While each listed trial was completed for the treatment of ALS or SCI, they varied widely with respect to graft cell type, stabilization method, targeting approach, dose delivered, and infusion parameters. All of the published works cited in **Table 2** did not provide consistent evidence of a prospective, controlled design with concomitant uniform recording of outcome measures.

The limited published data generally appear to support the safety achievable with direct cellular microinjection into the spinal cord. Data driven assessments regarding the superiority of specific targeting approaches, stabilization methods, cellular dosages, and infusion parameters in ALS and SCI will be forthcoming upon the conclusion of the current generation of clinical trials. Consideration of immunosuppression, largely outside of the scope of this manuscript, holds an uncertain future and is being evaluated in at least some of the trials in **Table 1** and **Table 2**.

3.3 FUTURE PERSPECTIVES

3.3.1 In Vivo Cell Graft Tracking

A critical issue faced in translating cell therapy from the bench to bedside is confirming the delivered dose and engraftment efficiency of cell grafts. Calculating dose certainty and engraftment efficiency depends on quantifying delivered and surviving graft cells at the target site. The delivered dose is affected by the delivery method, targeting accuracy, reflux from the tissue, and the quantity of cells delivered. Engraftment efficiency is dependent on survival, migration, and rejection by the immune system. In animal models, calculating dose and engraftment efficiency is easily achieved with post-mortem immunohistochemistry. Species-specific antibodies can be used to identify cell grafts when the donor and the recipient are of a different species. Post-mortem graft identification with histological methods in human patients has proved challenging due to the low number of engrafted cells and the limited methods for differentiating donor and recipient cells of the same species. Furthermore, post-mortem dose calculation only gives data from a single time point. The initial delivered dose cannot be calculated and longitudinal observations cannot be made. This critical issue highlights the need for a method to track cell grafts *in vivo*. Cells can be genetically modified to express reporter genes to improve graft identification and produce image contrast, but this is an invasive method that has consequences on cell function, toxicity, and immune response[67,83]. Moreover, such a label would complicate the regulatory approval process by altering the therapeutic biological product. Cells can also be labeled *ex vivo,* prior to transplantation, with a physical particle for identification. The cell internalizes the particles, but the

particle concentration can either be diluted with cellular divisions or internalized by host cells[78].

Many different approaches have been employed to label cellular grafts for *in vivo* tracking. Reporter gene systems have been designed for bioluminescence imaging[147], optical imaging[11], MRI[84,167], positron emission tomography (PET)[56,79], and near infrared imaging[93]. A PET reporter gene system was used to track cytotoxic T lymphocytes implanted in to the brain of a patient with Grade IV glioblastoma multiforme[163]. This was the first domestic, published reporter gene-based imaging method used to track implanted cells *in vivo* in humans. However, the limitation of the reporter gene approach is the risk associated with the random integration of reporter transgenes from viral vectors. This is considered an invasive approach. Additionally, the intensity of the signal produced by the reporter gene has been limited in some approaches. Methods of physically labeling stem cells *ex vivo*, prior to transplantation, have been used to track stem cells *in vivo*. These approaches include superparamagnetic iron oxide nanoparticles (SPINOP) for visualization with MRI[39,46] and radionuclides for PET. SPIONPs are FDA-approved for imaging contrast and are manufactured in the US. Additionally, they have been safely and effectively used outside of the US to track stem cell grafts in several clinical trials [27,155], including healthy controls[123], and trials in the central nervous system[15,62,166]. However, caution must be taken to: 1) confirm the cells internalized the particles, 2) calculate the contrast produced, and 3) characterize the effect the SPIONPs have on cell viability, function, and differentiation. For a full review on assessing the cytotoxicity of cells labeled with SPIONPs, please see this review[144].

While limitations exist in current methods for tracking cell grafts *in vivo* and identifying them post-mortem, determining delivered cell dose, confirming targeting accuracy, and calculating engraftment efficiency is essential for the successful translation of cellular therapeutics. SPIONP-labeled cells can be used to determine the initial location and dose of delivered cells and to track the cell graft longitudinally. Determining the initial graft location in the spinal cord can have a significant impact on expected graft survival, as grey and white mater have been shown to have different patterns of immune response[95]. Additionally, it may be possible to use SPIONPs to identify donor cells post-mortem[107]. SPIONP-labeled cell therapies may be used in upcoming clinical trials because of: 1) SPIONP FDA approval for different indications, 2) a clinical precedent with use in clinical trials, 3) a less invasive approach than reporter gene systems and PET tracers, and 4) definitive *in vitro* and *in vivo* evidence of unaltered cell properties can be collected as part of the pre-clinical data package for individual cell therapies before clinical use. Regardless, developing a reliable method for calculating delivered dose, the initial graft location, and engraftment efficiency is essential for widespread translation of cellular therapeutics in the spinal cord.

3.3.2 Image-Guided Delivery

Although the currently employed methods of direct intraparenchymal injection are reliable and safe, future approaches utilizing image-guidance for targeting and delivery could provide less invasive, more accurate methods to transplant cells into the spinal cord. Advanced intraoperative image-guided techniques offer an approach for improved direct targeting while percutaneous transplantation offers reduced

periprocedural inflammation and scarring. Computed Tomography (CT) and MRI have been used in the clinic for many years to guide percutaneous cordotomy procedures[57,58,94], and intraoperative MRI has been employed in surgical procedures in and around the spinal cord[30,104]. Furthermore, percutaneous transplant of a cellular graft to the canine spinal cord has been achieved under fluoroscopic guidance[74].

MRI is unparalleled in its spatial resolution and ability to visualize anatomy and pathology in the spinal cord, drastically improving targeting accuracy. Intraoperative MR targeting, trajectory planning, and cannula guidance are well established in the brain for the implantation of deep brain stimulation electrodes[72,88,146]. Sub-millimeter accuracy in placement of electrodes has been achieved with this MR-guided approach[72]. To translate MR-guided placement to the spinal cord, modifications to the current generation of platforms and cannulas are necessary. Extensive preclinical studies in large animal models must be conducted to evaluate the safety and accuracy of percutaneous, MR-guided spinal cord cell graft transplantation. Delivering cells percutaneously eliminates the need for an open surgical procedure. However, it raises other concerns, including: 1) cerebrospinal fluid leakage from needle puncture of the dura mater, 2) hemorrhage of spinal cord blood vessels from incidental needle puncture, 3) inaccurate targeting due to displacement of the cord from the resistance of the dura mater to needle puncture, 4) limited range of transplantation sites due to the vertebra, and 5) potential damage to the cord from needle puncture. While these concerns must be addressed before translation to the clinic, MR-guided delivery of stem cells to the cord remains particularly promising.

3.4 CONCLUSIONS

Cell-based therapies targeting varied spinal cord pathologies have proved efficacy in small animal models, feasibility in large animal studies, and safety in domestic and international clinical trials. The key to the successful, widespread clinical translation of cellular therapeutics is multi-faceted, including the optimization of: 1) patient selection, 2) cell line, 3) target site, and 4) delivery method. Intravascular, intrathecal, and intraparenchymal approaches offer distinct advantages/limitations and have been explored in the clinical setting. Future technical evolutionary advancements in delivery and tracking must occur to further optimize delivery of cellular therapeutics to the spinal cord.

CHAPTER 4

MAGNETIC NANOPARTICLE LABELING OF HUMAN CORTICAL NEUROSPHERES WITH FERUMOXYTOL FOR DIAGNOSTIC CELLULAR TRACKING (SPECIFIC AIM 1)

4.1 INTRODUCTION

Stem cell transplantation is a promising therapeutic strategy to overcome the regenerative limitations of the central nervous system (CNS). The aim is to replenish neuronal tissue and execute neuroprotective functions to counteract predominant degeneration caused by CNS pathologies such as amyotrophic lateral sclerosis (ALS), spinal cord injury (SCI), and multiple sclerosis [17,63,82,98]. Currently, clinical trials for ALS, SCI, and Parkinson's disease are ongoing and emerging evidence indicates that this approach is safe, feasible, and may have therapeutic effects [33,52,60,97,109]. The next step is to focus on ensuring accuracy and confirming delivered cell dosage to study the effectiveness of this approach. Therefore, it is critical to develop dynamic, non-invasive imaging technologies that may track cell graft delivery over time. The ability to localize cell engraftments in the clinic may also be used to assess cell distribution, differentiation, and viability to optimize treatment regimes[45].

The use of super paramagnetic iron oxide nanoparticles (SPION) has been validated as an imaging modality for tracking neural progenitor cells (NPC) using

MRI[8,19]. In animal models, cells are usually labeled using transfecting agents or reporter genes, but these techniques are difficult to use in humans due to overt complications that may arise. Novel labeling and optimization techniques need be developed to improve gradual signal disappearance and reduce cell toxicity[103]. Studies using simple SPION labeling for dissociated human neural stem cells show limited effect on cells' viability, tumor tropism, and lineage differentiation[8,19,26,51,140]. Most of these studies have employed nanoparticles that are not FDA approved or used Fedirex IV SPION, which has been discontinued in the United States[19].

This study aims to provide critical data on our ability to label human Neural Progenitor Cells (hNPCs) with ferumoxytol nanoparticles for diagnostic cellular tracking with MRI. Ferumoxytol is a SPION approved for clinical use by the US FDA as an intravenously administered MRI contrast agent. Currently, ferumoxytol is the only particle approved by the FDA and manufactured under Good Manufacturing Practice conditions. Ferumoxytol is a nanoparticle with an iron oxide core and a carboxydextran coat with a diameter of approximately 15 nanometers. The iron oxide core creates inhomogeneities in the local magnetic field, which can be detected with MRI, and provides a unique histological target for identifying grafted cells. We propose to use ferumoxytol "off label" as a cellular diagnostic marker to track transplanted cell grafts in the spinal cord with MRI. While the field of molecular imaging has employed SPION for cellular tracking, few clinical-grade human cell lines have been employed and limited data is available in the spinal cord. Furthermore, it is critical to rigorously establish safe labeling conditions and establish potential cytotoxicity for individual cell lines. Thus, the present study will help us define safe and effective ferumoxytol labeling conditions.

Currently there are only limited methods of identifying transplanted cell grafts, either *in vivo* or post-mortem, in clinical trials. This creates an unacceptable risk for failure because the investigators are unable to determine cell delivery, engraftment, migration, or survival. Potential therapeutic efficacy is difficult to attribute to the transplanted cells, as there is no diagnostic marker monitoring the therapy. SPION cell labeling with ferumoxytol for diagnostic monitoring of transplanted cell grafts provides a rapidly translatable method to identify *in vivo* and post-mortem the location of the transplanted graft. This will give insights in to delivery location, engraftment, survival, and potentially migration.

The aim of this study is to label a human cell line cultured as cortical neurospheres with ferumoxytol nanoparticles. Previous studies using SPION for molecular imaging have mostly employed non-human cell lines in monolayer culture systems. Neurospheres culture presents a unique problem in terms of cell access to SPION in the culture media, as effective ferumoxytol labeling requires most cells to internalize the particles. In monolayer culture systems, nearly all cells can directly access the media. However, only cells on the surface of the sphere will be able to directly access the media in a neurosphere culture system. This could create a heterogeneous population of labeled and unlabeled cells, complicating our ability to accurately track transplanted cell grafts. This methodological complication is relevant because many human neural stem cell lines are cultured as neurospheres.

We hypothesize that ferumoxytol can be internalized by hNPCs without significant cytotoxicity and produce adequate contrast for cellular tracking with MRI. The novel aspects of this aim pertain to the use of a clinical-grade human neural stem cell

line and the method it is cultured (cortical neurospheres). Limited studies have been performed on clinical-grade cell lines utilizing SPION with well-defined safety profiles. We aim to determine the optimal method for labeling hNPCs cultured as cortical neurospheres with ferumoxytol nanoparticles and to rigorously characterize the potential cytotoxic effects of labeling hNPCs with ferumoxytol with multiple independent assays quantifying viability, function, antigenicity, and the amount of internalized ferumoxytol. These studies present the possibility of generating a rapidly translatable approach for diagnostic cell tracking to large animal models and clinical studies.

4.2 METHODS

4.2.1 Human Neural Progenitor Cell Culture

Frozen stocks of early passage 21 hNPCs were graciously provided by the Clive Svendsen laboratory at Cedars-Sinai Regenerative Medicine Institute[64,149]. The hNPCs were originally isolated from eight-week-old postmortem fetal cortex of an aborted fetus with Institutional Review Board approval. Briefly, the intact cortical mantel was isolated and dissociated to a single cell suspension. The resulting cell line was expanded to free floating neurospheres of hNPCs and at passage 21 were frozen and sent to Emory University for the following studies.

The hNPCs were thawed and maintained as free floating neurospheres in T75 tissue culture flasks maintained with Neural Stem Cell Medium (Stemline Neural Stem Cell Expansion Medium, S3194, Sigma-Aldrich) supplemented with recombinant human Leukemia Inhibitory Factor (10 ng/mL, LIF1010, EMD Millipore), recombinant human Epidermal Growth Factor (100 ng/mL, GF003-AF, EMD Millipore), and

antimicrobial/bacterial reagent (15240062, Invitrogen) [Maintenance Medium]. The cells were cultured in a standard cell culture incubator at 37 °C and 5% CO_2. When the diameter of >75% of the neurospheres exceeded 500 micrometers, the neurospheres were passaged by mechanical sectioning[31]. Briefly, one flask of neurospheres were isolated from the media, placed in a plastic petri dish, orthogonally sectioned with an automatic tissue chopper (McIlwain Tissue Chopper, Lafayette Instrument Co.), and split in to two flasks with 50% fresh and 50% used maintenance media. The resulting clumps of cells reform spheres over the course of several days. The spheres were passaged approximately every eight days and 50% of the maintenance media was replaced with fresh maintenance media every 4 days. To prepare for transplantation and cytotoxicity assays, the neurospheres were chemically dissociated with trypsin (TrypeLE Express 1X, 11965092, Invitrogen) and DNAse (D4527, Sigma-Aldrich) and filtered with a 50 micron separation filter (130-041-407 Miltenyi Biotech) to a single cell suspension in Magnesium and Calcium free hibernation medium (Proprietary, provided by Svendsen lab). The cells were concentrated to 10,000 cells/μL and stored on ice. Cells between passage 25 and 35 were used for the labeling experiments on the same day of dissociation (**Figure 7**).

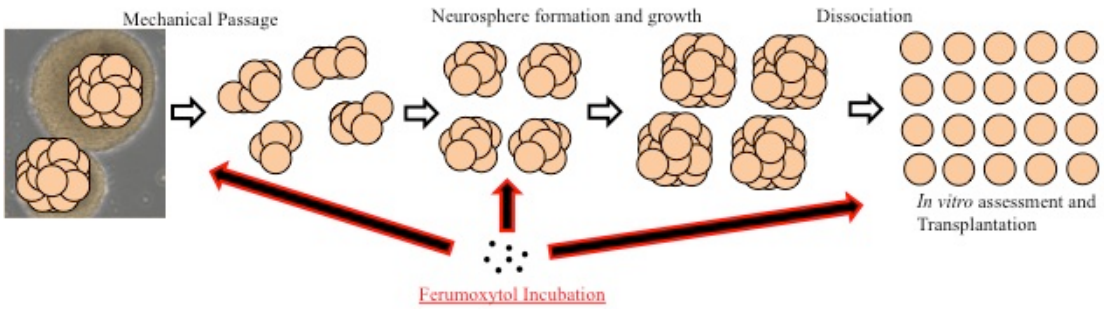

Figure 7. hNPC Culture and Ferumoxytol Incubation Schematic. Representative schematic of hNPC cultured from neurospheres, mechanical passage, neurospheres growth, and dissociation to single cells. The ferumoxytol nanoparticle were introduced to the cell culture medium at different time points.

4.2.2 Ferumoxytol Labeling of Human Neural Progenitor Cells

Three different strategies were employed to systematically induce hNPCs to internalize the ferumoxytol nanoparticles (**Figure 7)**. The first was to incubate dissociated cells, ready for transplantation, with increasing concentrations ferumoxytol in different conditions. The length of incubation, incubation media used, and the addition of transfection agents heparin (Hep) and/or protamine sulfate (PS) were all employed as outlined in **Table 3**. 24 hours was chosen as the maximum time point because of temporal viability limitations after dissociation. Transfection agents are charged reagents that potentially increase the efficiency of ferumoxytol internalization[18,153]. Two different incubation media were chosen because the neurospheres are cultured in maintenance medium, but transplanted as dissociated cells in hibernation medium.

Table 3: Dissociated Cells: Ferumoxytol Incubation Conditions

Incubation Medium	Ferumoxytol [µg/mL]	Time (hours)	PS [µg/mL] / Hep [IU/mL]
Hibernation	0, 100, 200, 400, or 1000	6, 12, or 24	0
Maintenance			
Hibernation	50 or 400	12	60 / 2 or 10 / 0, respectively
Maintenance			

The second approach was to incubate pre-formed neurospheres, four to six days after passage, with increasing concentration of ferumoxytol as outlined in **Table 4**. The third was to incubate neurospheres with increasing concentrations of ferumoxytol for seven days immediately following mechanical passage (**Table 5)**. At this time point, only small clumps remain and the neurospheres form over the course of several days. For all conditions, neurospheres were dissociated seven days after passage. Prior to dissociation, the neurospheres were washed twice with Dulbecco's Modified Eagle Medium and then after dissociation the cells were washed twice with hibernation medium to remove extracellular ferumoxytol nanoparticles.

Table 4: Formed Neurospheres: Ferumoxytol Incubation Conditions

Post-Passage Day	Ferumoxytol [µg/mL]	Time (hours)	PS [µg/mL] / Hep [IU/mL]
6	0, 100, 200, 400, or 1000	24	0
5		48	0
	50 or 400	48	60 / 2 or 10 / 0, respectively

Table 5: Passaged Neurospheres: Ferumoxytol Incubation Conditions

Post-Passage Day	Ferumoxytol [µg/mL]	Time (hours)	PS [µg/mL] / Hep [IU/mL]
0	0, 100, 200, 400, or 1000	168	0
	50 or 400		60 / 2 or 10 / 0, respectively

4.2.3 Rapid Assessment of Ferumoxytol Labeling

To rapidly assess the efficiency and effects of ferumoxytol uptake (labeling) for each of the different conditions, a viability assay and an *in vitro* MRI were performed. These assays were performed immediately following washing and dissociation. Cell viability was calculated using a trypan blue exclusion assay to measure live/dead cells on a hemocytometer under a microscope.

To assess the MRI contrast of the labeled cells, 250,000 cells in a pellet in a microcentrifuge tube were placed in a water bath in a 32-channel head radiofrequency coil in a Siemens 3T Trio Trim Full-Body MR scanner. The effect of the cells on the MR images contrast was calculated by determining the volume of the T2* signal generated by the cell pellet. A gradient echo (GRE) T2*-weighted sequence sensitive to magnetic field inhomogeneities was utilized [multiple echo time = 10 and 16 msec, pulse repetition time = 788 msec, number signal average = 4, field of view = 160 x 160 mm, matrix = 512 x 512, and slice thickness = 1.5mm)]. The two conditions that maximized MR contrast produced with optimal viability were chosen for further evaluation for potential cytotoxicity. Control (unlabeled) cells were evaluated further as a control.

4.2.4 Cellular MR Contrast Quantification

For the two optimal labeled cell conditions and the unlabeled cells, the following assays were performed to establish the amount of ferumoxytol internalized and evaluate any potential side effects of the ferumoxytol uptake.

MRI contrast was evaluated in the same system as section 4.2.3 (cell pellet in a microcentrifuge tube at 3T MRI). However, the scans were done in triplicate and MRI

contrast produced was measured in a quantitative method by calculating the Signal-to-Noise Ratio (SNR) of the cell pellet. Groups were compared with ANOVA and individual t tests ($p < 0.05$).

4.2.5 Ferumoxytol Internalization and Quantification

Ferumoxytol nanoparticle uptake/internalization by the cells was confirmed via microscopy. Immediately following labeling and dissociation, the cells were placed in Stemline Neural Stem Cell Medium supplemented with B-27 (17504044, Invitrogen) and antimicrobial/bacterial reagent (Invitrogen) [Plate Down Medium]. The cells in plate down medium were concentrated to 1,000 cells/μL and 40 μL of cells placed on ground glass coverslips coated with Poly-L-Ornithine (PLO) (P4638, Sigma Aldrich) and laminin (L2020, Sigma Aldrich) in 24 well tissue culture plates. The plates were placed in the incubator at 37 °C and 5% CO_2. After 1 hour, the wells were flooded with an additional 1 mL of plate down medium. After 24 hours, an aliquot of the cell-containing coverslips were fixed with 4% Paraformaldehyde (PFA) and washed three times with Phosphate Buffered Saline (PBS). The coverslips were then incubated with Hydrochloric Acid (2% solution) and Potassium Ferrocyanide (4% solution) for Perl's Prussian Blue (PB) histochemistry (CY005, Fisher Scientific). The Perl's reagent reacts with Iron in the ferumoxytol particles to generate histological blue precipitates. Nuclear Fast Red background stain was used to visualize the nuclei. The percentage of labeled cells with cytoplasmic Iron was calculated with ImageJ cell counter using a standard threshold for blue. Cells with threshold positive blue precipitates in the cytoplasm were considered "labeled". These experiments were done in triplicate and five slips/experiment/condition

were analyzed. Groups were compared with ANOVA and individual t tests ($p < 0.05$).

4.2.6 Transmission Electron Microscopy

A separate aliquot of cell-containing coverslips was fixed with glutaraldehyde and embedded in epon resin. The resin containing cells was sectioned at a thickness of 50 nanometeres. The sections were attached to a wire matrix and imaged with a JEOL JEM-1210 Transmission Electron Microscopy (TEM) to determine the intracellular location of the ferumoxytol nanoparticles.

4.2.7 Colorimetric Quantification of Cellular Iron

To quantify the amount of intracellular ferumoxytol, a Perl's colorimetric assay of Iron concentration was performed[14]. Briefly, aliquots of cells were lysed and mineralized with high concentration hydrochloric acid. Then the Perl's reagent was added to generate a blue solution, with color dependent on Iron concentration. The solutions were placed in 96 well plates and the absorbance of light at 630 nm was measured with an automated plate reader. The absorption of light from the cell samples was compared to a standard concentration curve of ferumoxytol particles. The absorbance of the cell sample was normalized to unlabeled cells and plotted on the standard curve to reveal the amount of Iron from ferumoxytol particles in individual cells (pico-grams per cell). Groups were compared with ANOVA and individual t tests ($p < 0.05$).

4.2.8 Cellular Viability Assays

Three separate assays were performed to accurately characterize the viability of the labeled cells. The trypan blue exclusion assay, as described earlier, was done five times for all groups. The trypan blue assay measures membrane permeability.

Quantitative flow cytometry live/dead staining (Life Technologies L34957) measuring membrane integrity was performed on recently dissociated cells. The samples were run on the LSRFortessa flow cytometer. Gating and quantification was performed using FlowJo software.

An 3-(4,5-dimethylthiazol-2-yl)-2,5-diphenyltetrazolium bromide (MTT) colorimetric assay (MTT Cell Growth Assay Kit, CT02, EMD Millipore) measuring mitochondrial metabolism was performed in duplicate on cells attached to coated coverslips for 24 hours. Cells were incubated with MTT agent for an additional 24 hours. Metabolically activate cells cleave MTT to create a byproduct with a different color absorption spectrum. After 48 hours, an expression agent was added to media and absorbance at 630 nm was measured for each coverslip (3 coverslips/condition). Groups were compared with ANOVA and individual t tests ($p < 0.05$).

4.2.9 Cellular Differentiation

To assess the differentiation capacity of labeled hNPCs, cells were placed on glass coverslips as previously described and incubated for an additional 7 days. 50% of the plate down media was replaced after 3 days. The coverslips were fixed with 4% PFA and prepared for immuncytochemistry. Briefly, the coverslips were washed with PBS, incubated in blocking buffer (PBST, 5% goat serum, 5% horse serum), and placed

directly in primary antibodies anti-Glial Fibrillary Acidic Protein (GFAP) [1:250, Sigma F0382] and anti-β-tubulin III (βTIII) [1:500, Sigma T8660] overnight at 4 °C. The slips were washed and placed in secondary antibodies goat-anti-rabbit Alexa-Fluor 594 (1:1000, A11037, Invitrogen) and goat-anti-mouse 488 (1:1000, A11001, Invitrogen) for one hour at room temperature. The coverslips were washed with PBS and mounted in vectashild with 4',6-diamidino-2-phenylindole (DAPI). The slips were visualized with a Nikon E400 Fluorescent microscope. Images of five High Power Fields at 40x were acquired. The percentage of GFAP+ (astrocytic differentiation) and βTIII+ (neuronal differentiation) cells for each condition was quantified using ImageJ cell counter. Three coverslips per condition performed in duplicate. Groups were compared with ANOVA and individual t tests ($p < 0.05$).

4.2.10 Cellular Antigenicity

As an estimate of potential increased antigenicity of ferumoxytol labeled cells, flow cytometry quantification of antigenic surface markers were quantified and compared to control cells. The cells were processed with the following antibodies: anti-Human Leukocyte Antigen (HLA)-DR APC (BD Biosciences 340549), anti-β2 microglobulin FITC (BD Biosciences 551338), anti-CD80 PE (BD Biosciences 560925), and anti CD86 PE (BD Biosciences 560957). The samples were run on the LSRFortessa flow cytometer. Gating and quantification was performed using FlowJo software.

4.3 RESULTS

4.3.1 Preliminary Studies on Ferumoxytol Labeling Methods

The first method of ferumoxytol labeling studies involved dissociated hNPCs. While the viability was relatively unaffected, all labeling conditions had limited uptake of ferumoxytol nanoparticles. Furthermore, with the longer incubation times, the amount of cells "recovered" after labeling was significantly less than the amount of cells initially incubated. Uptake of ferumoxytol by pre-formed neurospheres occurred, but at a low level. The incubation with ferumoxytol did not alter cell viability or change the morphology of the neurospheres. All conditions incubated with heparin showed significant decreases in viability and impaired neurospheres formation with no increase in labeling efficiency. The conditions incubated with protamine sulfate showed no change in viability or labeling efficiency. Finally, the conditions incubated with ferumoxytol immediately following mechanical passage showed significant particle uptake and little change in cell viability. These incubation conditions were explored further.

4.3.2 Ferumoxytol Dose Escalation

The passaged neurospheres had sufficient uptake of ferumoxytol nanoparticles. To properly assess optimal incubation concentration, a dose escalation paradigm was used. The growing spheres were incubated for 7 days (to reach dissociation size for transplantation) with a 50% fresh media change occurring at post passage day 4. The ferumoxytol labeling conditions did not alter neurospheres formation and were not toxic to the cells after dissociation, as measured by the trypan blue assay. With increased ferumoxytol concentration, no significant difference (ANOVA $p > 0.05$, individual t tests

$p > 0.05$) in viability measured by trypan blue was observed between different concentrations of ferumoxytol (**Figure 8 A)**. However, 50 μg/mL ferumoxytol, 60 μg/mL protamine sulfate and 2 IU/mL heparin was toxic to the neurospheres and excluded from analysis. The spheres dissolved in this condition and further analysis was not performed.

The contrast produced by the labeled cells was observed *in vitro* with MRI and quantified. The strong negative contrast produced by the labeled cells is best observed with gradient echo sequences (T2*). A dose-dependent increase in contrast (ANOVA $p < 0.0001$) was observed (**Figure 8 B, C**). The 400 μg/mL ferumoxytol and 10 μg/mL protamine sulfate condition was excluded from analysis because it provided no improvement in cell viability or MR contrast over [400 μg/mL] ferumoxytol alone. A statistically significant increase in contrast was observed between the 100 and 200 μg/mL conditions ($p < 0.05$). The difference between the 400 and 1000 μg/mL was non-significant ($p > 0.05$). Based on these observations and viability measurements, the passaged neurospheres incubated with 200 (hNPC-F^{Low}) and 400 (hNPC-F^{High}) μg/mL ferumoxytol for seven days immediately following mechanical passage were chosen for further evaluation.

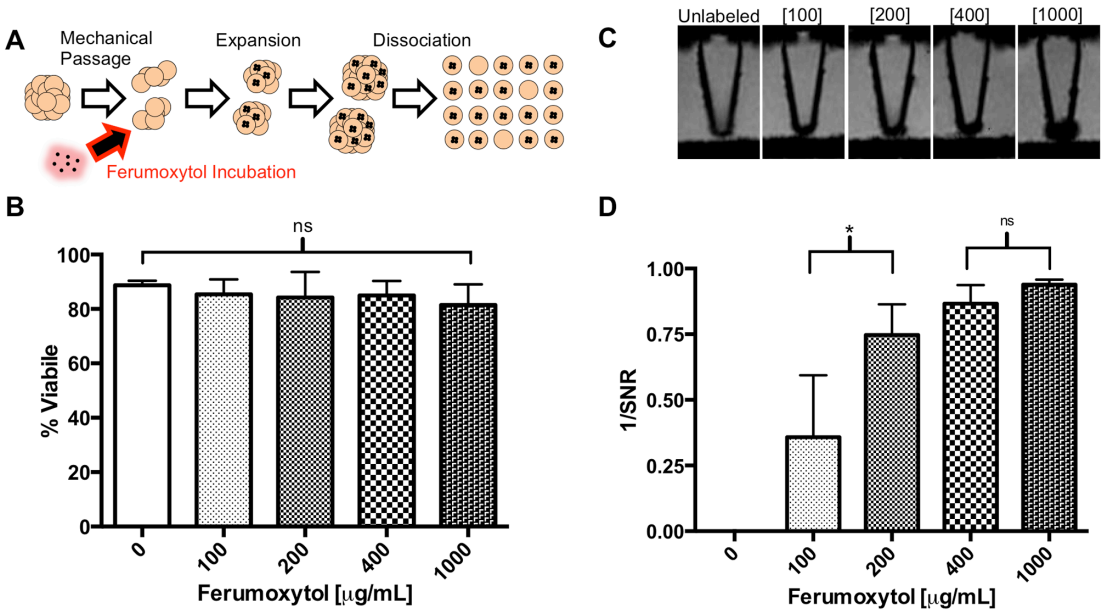

Figure 8. Incubation of human cortical neurospheres with ferumoxytol nanoparticles. Human neural progenitor cells cultured as free floating neurospheres were incubated with increasing concentrations [0 – 1000 μg/mL] of ferumoxytol nanoparticles for 7 days. Following incubation, the neurospheres were washed and chemically dissociated to a single cell suspension (**A**). No significant change in cell viability assessed by trypan blue exclusion assay was observed with increased ferumoxytol concentrations (**B**). Microcentrifuge tubes with a $2.5x10^6$ cell pellet were immersed in water and imaged with a gradient echo T2*-weighted sequence on a clinical 3T Magnetic Resonance Imaging scanner. Representative images show a signal void in the region of the cell pellet produced by ferumoxytol (**C**). The signal-to-noise ratio (SNR) for the volume of the cell pellet was calculated and a dose-dependent decrease in SNR was observed with increased ferumoxytol concentrations (**D**). A significant difference was observed between [100 μg/mL] and [200] conditions. No significant difference was observed between [200] and [400]. Ordinary one-way ANOVA and individual unpaired t-tests were performed (n = 5 / group). *Significant, $P < 0.05$; **Significant, $P < 0.005$; ***Significant, $P < 0.0005$. Graphs displayed as mean ± SD.

4.3.3 Ferumoxytol Particle Internalization

HNPCs labeled with 200 and 400 μg/mL ferumoxytol [(hNPC-F^{Low}) and (hNPC-F^{High}), respectively) and unlabeled hNPCs (0 μg/mL ferumoxytol) cells were plated on glass coverslips for 24 hours were evaluated for the internalization of ferumoxytol nanoparticles. An aliquot of coverslips stained with the Prussian blue reagent with nuclear fast red background were analyzed for the presence of ferumoxytol "labeled" cells with characteristic perinuclear blue precipitates in the cytoplasm. High-powered field micrographs show numerous labeled cells in both hNPC-F^{Low} and hNPC-F^{High} cells but not in unlabeled hNPCs (**Figure 9 A - C**). Quantification of labeled cells with ImageJ minimum threshold method of cytoplasmic blue precipitates yields 53.3% of hNPC-F^{Low} and 77.2% of hNPC-F^{High} cells were labeled, which was a significant increase over unlabeled hNPCs (ANOVA, $p < 0.005$) (**Figure 9 D**). Furthermore, the increase in labeling between hNPC-F^{Low} and hNPC-F^{High} was significant ($p < 0.005$).

Transmission Electron Microscopy (TEM) micrographs of both hNPC-F^{Low} and hNPC-F^{High} cells showed abundant endosomes and lysosomes laden with 10 - 20 nm ferumoxytol nanoparticles (**Figure 9 E - G**). Nanoparticles were confined to intracellular structures and not observed on the cell membrane or in the extracellular space. Furthermore, the internal architecture of the cells was consistently healthy with ample mitochondria, organelles, and neurites observed. Control hNPCs contained few lysosomes or endosomes and they did not contain nanoparticles.

The cellular concentration of iron from ferumoxytol nanoparticles was calculated using a PB colorimetric digestion assay. A statistically significant difference was observed between all groups ($p = 0.005$) with 1.46 and 2.82 ρg ferumoxytol iron/cell for

hNPC-F^{Low} and hNPC-F^{High} cells, respectively (**Figure 9H**). The intracellular iron was normalized to unlabeled cells, revealing only iron from ferumoxytol nanoparticles and excluding physiologic cellular iron.

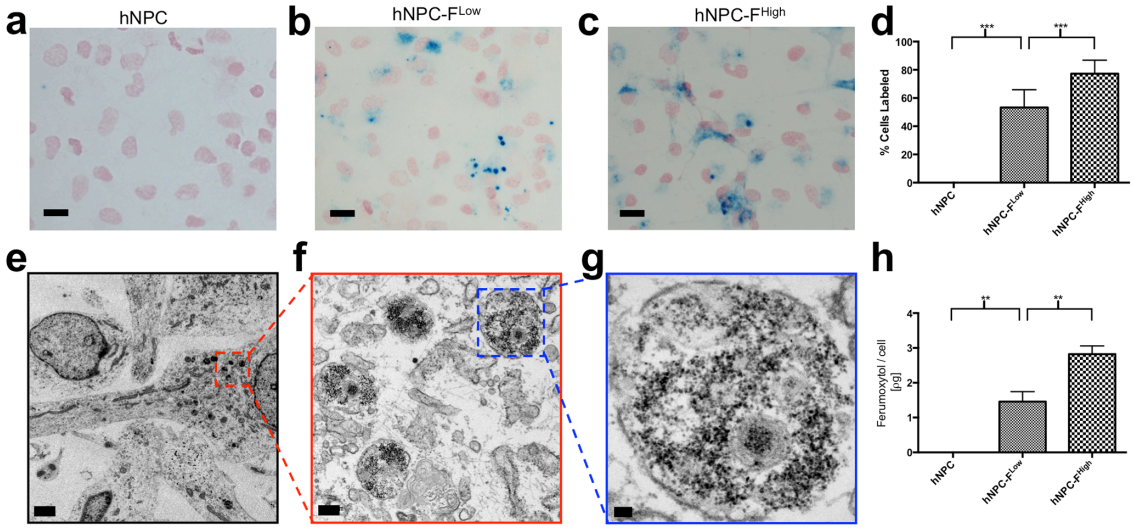

Figure 9. Cellular internalization of ferumoxytol nanoparticles. Representative light microscopy images of cytochemical staining for cellular iron with Prussian Blue (PB) for unlabeled hNPCs (**A**), hNPC-F^{Low} (**B**), and hNPC-F^{High} (**C**) labeled cells are shown. Characteristic blue precipitates of iron oxide nanoparticles were observed in the cytoplasm of ferumoxytol-labeled cells. A statistically significant difference was observed between all groups with 53.3% and 77.2% of hNPC-F^{Low} and hNPC-F^{High} cells labeled, respectively (**D**). Transmission Electron Microscopy of hNPC-F^{Low} and hNPC-F^{High} cells (**E**) revealed numerous iron-laden, electron-dense endosomes (**F**) containing nanoparticles (**G**). The cellular concentration of iron from ferumoxytol nanoparticles was calculated using a PB colorimetric digestion assay. A significant difference was observed with 1.46 and 2.82 ρg iron/cell for hNPC-F^{Low} and hNPC-F^{High}, respectively (**H**). Scale bars: (**A – C**) 10 μm; (**E**) 3 μm; (**F**) 0.3 μm; and (**G**) 50 nm. Ordinary one-way ANOVA and individual unpaired t-tests were performed (n = 5 / group). *Significant, $P < 0.05$; **Significant, $P < 0.005$; ***Significant, $P < 0.0005$. hNPC,

human neural progenitor cell; F, ferumoxytol; PB, Prussian Blue. Graphs displayed as mean ± SD.

4.3.4 In Vitro Cellular Dynamics

Ferumoxytol labeled hNPC-F^{Low} and hNPC-F^{High} cells, and unlabeled hNPCs were plated on glass coverslips for 7 days for evaluation of cellular differentiation of attached neural progenitor cells. Representative micrographs of unlabeled hNPCs, hNPC-F^{Low} and hNPC-F^{High} cells (**Figure 10 A – C**) show numerous GFAP+ astrocytes (red) and βTIII+ neuronal cells (green). The morphology of the differentiated cells is similar between groups. Quantification of differentiation reveals a statistically significant decrease in neuronal differentiation (35.0% hNPC, 30.0% hNPC-F^{Low}, 21.5% hNPC-F^{High}, ANOVA $p < 0.005$) (**Figure 10 D**) with a concurrent statistically significant increase in astrocytic differentiation (64.6% hNPC, 70.0% hNPC-F^{Low}, 78.5% hNPC-F^{High}, ANOVA $p < 0.005$) (**Figure 10 E**). However, a non-significant difference was observed between hNPCs and hNPC-F^{Low} for differentiation to neuronal cells ($p > 0.05$) and astrocytes ($p > 0.05$). Total differentiation was greater than 99% of cells for all conditions. Furthermore, the cellular morphology of the differentiated cells appears unchanged between groups.

Trypan blue exclusion assay of cell viability between hNPC, hNPC-F^{Low} and hNPC-F^{High} showed no difference (**Figure 10 F**). Flow cytometry live/dead staining was used as an independent measure of cell viability and cell membrane integrity. hNPC-F^{Low} and hNPC-F^{High} tended to be smaller (decreased forward scatter) and more granular (increased side scatter) than unlabeled hNPCs. Viability was calculated at 92.5% hNPC, 83.2% hNPC-F^{Low}, and 83.3% hNPC-F^{High} (**Figure 10 G**).

MTT mitochondrial metabolism assay showed a significant increase (ANOVA $p < 0.005$) in metabolism between groups (**Figure 10 H**). The difference remained significant between all groups ($p < 0.05$). Metabolism was significantly greater and normalized to dead, unlabeled cells.

Analysis of cell surface antigens HLA-DR (**Figure 10 I**), β2 microglobulin (**Figure 10 J**), CD80 (not shown), and CD86 (**Figure 10 K**) with flow cytometry quantification revealed no change in expression between labeled and unlabeled cells. Furthermore, all cell types expressed Major Histocompatibility Complex (MHC) 1 (β2 microglobulin) and MHC II (HLA-DR) proteins, but not co-stimulatory CD80/86 antigens.

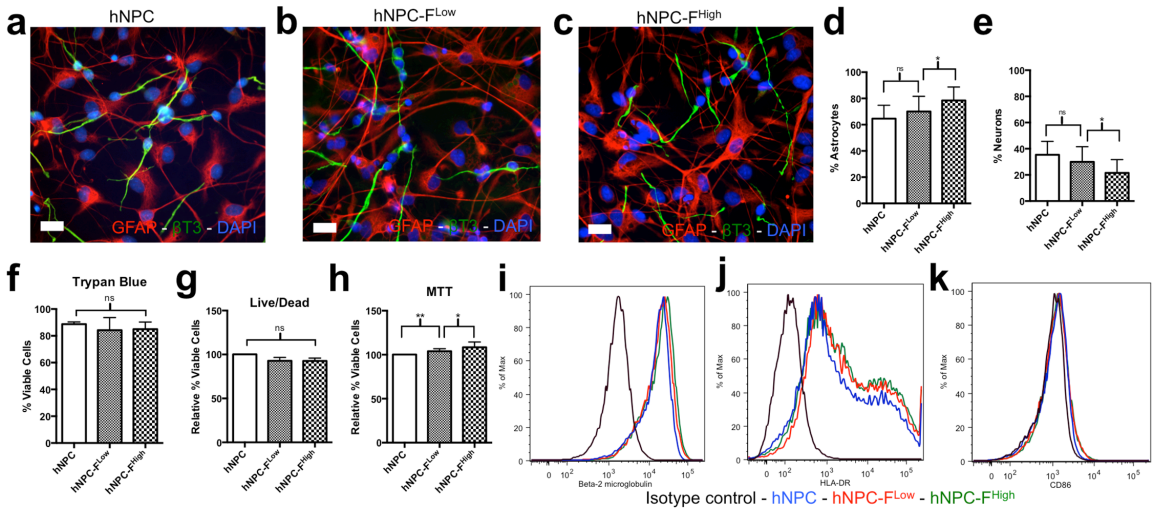

Figure 10. Cell dynamics following ferumoxytol labeling. Representative images of immunohistochemical staining of unlabeled hNPC (**A**), hNPC-F^{Low} (**B**), and hNPC-F^{High} (**C**) labeled cells expressing the astrocytic marker GFAP (red) and the neuronal marker βT3 (green). Five high power fields (40X) were analyzed for each of five coverslips from each condition. A significant decrease in neuronal differentiation was observed between hNPC-F^{Low} and hNPC-F^{High} conditions, but not between unlabeled hNPC and

hNPC-F^{Low} (**D**). A concurrent, significant increase in astrocytic differentiation was observed (**E**). Trypan Blue exclusion assay (**F**) and flow cytometry live/dead stain with AquaBlue (**G**) showed no change in cell viability across groups. MTT cellular metabolism assay showed a significant increase in cellular metabolism with ferumoxytol labeling (**H**). No change was observed in expression of cellular antigens Beta-2 microglobulin (**I**), HLA-DR (**J**), or co-stimulatory molecules CD80 (now shown) and CD86 (**K**). Scale bars: (**A – C**) 10 μm. Ordinary one-way ANOVA and individual unpaired t-tests were performed. *Significant, $P < 0.05$; **Significant, $P < 0.005$; ***Significant, $P < 0.0005$. hNPC, human neural progenitor cell; F, ferumoxytol; GFAP, glial fibrillary acidic protein; βT3, Beta Tubulin III; MTT, 3-(4,5-dimethylthiazol-2-yl)-2,5-diphenyltetrazolium bromide; HLA, Human Leukocyte Antigen; CD, Cluster of Differentiation. Graphs displayed as mean ± SD.

4.4 DISCUSSION

Sufficient uptake of ferumoxytol nanoparticles with cellular internalization was observed with ferumoxytol nanoparticle incubation for seven days immediately following mechanical passage of clinical grade human neural progenitor cells. A dose escalation study revealed two conditions ([200] and [400] μg/mL ferumoxytol incubation; hNPC-F^{Low} and hNPC-F^{High} cells, respectively) that produced adequate cellular MR contrast without significantly altering cell viability. The uptake of ferumoxytol particles from the extracellular environment is most likely achieved by active processes requiring endocytosis[76]. Following mechanical passage, the small clumps of cells remain stable with cell-to-cell contact, are metabolically active, replicating, and reforming neurospheres. In this time they are most likely actively sampling their environment, leading to increased uptake of ferumoxytol nanoparticles. Furthermore, it is possible that slight membrane damage increases permeability and the ability of ferumoxytol particles

to enter the cell. The small clumps of cells render this approach spatially advantageous. The long incubation time also renders this approach temporally advantageous to increased particle uptake. Previous studies have employed much shorter incubation times and lower concentrations of nanoparticles to achieve cellular labeling with SPION. However, the cell culture system used in this study proved unique in that the cells were both non-adherent and non-phagocytic. Adherent cell lines cultured in monolayer allow easy access of all cells in culture to the incubated nanoparticles, resulting in much shorter incubation times and nanoparticle concentrations[20,114,145,153]. Phagocytic cells also reduce the time and amount of particles required because they are more actively sampling their environment[13].

Dissociated cells in hibernate medium are dormant and those in maintenance medium are unstable, attempting to regain cell to cell contain by reforming neurospheres. Both situations are not conductive to active environmental sampling and particle uptake. Furthermore, incubation of pre-formed neurospheres proved insufficient. The failure of this approach was most likely due to heterogeneous labeling of cells where those on the surface had adequate uptake and those in the center had none. The ferumoxytol nanoparticles were unable to penetrate the large neurospheres.

Particle uptake and intracellular location in endosomes/lysosomes was confirmed with histochemistry and TEM. The localization of particles in organelles suggests an active endocytic mechanism of uptake. 53.3% of hNPC-F^{Low} and 77.2% of hNPC-F^{High} cells were labeled with ferumoxytol. While the percentage of labeled cells is lower, the amount of internalized ferumoxytol (1.46 and 2.82 ρg ferumoxytol, respectively) is similar to previously published reports[45,153]. The difference in percentage of labeled cells

could be explained by the different histochemical approach used in our study. The previous reports used a DAB enhanced Prussian blue stain with a higher sensitivity than standard Prussian blue staining used in our study[145].

Biosafety and unaltered cellular features are essential to the successful translation of diagnostic molecular imaging approaches. In this study, we employed multiple, independent measures of cellular dynamics to assess potential effects of ferumoxytol labeling. The differentiation of neural progenitor cells to terminal cell types (neurons and astrocytes) changed with ferumoxytol labeling. A decrease in neuronal differentiation was observed with a concurrent increase in astrocytic differentiation. However, the difference between the unlabeled hNPCs and hNPC-F^{Low} cells was not significant with this sample size. Furthermore, the primary objective of this cell line is to generate astrocytes for trophic support of motor neurons[41]. The change in differentiation should not have an effect on the overall therapy.

Cell viability calculated by flow cytometry live/dead staining and MTT assay for mitochondrial metabolism showed little change in viability. The increased metabolism of the labeled cells observed with the MTT assay has been previously described in the literature[145]. This change is most likely due to the increased metabolism resulting from the excess cellular Iron or from the ferumoxytol particles themselves altering the absorbance of light in the assay.

Analysis of cellular surface antigens revealed an interesting pattern of expression in the hNPCs. The cells possess both MHC I and MHC II antigens, which suggests the cells are capable of directly presenting antigens to the immune system. Expression of MHC antigens on human neural stem cells is previously described[96]. However, the cells

do not express co-stimulatory CD80 or CD86 molecules so they are unable to directly active T lymphocytes. Importantly, the expression of these surface antigens is not altered by the ferumoxytol labeling approach employed in this study.

4.5 CONCLUSIONS

The present study developed a straightforward, rapidly translatable incubation method to label clinical grade human neural progenitor cells with ferumoxytol nanoparticles for diagnostic cellular imaging. The method does not use transfection agents and employs an FDA approved clinical nanoparticle. Minimal adverse effects on the biological properties of the ferumoxytol labeled cells were observed.

CHAPTER 5

LONG-TERM MR TRACKING AND STEREOLOGICAL QUANTIFICATION OF FERUMOXYTOL LABELED HUMAN NEURAL PROGENITOR CELLS TRANSPLANTED INTO THE PORCINE SPINAL CORD* (SPECIFIC AIM 2)

5.1 ABSTRACT

Transplantation of stem cells into the spinal cord has been explored as treatment for a range of diseases. The post-transplantation fate of cellular therapeutics is poorly understood in both large animal models and in human studies because of limitations in cell graft detection. A minimally invasive technology for cellular graft tracking to visualize grafts *in vivo* is needed. However, it is important that the diagnostic marker does not impact engraftment of transplanted cells. We report on surgical transplantation of ferumoxytol labeled human neural progenitor cells into the spinal cord of a large animal with *in vivo* MRI graft tracking, quantification of cell engraftment post-mortem, and preliminary MR-guided delivery.

Human neural progenitor cells were labeled with multiple concentrations of ferumoxytol ([0], [200], and [400 μg/mL]). For each of the three labeling conditions, four 250,000 cell grafts (n=12 grafts/pig) were transplanted into the ventral horn of the thoracolumbar spinal cord of minipigs via direct intraspinal microinjection using a spine-

mounted platform following laminectomy. No post-operative deficits were observed and the pigs were maintained for 28 (n=3 pigs), 42 (n=3), and 105 days (n=5) after surgery. All [200] and [400] transplanted cell grafts (n=88) were visualized *in vivo* with 3T full-body MRI using a T2*-weighted gradient echo sequence 14 days after transplantation. 63.6% of grafts were 'on target' in the ventral horn. The grafts were tracked longitudinally with serial MRI and signal intensity quantified with a minimum threshold method. The mean volume after transplantation was 2.3 and 13.9 μL for [200] and [400] grafts. Furthermore, 75% of [200] and 100% of [400] grafts were identified at post-operative day 105 with a mean volume of 1.1 and 9.6 μL.

The pigs were sacrificed and the spinal cords harvested. The cords were sectioned at 50 μm intervals and every 6th section immunostained for the human nucleus (HuNu). The engraftment of individual cell grafts was quantified using stereology for the 42-day cohort. The engraftment was calculated for [0] (mean 24.0% cell engraftment, range of 0.0-65.7%), [200] (17.1, 1.0-35.9), and [400] (25.0, 0.0-45.6) and no statistically significant difference was observed. Degradation of MR signal between 14 and 28 days for [200] and [400] grafts correlated with graft survival ($r=0.47$, $p=0.02$) in the 42-day cohort. Stereology is ongoing for the other cohorts. Prussian Blue-HuNu co-staining and transmission electron microscopy of tissue sections confirmed the presence of intracellular iron deposits.

Ferumoxytol labeling allows for immediate and long-term identification of cell grafts *in vivo* with MRI without impacting cell engraftment in a large animal xenograft

model. The ferumoxytol nanoparticles were observed in the cytoplasm of transplanted, labeled cells. This approach has the potential to be used in ongoing and upcoming clinical trials to monitor cell-based therapies. Furthermore, ferumoxytol labeling allows for immediate visualization of stem cells transplanted into the spinal cord percutaneously under MR-guidance.

***Lamanna JJ,** Gutierrez J, Urquia L, Federici T, Oshinski J, Boulis N. Long-term MR tracking and stereological quantification of ferumoxytol labeled human neural progenitor cells transplanted into the porcine spinal cord. *World Molecular Imaging Congress 2014* (Honolulu, September 2015).

5.2 INTRODUCTION

Transplantation of stem cells into the spinal cord has been explored is a promising therapeutic strategy to overcome the regenerative limitations of the central nervous system (CNS). The aim of stem cell therapy is both neuroregeneration and neuroprotection to counteract degeneration caused by CNS pathologies such as amyotrophic lateral sclerosis (ALS), spinal cord injury (SCI), and multiple sclerosis (MS) [17,63,82,98]. Clinical trials for ALS, SCI, and MS are ongoing and emerging evidence indicates that this approach is safe, feasible, and may have therapeutic effects [33,52,60,97,109]. To properly assess the therapeutic efficacy of these early-stage therapies, it is essential to confirm the accuracy of the transplantation site, the delivered dose, and the survival of the cellular therapeutic *in vivo*. Therefore, it is critical to develop diagnostic, non-invasive imaging technologies that may track the cell graft over time *in vivo* and identify the graft post-mortem in histological sections. However, it is essential that the diagnostic marker does not impact the survival or biological properties of transplanted cells.

Previous groups have employed super paramagnetic iron oxide nanoparticles (SPION) as a diagnostic marker for tracking transplanted cellular therapeutics using Magnetic Resonance Imaging (MRI)[8,19]. Studies have shown that SPION labeling of human neural stem cells has limited effect on its biological properties[8,19,26,51,140]. Most of these studies have employed nanoparticles that are not currently approved by the Food and Drug Administration or manufactured in the United States[19]. Furthermore, most of these *in vivo* studies were conducted in the CNS of a small animal model, limiting its ability to predict clinical utility[9,39,46,107].

The only SPION currently FDA approved and manufactured is ferumoxytol. Ferumoxytol is an ultra-small nanoparticle with an iron oxide core and a carboxydextran coat with a diameter of approximately 15 nanometers. While several studies have investigated the use of ferumoxytol as a cell label, no studies have been published in the CNS of a large animal model. Furthermore, limited quantitative studies assessing transplanted cell graft survival have been published.

We propose to transplant ferumoxytol labeled human neural progenitor cells (hNPCs) into the spinal cord of a large animal (porcine) model and track them *in vivo* with clinical MRI. The use of large animals is considered critical for validating the combination of the surgical procedure, device, feasibility of tracking *in vivo*, and safety of the final product for human use. The size, anatomy, and general vulnerability of the porcine spine and spinal cord better models the human. The surgical process of exposing and manipulating the spinal cord as well as closing the wound in the pig is virtually indistinguishable from the human. Consequently, the pig is subject to the same fundamental complications including spinal cord injury, epidural hematoma, abscess, and CSF leakage. The devices that we have designed for human surgery fit the porcine spine, meeting the FDA requirement that the safety of the device, technique, and cells to be tested as a unit.

The MR tracking, conducted in a clinical 3T scanner, will allow us to assess our ability to track stem cell grafts *in vivo* in a model that is directly translatable to clinical trials. At the conclusion of this study, we will compare the MRI signal *in vivo* with *post-mortem* histological measures of labeled cells. Furthermore, we will directly compare survival of ferumoxytol-labeled and unlabeled cell grafts with graft-specific stereological

quantification. The objectives of this study are to: 1) identify the location of transplanted cell grafts *in* vivo with MRI; 2) quantify ferumoxytol-labeled cell graft survival; and 3) correlate MR findings, histological measures of Iron deposits and graft survival.

5.3 METHODS

5.3.1 Experimental Design

Female Göttingen minipigs were divided into 5 groups according to their survival time and transplantation strategy (**Table 4**). The pigs received multiple, independent grafts of ferumoxytol labeled hNPC-F^{Low} and hNPC-F^{High} cells, and unlabeled hNPCs (**Figure 11**). Cell grafts were transplanted into the pig thoracolumbar spinal cord bilaterally. The volume of each injection was 10 or 25 microliters with a concentration of 10,000 cells/μL. Grafts containing two concentrations of iron (hNPC-F^{Low} and hNPC-F^{High}) from the *in vitro* experiments were compared to control unlabeled hNPCs in the same animal. Inter-graft distances of 4 mm were used. Each animal received a total of 12 to 15 injections based on their cohort. The hNPC-F^{High} grafts were transplanted into the rostral spinal cord segment, the hNPC grafts into the middle segment, and the hNPC-F^{Low} grafts into the caudal segment. The injections aimed to transplant the cell grafts into the motor-neuron containing ventral horn of the spinal cord. Injected segments were identified by rostral and caudal 5-0 blue prolene dural stitches to facilitate histological graft identification. Immunosuppression consisted of a monotherapy with Tacrolimus (0.025mg/kg, BID, IV). Animals were switched to Cyclosporine (10mg/kg, BID, oral) for immunosuppression after 28 days.

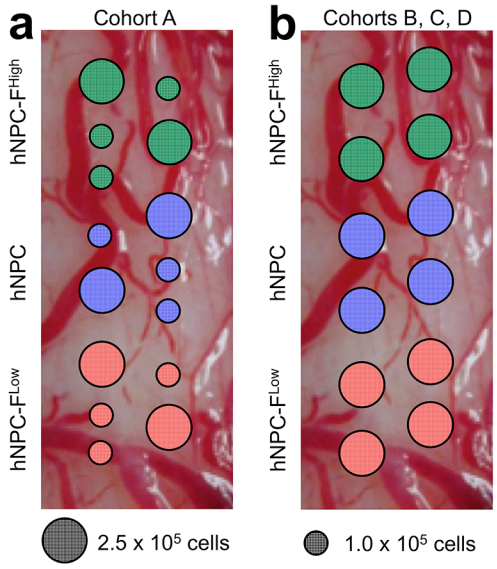

Figure 11. Spinal Cord Transplantation Schematic. A representative schematic of the spinal cord stem cell transplantation strategy is shown. Individual injections of unlabeled hNPC, and ferumoxytol-labeled hNPC-F^{Low} and hNPC-F^{High} cell grafts were bilaterally transplanted into the porcine spinal cord with a stabilized stereotactic injection system. Cohort A (n = 3) received 15 total injections of 2.5 x 10^5 and 1.0 x 10^5 cells. Cohorts B (n = 3), C (n = 3), and D (n = 5) received 12 injections of 2.5 x 10^5 cells. hNPC-F^{High} cell grafts were transplanted into the rostral spinal cord segment, unlabeled hNPC grafts into the center segment, and hNPC-F^{Low} grafts were transplanted into the caudal segment.

Table 6. Pig Cohorts. 14 female Göttingen minipigs were enrolled in the study and divided into 4 cohorts. The pigs received pre-operative MRI and serial MRI after surgical transplantation of hNPCs into the spinal cord.

Cohorts	N of animals	MRI (Post-Operative Day)	Survival (Days)
A	3	0, 14	14
B	3	0, 14, 28	28
C	3	0, 14, 28, 42	42
D	5	0, 14, 42, 63, 84, 105	105

5.3.2 Intrajugular Catheter Placement

Before the spinal incision, the neck of the pig was prepped and draped. The internal jugular was exposed surgically and cannulated with a central catheter, which was secured with a 3-0 silk tie. The proximal end of the internal jugular was ligated with a 3-0 silk tie. The catheter was then tunneled out of the neck skin dorsally and secured with 3-0 nylon stitches. The wound was irrigated and closed with a running 3-0 nylon stitch. The catheter was used to administer all IV medication for the duration of the experiments.

5.3.3 Thoracolumbar Transplantation

Pigs were placed in the prone position, with appropriate draping of the operative area. An approximately 10-15 cm incision was performed over the spine and a multi-level laminectomy was performed over the thoracolumbar spinal cord. Following laminectomy, the percutaneous posts were placed through 1 cm skin incisions above and below the primary incision. The upper and lower posts were mounted to lamina above and below the primary incision through small percutaneous incisions. The microinjection platform was attached to the four posts, allowing the device to span the laminectomy. At this point, a 2-4 cm incision was made into the dura mater, allowing exposure of the spinal cord. The dura mater was then tacked away using 4.0 nurulon suture. At this point, the microinjection device was placed and adjusted. Targeting to the area of interest within the spinal cord was achieved with the use of coordinate-based microinjection and visual observation. The injections followed placement of the cannula. Immediately prior to this, a bolus of Methylprednisolone (125mg, Intravenous) was given in an attempt to

prevent spinal cord swelling. A custom infusion cannula of narrow diameter was used. For each injection, the appropriate volume of cell suspension was infused by a microprocessor-controlled syringe pump at the rate of 5 microliters per minute. The needle was left in place for an additional 1 minute to prevent cell reflux up the cannula injection tract before extraction. Following needle removal, the stereotaxic apparatus was relocated to the next target site, separated by 4 mm as necessary to avoid visible blood vessels on the dorsal surface of the spinal cord. This process was repeated as proposed for each cohort. Once all injections were made, the injection apparatus was removed and the incisions were closed in four layers. The dura was closed using a 4.0 nurulon stitch, in a watertight fashion. A 0 vicryl suture was used for the deep muscular layer. The second layer, fascia, was also closed using 0 vicryl suture in a watertight fashion. The dermal layer was closed with 2.0 ethylon, with a running stitch.

5.3.4 Post-Operative Assessment

Animals underwent a general neurological examination/observation before surgery and following complete recovery from the procedure. Behavioral assessment of spinal cord function was performed daily during the 14 first post-operative days and then 2 times per week until euthanasia. Sensory evaluation took place in the form of a tactile stimulus to the perianal region. Also, all four limbs were assessed. This stimulus is not noxious or painful but allows assessment of both sensation and motor function in response to limb retraction from a steadily applied force (withdrawal response to a mechanical stimulus). Gait and motor function was assessed according to the Tarlov scale. This scale provides objective criteria by which to evaluate ability to ambulate as a

surrogate measure of motor function. The score is as follows: (0) no voluntary limb function; (1) only perceptible joint movement; (2) active movement but unable to stand; (3) to be able to stand but unable to walk; (4) complete normal hind-limb motor function.

5.3.5 In Vivo Magnetic Resonance Imaging

Pig MRI was performed on a Siemens Trio Trim 3T Full Body MR Scanner with a table-integrated spine matrix coil. Pigs were sedated with ketamine (35 mgs/kg, IM) and acepromazine (0.8 mgs/kg, IM), and maintained with isofluorane inhalation (1 – 2%). Pigs were placed in the scanner in the head first supine position. MRI was acquired as outlined in the experimental design. Structural MR images were obtained using standard Sagittal T2-weighted spin echo and Coronal T1-weighted 3D sequences. For grafted cell detection, a gradient echo (GRE) T2*-weighted axial sequence sensitive to magnetic field inhomogeneities was utilized [multiple echo time = 10 and 16 msec, pulse repetition time = 788 msec, average = 4, field of view = 160 x 160 mm, matrix = 512 x 512, and slice thickness = 1.5mm)]. The GRE sequence was acquired a second time with a shift of 0.75 mm to avoid partial volume effects.

5.3.6 Image Analysis

MR Images of the spinal cord containing cell grafts were analyzed with ImageJ. Anatomical position of each graft was determined by observing the distance anterior/posterior and left/right from the center of the spinal cord. Anatomical landmarks such as the grey/white junction and location of CSF were also used. Three blinded expert

observers viewed 20 grafts and scored them as on or off target. On target was defined as 50% of the graft contacting the ventral horn. This data was used to determine on/off target transplantation using a Chi squared table to generate sensitivity and specificity for both hNPC-F^{Low} and hNPC-F^{High} grafts. The volume of the individual grafts was calculated using the ImageJ, adapting a previously described method for quantifying SPION signal in the rodent brain[9]. Briefly, regions of interest in GRE MR images were set over half the spinal cord of individual hNPC-F^{Low} and hNPC-F^{High} grafts, encompassing the entire graft. Regions of interest over the entire cord were set in areas containing control hNPCs. For these control regions, a value for the average voxel intensity minus two standard deviations was calculated. This value was used as a threshold for the regions containing labeled cells. The number of voxels below the threshold was calculated for each graft and was recorded in volume (μL). Groups were compared with ANOVA ($p < 0.05$ significance) with multiple comparisons (t tests, $p < 0.05$).

5.3.7 Euthanasia, Perfusion, and Necropsy

At endpoints, animals were sedated with ketamine (35 mgs/kg, IM), acepromazine (0.8 mgs/kg, IM) and Euthasol (1 ml/10 lbs, IV). Following sedation, 10,000 USP Units/ml of Heparin Sodium were administered IV five minutes before euthanasia, while the heart was still beating. Transcardiac perfusion with a 0.9% NaCl solution followed by a 4% Paraformaldehyde (PFA) solution was then performed to improve the quality of the tissue for immunohistochemistry. A peristaltic pump (Masterflex Console Drive pump (model 71-1420) was used for perfusions. Spinal cords

with dura mater intact were harvested by dissection in necropsy. The cords were placed in 4% PFA for 24 hours and then 30% sucrose solution for one week. The dura mater was removed and the region of interested containing cell grafts (marked with prolene sutures) was isolated and flash frozen in blocks. Tissue was then frozen in optimal cutting temperature gel and cryosectioned transaxially in 50 micrometer sections. The tissue was placed in cryopreservative for histological analysis.

5.3.8 Histological Staining for Transplanted Human Cells

An antibody specific to the human nuclear (HuNu) antigen (1:250; Millipore MAB1281) was used to determine the location of transplanted cell grafts. DAB-enhanced HuNu immunohistochemistry was performed on every 6^{th} section of tissue throughout the ROI. Briefly, Sections were washed in 1X phosphate buffered saline (PBS) for 3 x 10 minutes while shaking at room temperature (RT) to remove cryoprotectant and thaw. Next, sections were treated with hydrogen peroxide (3% H_2O_2 in 1X PBS + 0.1% triton [PBST]) for 15 minutes while shaking at RT. This was performed to block endogenous peroxidase activity, reducing non-specific background staining in horseradish peroxidase-conjugated antibody steps below. After treatment, sections were washed with 1X PBST for 3 x 10 minutes while shaking at RT. Sections were then incubated in blocking buffer (5% horse serum in PBST) for 30 minutes while shaking at RT. Horse serum was chosen to prevent nonspecific epitope binding of the secondary antibody. Once blocked, sections were transferred to anti-human nuclei (HuNu) primary antibody reagent (dilution in 2% NGS in 1X PBS) and stored overnight on shaker at 4 ^{o}C.

Tissue sections were washed in 1X PBS for 3 x 10 minutes while shaking at RT. Biotinylated horse α mouse antibody was prepared at 1:250 (2% NGS in 1X PBS). Sections were incubated in this secondary antibody for 2 hours while shaking at RT. 3 x 10 minute 1X PBST washes were then performed. Tertiary antibody (ABC kit from Vector Labs: [50uL A, 50uL B]/10mL PBST) was prepared 30 minutes prior to use and stored while shaking at RT. Following 3 x 1X PBST washes, tissue sections were transferred to the tertiary antibody and stored overnight on shaker at 4 ^{o}C.

Tissue sections were then washed in 1X PBS for 3 x 10 minutes while shaking at RT. DAB peroxidase substrate was prepared immediately before use, and sections were incubated until a dark signal was seen. The maximum recommended DAB incubation time is 10 minutes. Tissue sections were then transferred to 1X PBS and washed thoroughly for 5 minutes. If Prussian blue costain was desired, sections were kept floating and the PB protocol described below was followed. For anti-HuNu staining only, sections were transferred to distilled water, mounted onto slides, and allowed to dry overnight. Once dry, a cresyl violet background stain was performed, followed by dehydration and coverslip.

5.3.9 Stereological Quantification of Engrafted Human Cells

Stereology constitutes an interdisciplinary field that is largely concerned with the three-dimensional interpretation of planar sections of materials or tissues. It uses techniques for extracting quantitative information about a three-dimensional material from measurements made on two-dimensional planar sections of the material. A random, systematic sampling approach is used to provide potentially unbiased and quantitative

data and is an important and efficient tool in many applications of microscopy. It may thus provide estimates of cell numbers, object size and shape with precision [43,138].

Briefly, the transplanted area of each individual graft in the spinal cord of every pig was sampled using unbiased random uniform sampling. All sections with grafted HuNu+ cells were considered for the sample, sections without grafted cells were discarded. One out of every six sections was included in the sample for analysis with a total distance between sections of 300 μm. A combination of the Cavalieri principle and the optical disector was applied to the neuron and grafted cell counting. The equipment used for the optical disector included a microscope (Leica DM2500) with a motorized x–y stage, an electronic microcator (Applied Scientific Instrumentation), which was used for measuring movements in the z direction, and the PC software Stereologer™ for cell counting. The optical disector frame provided inclusion and exclusion lines to prevent edge effects arising from sub-sampling. All grafted cells that came into focus within the disector height (15 μm) were counted, provided they did not touch any of the exclusion lines and fell in the inclusion lines. The sections were counted with a 60X oil-immersion objective (final magnification, 2000X). Groups were compared with ANOVA ($p < 0.05$ significance) with multiple comparisons (t tests, $p < 0.05$).

5.3.10 Histological Staining for Iron

Perl's Prussian Blue (PB) histochemistry was performed at the center and on the periphery (600 μm from graft center both rostral and caudal) of all grafts identified with HuNu to estimate the amount of iron from ferumoxytol located in each graft. Briefly, the

sections were washed with PBS, incubated with hydrogen peroxide (1%) for 15 minutes, washed 3x with distilled water, incubated with Perl's Prussian Blue reagent (6% HCl + 2% KFe_6CN) for 30 minutes, washed 3x with distilled water, and mounted on glass slides. Eosin background staining was performed and the slides were cover slipped.

5.3.11 Quantification of Histological Iron

Perl's Prussian Blue stained grafts were visualized with a Nikon E400 light microscope. Images of the grafts at 4x were acquired under the same exposure conditions. The Perl's signal was quantified using a threshold technique in ImageJ. An open filter was applied to the entire green and blue channels. A closed filter was applied to peak of the red signal. This approach negated all signal except that from the characteristic blue precipitates. The total volume of Iron was calculated in microliters per graft. Groups were compared with ANOVA ($p < 0.05$ significance) with multiple comparisons (t tests, $p < 0.05$).

5.3.12 Histological Staining for Human Cell Differentiation

To assess the differentiation capacity of transplanted, labeled hNPCs, select sections containing well-integrated grafts from group D (105 cohort) were stained for the presence of human Glial Fibrillary Acidic Protein (GFAP). Briefly, the sections were washed with PBS, incubated in blocking buffer (PBST, 5% goat serum, 5% horse serum), and placed directly in a primary mouse antibody anti-human GFAP [1:500, Takara Bio STEM123] overnight at 4 °C. The sections were washed and placed in a secondary

antibody goat-anti-mouse 488 (1:1000, A11001, Invitrogen) for one hour at room temperature. The coverslips were washed with PBS and mounted in vectashild with DAPI. The slips were visualized with a Nikon E400 Fluorescent microscope. Images of High Power Fields (HPF) at 40x and 100X were acquired. The presence of human GFAP+ cells was qualitatively assessed.

5.3.13 Histological Co-Staining for Human Nuclei and Iron

Co-staining for human nuclei and iron was performed on select grafts (largest engraftment) from each time point. 5 grafts per labeling condition per time point were stained in the graft center and periphery. The immunohistochemical method starts with the same method as standard human nuclei staining, but following incubation with DAB peroxidase and 1X PBS wash, tissue sections were transferred to distilled water. 3 x 5 minute distilled water washes were performed on a shaker at RT. The PB reagent (6% HCl, 2% KFe_6CN at 1:1 dilution) was made under a fume hood immediately prior to use. Sections were transferred to the reagent and incubated at 52^{o}C for 20-45 minutes. Next, sections were washed for 3 x 5 minutes in distilled water while shaking. Tissue was mounted on slides and allowed to dry overnight. Once dry, an eosin background stain was performed, followed by dehydration and coverslip.

5.3.14 Immunoperoxidase labeling and tissue preparation for Transmission Electron Microscopy

A section of graft-containing tissue was embedded in wax, sectioned at 50 nanometers, stained for HuNu, and mounted for analysis with TEM. Immunoperoxidase

labeling was carried out before sample embedding. Pig spinal cord containing transplanted human neural stem cells was fixed with 4% paraformaldehyde in 0.1 M phosphate buffer and then stored in cryoprotectant for a period of time before frozen sectioning at 50 micrometers. Frozen sections were then thawed and washed thoroughly with 0.1 M PB to get rid of cryoprotectant. For immunoperoxidase labeling, sections were first incubated in blocking solution for 30 min at 4°C to minimize non-specific labeling. The blocking solution was phosphate buffered saline (PBS) containing 5% normal goat serum (NGS), 5% bovine serum albumin (BSA), and 0.1% cold water fish gelatin. Sections were then incubated in the primary antibody against the human nuclear antigen (Millipore MAB1281) diluted with PBS containing 0.1% acetylated BSA (BSA-c) to 5 μg/ml overnight at 4 degree with gentle agitation. After 6 washes (5 min each) with PBS/BSA-c, sections were incubated overnight at 4 degree in biotinylated secondary antibody (Vector) at 1:200 dilution. Following 3 washes with PBS/BSA-c and 3 washes with PBS, sections were incubated in avidin-biotin complex from ABC kit (Vector) for 3 hours and washed again for 6 times with PBS. Finally, the enzyme reaction was carried. Sections were placed in 0.05 M Tris buffer (pH 7.3) containing 0.05% diaminobenzidine and 0.003% hydrogen peroxide for 5-10 minutes at room temperature. Sections were then washed, fixed with 2.5% glutaraldehyde in 0.1 M PB and embedded in Eponate 12 resin. Ultrathin sections were cut at 70 nanometer thick using a Leica UltraCut S ultramicrotome, counterstained with 5% uranyl acetate and 2% lead citrate, and examined on an JEOL JEM-1400 transmission electron microscope (Tokyo, Japan) equipped with a Gatan 2k x 2k US1000 CCD camera (Pleasanton, CA).

5.3.15 Data Analysis

Individual cell graft-specific information of quantified surviving human cells, histological Iron, and MRI volume was compared between individual grafts of the same ferumoxytol labeling condition and between conditions. The primary objectives were to correlate the MRI signal with histological iron, cell survival with histological iron, and cell survival with MRI. Linear regression and correlation analysis were done with a one-sided p value ($p < 0.05$).

5.4 RESULTS

5.4.1 Post-Operative Assessment

Following transplantation, expected post-operative transient morbidity was observed (**Figure 12**). Transient deficits were observed in the neurological exam, limb retraction to applied force, and the Tarlov score. The animals experienced pain, lethargy, and reduced diet immediately following surgery. However, all animals returned to neurologic baseline 7 days after surgery.

Two animals from group D experienced adverse events related to immunosuppression. The jugular catheter on pig #4 became unusable after post-operative day (POD) 3 and the animal was switched to oral cyclosporine for the remainder of the study. Pig #3 experienced an adverse reaction to the anesthesia or immunosuppression and developed a coagulopathy that required blood transfusion from a donor pig on POD 16. The pig was switched to oral cyclosporine on POD 3 and all immunosuppression was discontinued on POD 15. The pig fully recovered with blood transfusion and continued for the duration of the study.

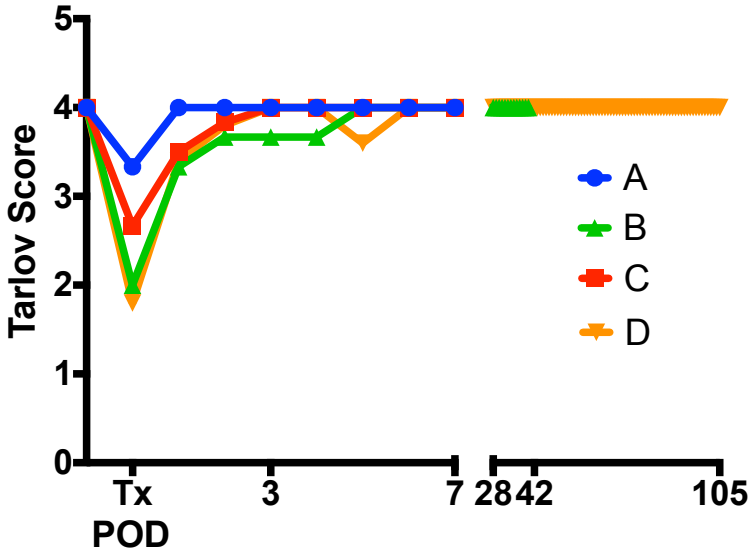

Figure 12. Motor Function Assessed with the Tarlov Scale. The Tarlov scale was used to assess gait and motor function in cohorts A – D that underwent transplantation. The score is as follows: (0) no voluntary limb function; (1) only perceptible joint movement; (2) active movement but unable to stand; (3) to be able to stand but unable to walk; (4) complete normal hind-limb motor function. Transient morbidity was observed in all groups, but all animals returned to baseline after seven days. Post-Operative Day (POD).

5.4.2 Pilot Study and Preliminary Graft Identification of Ferumoxytol-Labeled Human Neural Progenitor Cell Grafts in the Porcine Spinal Cord

To inform long-term pig studies (groups B, C, and D), a short-term pilot study with 3 pigs (group A) was conducted using multiple graft sizes per labeling condition. 15 cell grafts were transplanted into the thoracolumbar spine of the pigs. Two 25 µL and three 10 µL grafts were transplanted per condition (unlabeled hNPC, hNPC-F^{Low}, and hNPC-F^{High}). Unlabeled hNPC graft survival was confirmed (100% of grafts identified)

with human nuclear antigen staining (HuNu), but the grafts were not visualized with MRI or identified with PB staining (**Figure 13 A – F**). HNPC-F^{Low} cells grafts were identified with HuNu (100% 25 μL, 100% 10 μL) and PB staining. 100% of hNPC-F^{Low} 25 μL, but only 67% of 10 μL were identified with MRI (**Figure 13 G – L**). HNPC-F^{High} cell grafts were identified with HuNu, PB, and MRI (100% 25 μL, 100% 10 μL) (**Figure 13 M – R**). Transplanted cell grafts of 25 μL were used for the remainder of the study based on MR visualization and the completion of a dose escalation study by our group[44].

5.4.3 *In Vivo* Visualization and Quantification of Ferumoxytol-labeled Neural Progenitor Cell Grafts in the Porcine Spinal Cord with MRI

Each pig received four 25 μL unlabeled hNPC, hNPC-F^{Low}, and hNPC-F^{High} cell grafts into the spinal cord with direct injection (**Figure 14 C**). The pigs were maintained 4 (n =3), 6 (n =3), and 15 (n = 5) weeks after transplantation with serial MRI every 2-3 weeks. Axial GRE T2* images acquired through the transplanted cell graft sites were converted to coronal sections using 3D Slicer (**Figure 14**). Pre-operative imaging in all animals showed normal spinal cord anatomy with no hypointense regions observed in the spinal cord. Two weeks after transplantation, all hNPC-F^{Low}, and hNPC-F^{High} cell grafts were visualized as hypointense foci with T2*-weighted MRI. Hypointense foci were not observed in the area containing unlabeled cell grafts.

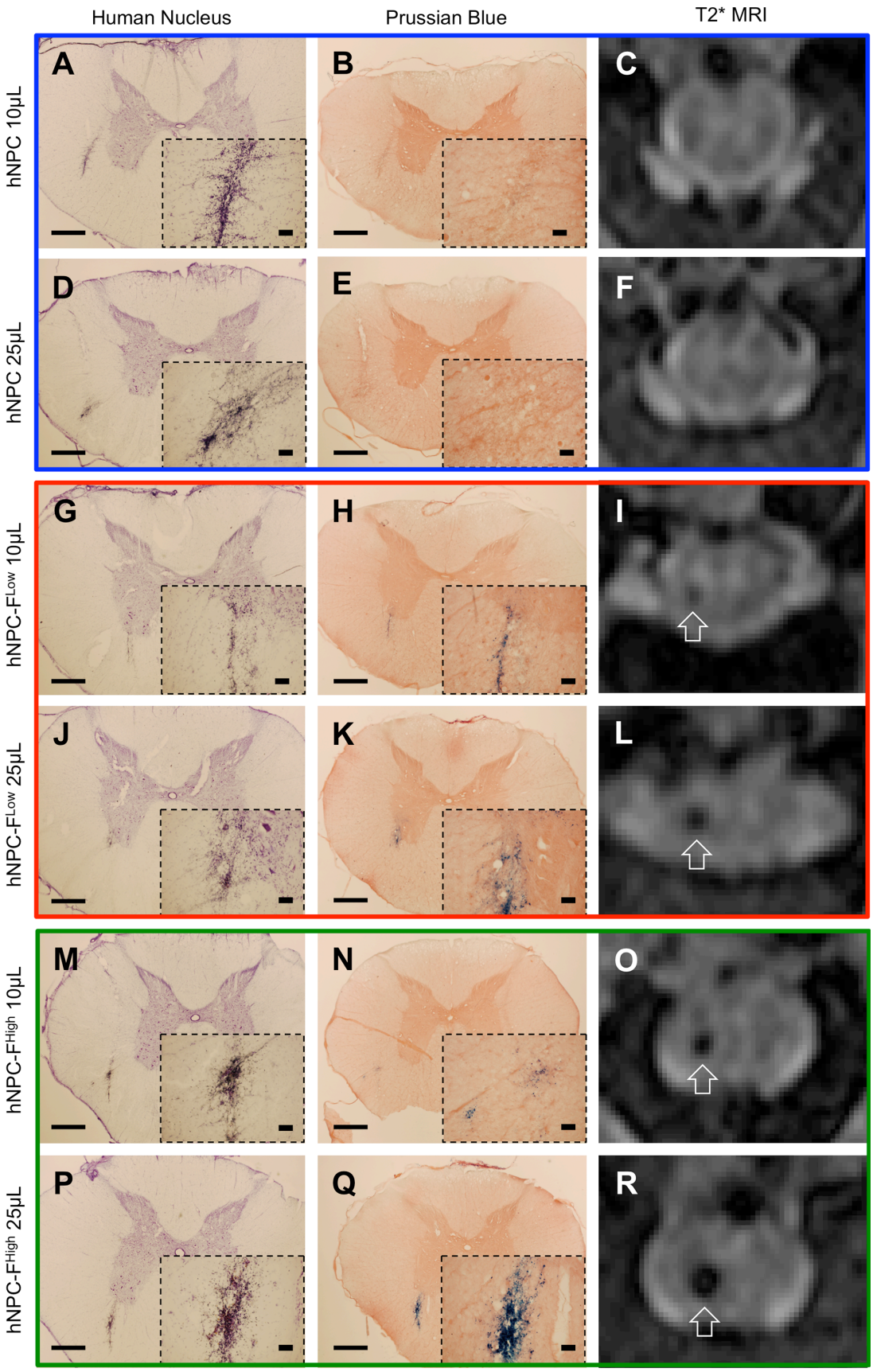
Human Nucleus
Prussian Blue
T2* MRI
hNPC 10µL
hNPC 25µL
hNPC-F^Low 10µL
hNPC-F^Low 25µL
hNPC-F^High 10µL
hNPC-F^High 25µL
A
B
C
D
E
F
G
H
I
J
K
L
M
N
O
P
Q
R

Figure 13. Preliminary Identification of Ferumoxytol Labeled Cell Grafts in the Porcine Spinal Cord. Representative micrographs and MR images from cohort A (14 day survival) are shown. **[A – F]** Unlabeled hNPC cell grafts of 1.0 x 10^5 and 2.5 x 10^5 cells were not observed with T2*-weighted MRI **(C, F)** or detected histologically with Perl's Prussian Blue (PB) iron staining **(B, E)**. The grafts were detected in the spinal cord with DAB-enhanced human nuclear antigen staining (black nuclei) **(A, D).** **[G - L]** Ferumoxytol labeled hNPC-F^{Low} cell grafts of both 1.0 x 10^5 and 2.5 x 10^5 were identified as multiple black nuclei with human nucleus staining (**G, J**), as characteristic blue precipitates with PB (**H, K**), and as a hypointense focus (white arrow) with MRI (**I, L**). **[M – R]** Ferumoxytol labeled hNPC-F^{High} cell grafts of both 1.0 x 10^5 and 2.5 x 10^5 were identified with HuNu (**M, P**), PB (**N, Q**), and MRI (**O, R**). Scale bars: main panels, 2 mm; insets, 100 µm.

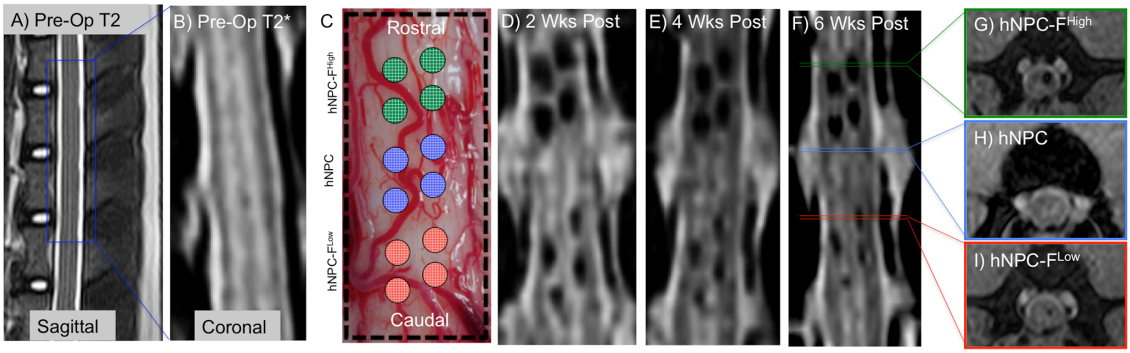

Figure 14: *In vivo* identification and tracking of ferumoxytol-labeled grafts (Cohort C). Pre-operative sagittal T2-weighted **(A)** and coronal T2*-weighted **(B)** images demonstrate normal spinal cord anatomy and the target site for transplantation. Unlabeled hNPCs and ferumoxytol-labeled hNPC-F^{Low} and hNPC-F^{High} 2.5 x 10^5 (25 µL) cell grafts were transplanted in to the pig spinal cord bilaterally **(C)**. Hypointense foci, representative of hNPC-F^{Low} and hNPC-F^{High} labeled cell grafts were observed on post-operative week 2 **(D)**, 4, **(E)**, and 6 **(F)** in coronal T2*-weighted images. Unlabeled cell grafts were not visualized. Axial T2* images show individual hypointense foci representing ferumoxytol-labeled hNPC-F^{High} **(G)** and hNPC-F^{Low} **(I)**, but not unlabeled [0] **(H)** grafts.

Ferumoxytol-labeled cell grafts were quantified using a region of interest and minimum threshold in ImageJ (**Figure 15 A – N**). The average volume of hNPC-F^{Low} and hNPC-F^{High} cell graft two weeks after transplantation was 5.3 ± 2.4 µL and 19.6 ± 5.7 µL, respectively. A significant decrease in graft volume was observed for both hNPC-F^{Low} and hNPC-F^{High} cell grafts over time (ANOVA, $p < 0.0005$) (**Figure 15 O – Q**). A significant decrease in signal was observed between two and four weeks for the hNPC-F^{Low} cell grafts and decreases at later time point was non-significant. For the hNPC-F^{High} cell grafts, significant signal decreases were observed between two, four, six, and nice weeks after transplantation.

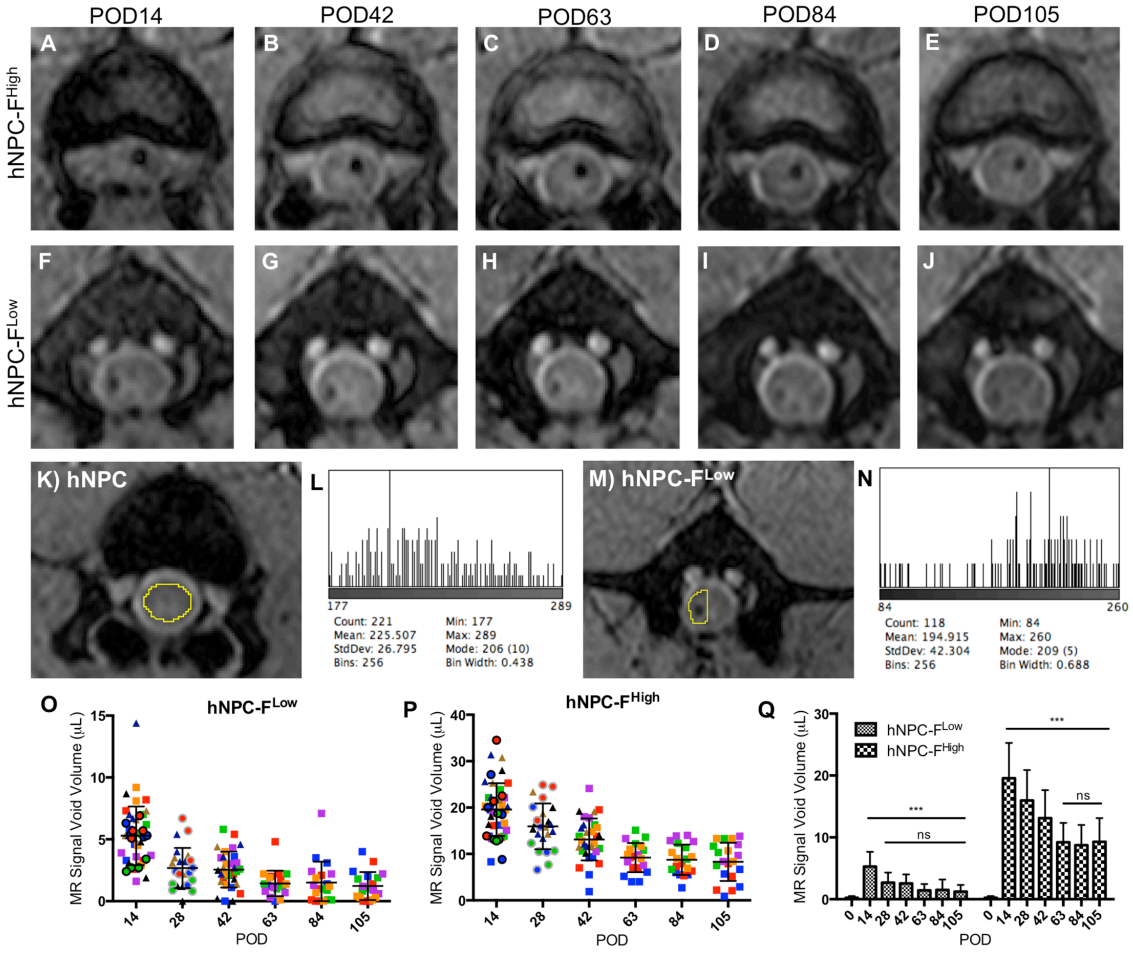

Figure 15: *In vivo* tracking and quantification of ferumoxytol-labeled grafts. A representative hNPC-F^{High} (**A – E**) and hNPC-F^{Low} (**F – J**) cell graft tracked with T2*-weighted gradient echo MRI from post-operative day (POD) 14 to 105 are shown. A region of interest was created over the unlabeled grafts (**K**) and a histogram of the voxel intensities was calculated using ImageJ (**L**). The minimum threshold for the labeled grafts was the mean voxel intensity of the unlabeled grafts minus two standard deviations to account for the decrease in signal associated with the negative contrast agent ferumoxytol. A representative hNPC-F^{Low} graft is shown (**M**) with its histogram (**N**). The graft volumes were calculated for all hNPC-F^{Low} (**O**) and hNPC-F^{High} (**P**) grafts at all time points. Data points are of individual cell grafts and are colored by animal and shaped by cohort (cohort B, triangle; C, circle; D, square). Summary data represented as the mean signal intensity at each time point is shown (**Q**). Ordinary one-way ANOVA and individual unpaired t-tests were performed. *Significant, $P < 0.05$; **Significant, $P < 0.005$; ***Significant, $P < 0.0005$. hNPC, human neural progenitor cell; F, ferumoxytol; POD, Post-Operative Day. Graphs displayed as mean ± SD.

5.4.4 Diagnostic Magnetic Resonance Imaging of Ferumoxytol-Labeled Cell Grafts for Predicting On/Off Target Transplantation Site

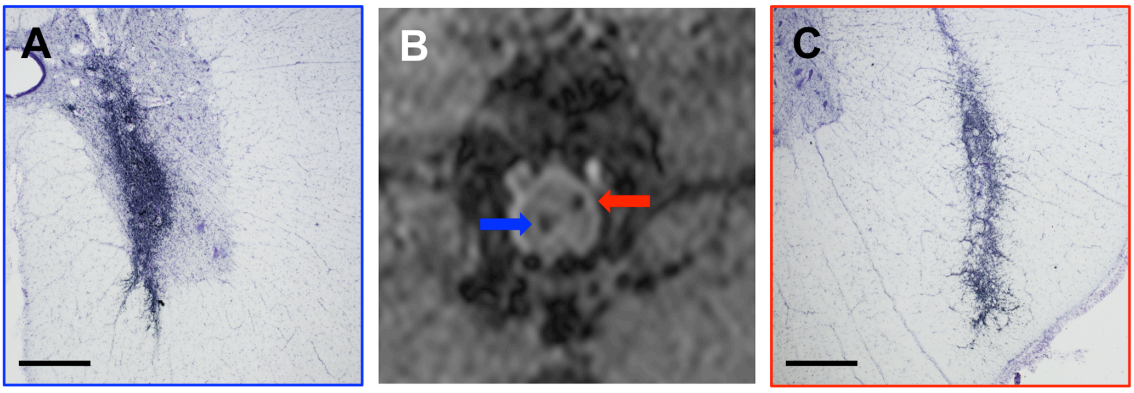

Figure 16. Representative Micrographs of On and Off Target Cell Grafts. A representative "on target" (**A**) and "off target" (**C**) micrograph of a hNPC-F^{High} cell graft stained for the human nuclear antigen (black nuclei). On target was defined as greater than 50% of the cell graft contacting the motor neuron-containing ventral horn. T2*-

weighted MRI showed both an on target (blue arrow) and an off target (red arrow) graft in the spinal cord (**B**). Scale bars: 1 mm.

Table 7: Contingency table for hNPC-F^{Low} cell grafts. Sensitivity 86.7%, Specificity 93.3%. Data shown from identification of images from three blinded expert observers.

hNPC-F^{Low} Grafts	**On Target**	**Off Target**
MRI On Target	13	1
MRI Off Target	2	14

Table 8: Contingency table for hNPC-F^{High} cell grafts. Sensitivity 86.7%, Specificity 80.0%. Data shown from identification of images from three blinded expert observers.

hNPC-F^{High} Grafts	**On Target**	**Off Target**
MRI On Target	13	3
MRI Off Target	2	12

To determine the diagnostic capability of ferumoxytol in predicting on and off target graft location, T2*-weighted MR images were used to predict on or off target (diagnostic test) (**Figure 16 B**). The gold standard was histological confirmation of graft location with human nuclear antigen staining. The representative on target graft is located in the center of the grey mater of the ventral horn (**Figure 16 A**). The representative off target graft is located in the ventral lateral white water (**Figure 16 C**). On target was defined as greater than 50% of the cell graft contacting the motor neuron-containing ventral horn. Using contingency tables, the utility of identifying transplantation location hNPC-F^{Low} and hNPC-F^{High} cell graft was assessed. Using three blinded expert observers, T2*-weighted MRI immediately prior to sacrifice of hNPC-F^{Low} grafts had a sensitivity of 86.7% and specificity of 93.3% in predicting targeting

(**Table 7**). MRI of hNPC-F^{High} cell grafts had a sensitivity of 86.7% and specificity of 80.0% in predicting targeting (**Table 8**).

5.4.5 Histological Identification and Quantification of Ferumoxytol-Labeled Grafts

Pigs were euthanized at the previously described endpoints (Post-Operative Day 28, 42, or 105) and the spinal cords harvested, sectioned, and stained for Human Nuclear antigen (HuNu) with Cresyl violet background stain and Iron with Perl's Prussian Blue (PB) with Eosin background stain. Representative T2*-weighted axial MR images and micrographs for HuNu and PB staining are presented for each cohort.

In the Post-Operative Day 28 cohort B, all hNPC-F^{Low} and hNPC-F^{High} cell grafts were identified two weeks after transplantation with an average volume of 4.7 ± 1.5 μL and 18.7 ± 7.1 μL, respectively (mean ± standard deviation) and immediately prior to sacrifice with a volume of 2.6 ± 1.8 μL and 15.2 ± 6.5 μL, respectively (mean ± standard deviation). Regions containing unlabeled hNPC graft did not contain hypointense foci representative of labeled grafts. These grafts were quantified to have a volume of 0.4 ± 0.5 μL after transplantation and 0.4 ± 0.7 μL prior to sacrifice. A significant trend for increased MR hypointense signal with increased ferumoxytol dose was observed for all groups (ANOVA, $P < 0.0005$). Multiple comparison analysis showed a significant difference between hNPC-F^{High} grafts and control grafts (t test, $p < 0.0005$), but not between hNPC-F^{Low} grafts.

Stereological quantification of cell survival revealed an average engraftment of 25.6 ± 3.4 %, 13.4 ± 2.0 %, and 18.8 ± 2.7 % for individual hNPC, hNPC-F^{Low} and hNPC-F^{High} cell grafts, respectively (mean ± standard deviation). Engraftment

Percentage is defined as the relative percentage of surviving cells quantified with stereology compared to the number of cells originally transplanted. A significant increase in survival was observed for hNPC over hNPC-F^{Low} cell grafts (t test, $p < 0.05$). Quantification of histological iron with PB staining and ImageJ minimum threshold revealed an average of 0.1 ± 0.2 μL, 2.3 ± 1.4 μL and 7.2 ± 3.0 μL histological iron for individual hNPC, hNPC-F^{Low} and hNPC-F^{High} cell grafts, respectively (mean ± standard deviation) with a statistically significant trend of increasing histological iron with ferumoxytol dose (ANOVA, $p < 0.0005$).

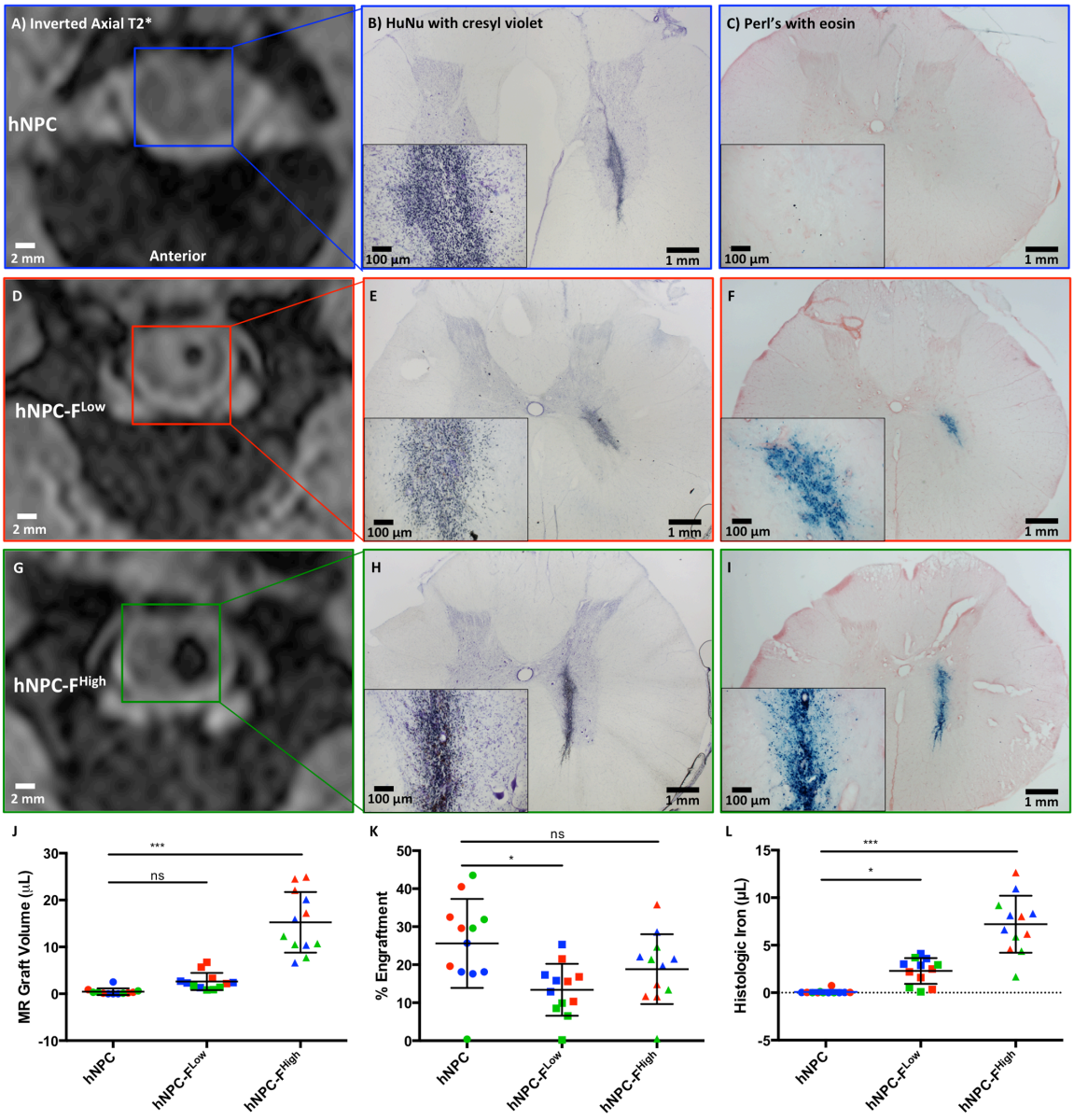

Figure 17. Ferumoxytol-labeled grafts identified postmortem (28 day cohort B). A representative unlabeled hNPC cell graft six weeks after transplantation was not observed with MRI **(A)** or Perl's Prussian Blue (Perl's) Iron staining **(C)**. It was detected with post-mortem human nuclear (HuNu – black) antigen staining **(B).** However, both hNPC-F^{Low} and hNPC-F^{High} grafts were observed with MRI **(D), (G)**, HuNu **(E), (H)**, and Perl's **(F), (I)**. The quantification data is from all 36 grafts in the 28 day survival group (n = 3 pigs). Volumetric quantification of MR signal from hNPC, hNPC-F^{Low} and hNPC-F^{High} cell grafts are shown (**J**). Stereological quantification of surviving human nuclei is

shown for all groups (**K**). Histological Iron quantification was shown for all groups **(L)**. Individual data points on figures are color coded by animal. Scale bars: main panels, 1 mm; insets, 100 μm; MRI, 2mm. Ordinary one-way ANOVA and multiple comparison unpaired t-tests were performed. *Significant, $P < 0.05$; **Significant, $P < 0.005$; ***Significant, $P < 0.0005$. hNPC, human neural progenitor cell; F, ferumoxytol. Graphs displayed as mean ± SD.

In the Post-Operative Day 42 cohort C, all hNPC-F^{Low} and hNPC-F^{High} cell grafts were identified two weeks after transplantation with a volume of 6.4 ± 3.1 μL and 23.4 ± 4.9 μL, respectively (mean ± standard deviation). Immediately prior to sacrifice at POD 42, 83.3% of hNPC-F^{Low} and 100% of hNPC-F^{High} cell grafts were identified with an average volume of 2.3 ± 1.5 μL and 14.0 ± 3.0 μL, respectively (mean ± standard deviation). Grafts with a volume of less than 0.5 μL were considered not identified. A statistically significant decrease was observed in both hNPC-F^{Low} and hNPC-F^{High} cell grafts over time (ANOVA, $p < 0.0005$). Stereological quantification of cell survival revealed a non-significant difference of average engraftment of 24.0 ± 6.5 %, 17.1 ± 3.9 %, and 25.0 ± 5.4 % for individual hNPC, hNPC-F^{Low} and hNPC-F^{High} cell grafts, respectively (ANOVA, $p > 0.05$). Quantification of histological iron with PB staining and ImageJ minimum threshold revealed an average of 0.1 ± 0.0 μL, 3.1 ± 0.5 μL and 5.0 ± 0.4 μL histological iron for individual hNPC, hNPC-F^{Low} and hNPC-F^{High} cell grafts, respectively (ANOVA, $p < 0.0005$).

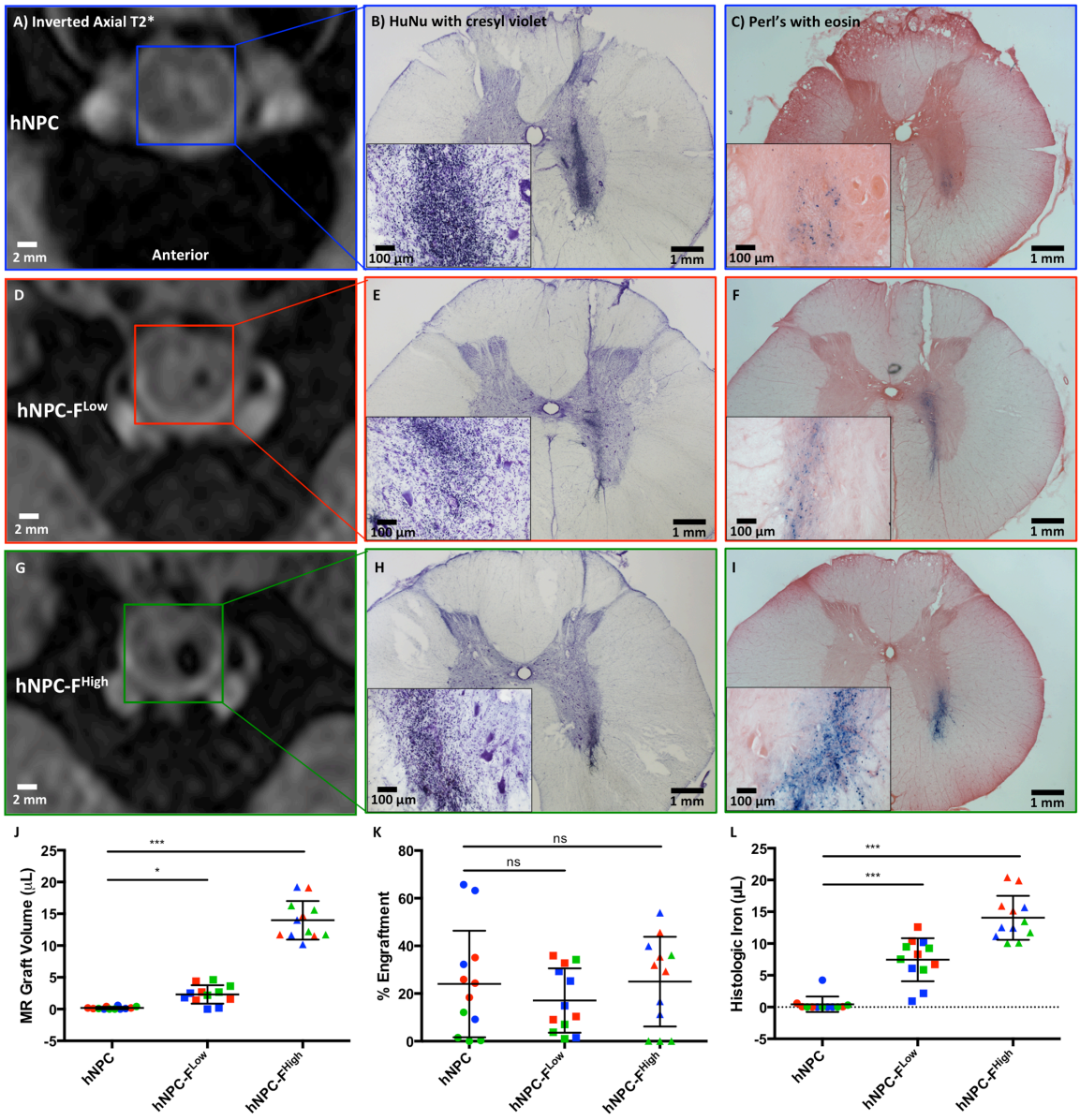

Figure 18. Ferumoxytol-labeled grafts identified postmortem (42 day cohort C). A representative unlabeled hNPC cell graft six weeks after transplantation was not observed with MRI **(A)** or Perl's Prussian Blue (Perl's) Iron staining **(C)**. It was detected with post-mortem human nuclear (HuNu – black) antigen staining **(B).** However, both hNPC-F^{Low} and hNPC-F^{High} grafts were observed with MRI **(D), (G)**, HuNu **(E), (H)**, and Perl's **(F), (I)**. The quantification data is from all 36 grafts in the 42 day survival group (n = 3 pigs). Volumetric quantification of MR signal from hNPC, hNPC-F^{Low} and hNPC-F^{High} cell grafts are shown (**J**). Stereological quantification of surviving human nuclei is

shown for all groups (**K**). Histological Iron quantification was shown for all groups **(L)**. Scale bars: main panels, 1 mm; insets, 100 µm; MRI, 2mm. Ordinary one-way ANOVA and multiple comparison unpaired t-tests were performed. *Significant, $P < 0.05$; **Significant, $P < 0.005$; ***Significant, $P < 0.0005$. hNPC, human neural progenitor cell; F, ferumoxytol. Graphs displayed as mean ± SD.

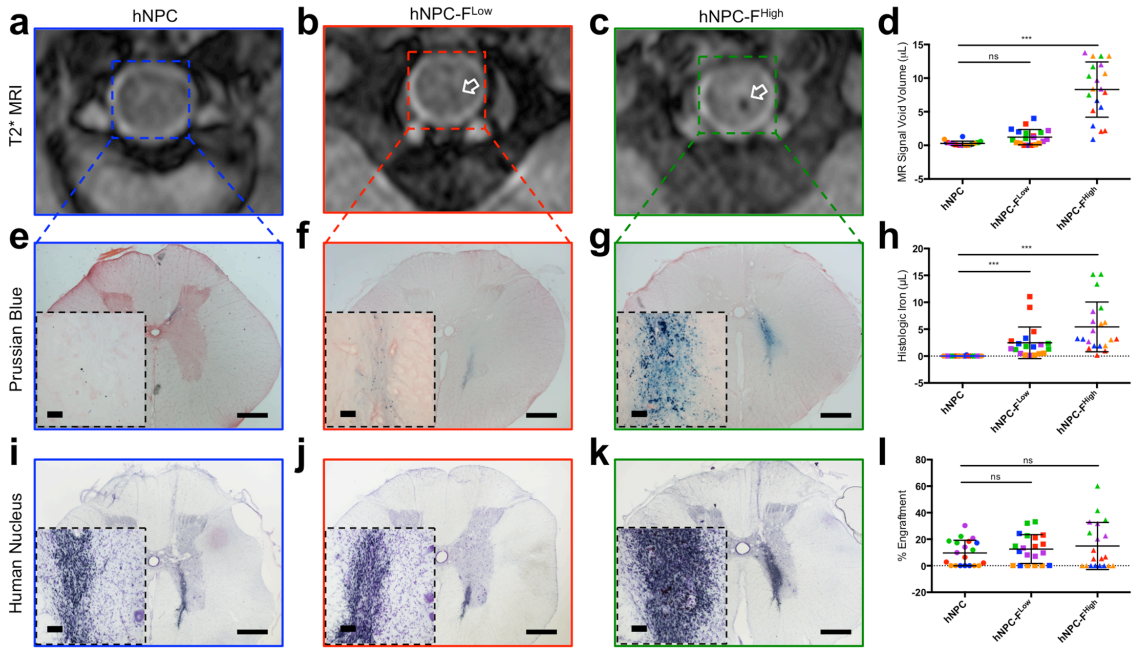

Figure 19. Ferumoxytol-labeled grafts identified postmortem (105 day cohort D). A representative T2*-weighted MR image of the region containing a hNPC unlabeled graft 105 days after transplantation showed no hypointense focus (**A**). Representative MR images from representative hNPC-F^{Low} (**B**) and hNPC-F^{High} (**C**) cell grafts showed hypointense foci (white arrows) representative of the negative contrast produced by ferumoxytol. The MR signal void volume for all grafts was calculated for the terminal time point (**D**). Representative micrographs from Prussian Blue iron staining are shown for hNPC (**E**), hNPC-F^{Low} (**F**) and hNPC-F^{High} (**G**) cell grafts. Characteristic blue precipitates were observed in hNPC-F^{Low} and hNPC-F^{High} cell grafts. Graft-specific histological iron was quantified (**H**). Representative micrographs of human nuclear antigen staining for hNPC (**I**), hNPC-F^{Low} (**J**) and hNPC-F^{High} (**K**) cell grafts are shown.

Engraftment was quantified with stereology (**I**). Individual data points on figures are color coded by animal. Scale bars: 1 mm; insert, 50 μm. Ordinary one-way ANOVA and multiple comparison unpaired t-tests were performed. *Significant, $P < 0.05$; **Significant, $P < 0.005$; ***Significant, $P < 0.0005$. hNPC, human neural progenitor cell; F, ferumoxytol. Graphs displayed as mean ± SD.

In the Post-Operative Day 105 cohort, all hNPC-F^{Low} and hNPC-F^{High} cell grafts were identified two weeks after transplantation with a volume of 5.1 ± 2.1 μL and 17.8 ± 4.2 μL, respectively (mean ± standard deviation). Immediately prior to sacrifice at POD42, 65.0% of hNPC-F^{Low} and 100% of hNPC-F^{High} grafts were identified with an average volume of 1.2 ± 1.1 μL and 8.3 ± 4.1 μL, respectively (mean ± standard deviation). Grafts with a volume less than 0.5 μL were not considered identified. The difference in MR signal at POD 105 between hNPC grafts and hNPC-F^{Low} was non-significant. Stereological quantification of cell survival revealed an average engraftment of 9.6 ± 9.6 %, 12.6 ± 10.9 %, and 14.9 ± 17.7 % for individual hNPC, hNPC-F^{Low} and hNPC-F^{High} cell grafts, respectively (mean ± standard deviation). The difference in cell survival was non-significant (ANOVA, $p > 0.05$). Quantification of histological iron with PB staining and ImageJ minimum threshold revealed an average of 0.0 ± 0.0 μL, 2.5 ± 2.9 μL and 5.4 ± 4.6 μL histological iron for hNPC, hNPC-F^{Low} and hNPC-F^{High} cell grafts, respectively. One of the hNPC-F^{Low} grafts was excluded form analysis due to a histological anomaly that complicated analysis.

Further analysis of the stereological quantification of human cell survival revealed a significant decrease in survival of unlabeled hNPC cell grafts over time with an average engraftment of 25.6 ± 3.4 %, 24.0 ± 6.5 %, and 9.6 ± 2.1 % for POD 28, 42, and 105,

respectively (ANOVA, $p < 0.005$) (**Figure 20**). The average survival of hNPC-F^{Low} and hNPC-F^{High} cell grafts remained relatively constant over time.

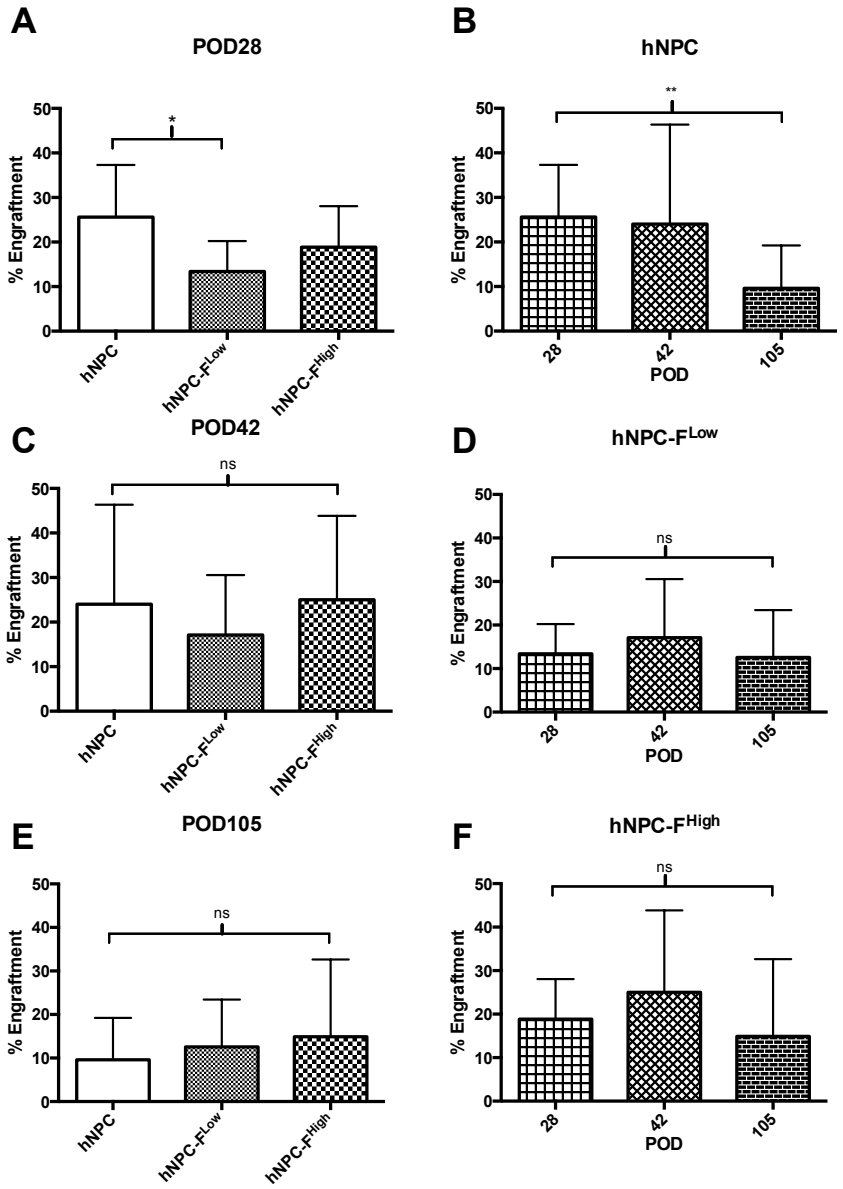

Figure 20. Quantification of Transplanted Cell Graft Survival with Stereology of Human Nuclei. Stereological quantification was done for each individual cell graft in each animal for all cohorts. Engraftment % is defined as the relative percentage of surviving human cells compared to the amount originally transplanted. Ordinary one-

way ANOVA and multiple comparison unpaired t-tests were performed. *Significant, P < 0.05; **Significant, P < 0.005; ***Significant, P < 0.0005. hNPC, human neural progenitor cell; F, ferumoxytol. Graphs displayed as mean ± SD.

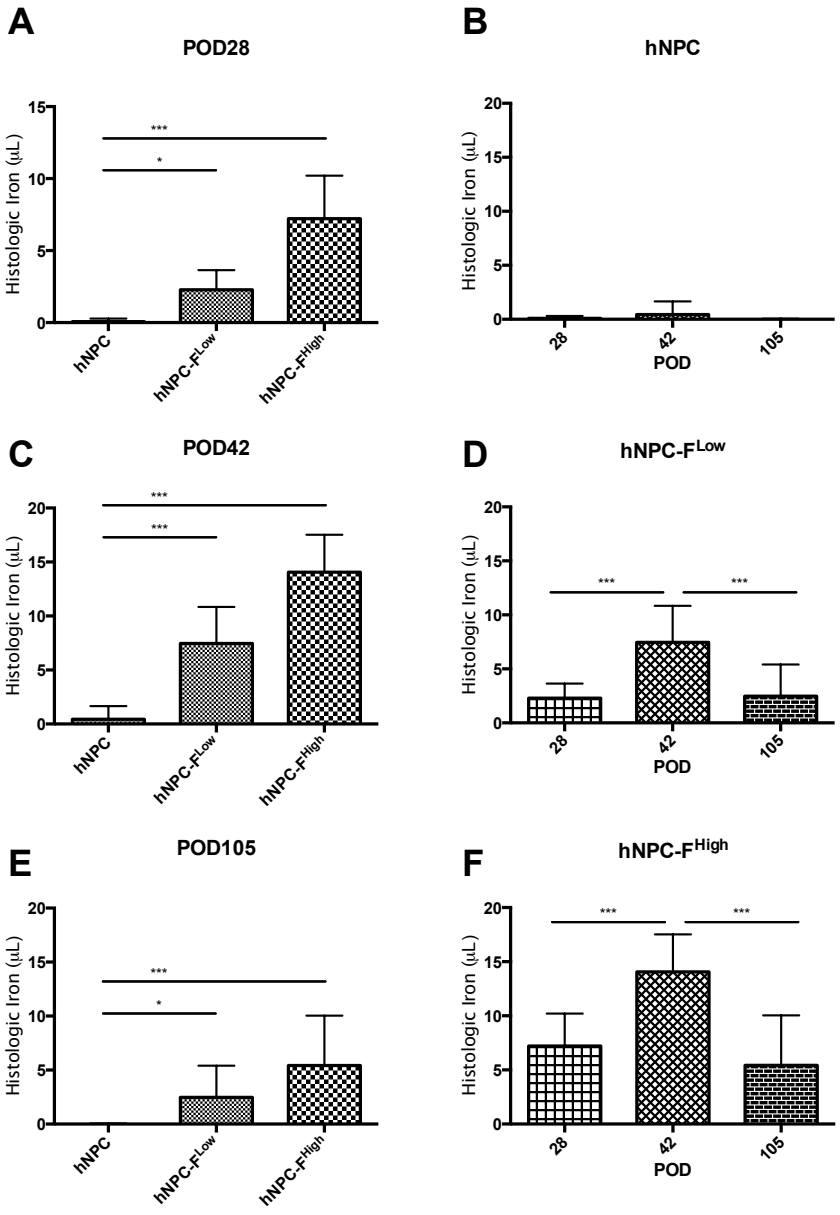

Figure 21. Quantification of Histological Iron in Transplanted Cell Grafts. Quantification of histological iron was done for each individual cell graft in each animal for all cohorts. Using a threshold method on ImageJ, a volume of histological iron was

calculated. Ordinary one-way ANOVA and multiple comparison unpaired t-tests were performed. *Significant, $P < 0.05$; **Significant, $P < 0.005$; ***Significant, $P < 0.0005$. hNPC, human neural progenitor cell; F, ferumoxytol. Graphs displayed as mean ± SD.

Further analysis of the quantification of transplanted cell graft histological iron from the ferumoxytol nanoparticles revealed a significant increase between hNPC, hNPC-F^{Low} and hNPC-F^{High} cell grafts at all time points (ANOVA, $p < 0.005$) (**Figure 21**). The average volume of histological iron content remained relatively stable between POD 28, 42, and 105 time points for hNPC, hNPC-F^{Low} and hNPC-F^{High} cell grafts.

5.4.6 Correlation Analysis of MR Graft Volume, Histological Iron, and Cell Survival of Transplanted Ferumoxytol-Labeled Human Neural Progenitor Cell Grafts

Group analysis revealed a statistically significant difference in change of MRI signal between POD 14 and 28 or 42 between rejected and surviving hNPC-F^{High} cell grafts (**Figure 22 A, B**). The hNPC-F^{High} cell grafts were grouped by engraftment percentage where surviving grafts have over 5% engraftment. Correlation analysis between terminal MR graft volume and graft histological iron revealed a linear correlation for hNPC-F^{High} cell grafts ($r = 0.52$, $p < 0.0005$) (**Figure 22 C**). The graft volume observed on T2*-weighted MRI was predictive of the amount of ferumoxytol nanoparticles in the tissue. Furthermore, correlation analysis between histological iron and % engraftment showed a strong linear correlation for hNPC-F^{High} cell grafts ($r = 0.63$, $p < 0.0005$) conditions (**Figure 22 D**). The histological iron observed with PB staining was predictive of the survival of the cell graft measured by stereological quantification of

surviving human nuclei. A correlation was not observed between MR graft volume, histological iron, or cell engraftment for hNPC-F^{Low} cell grafts.

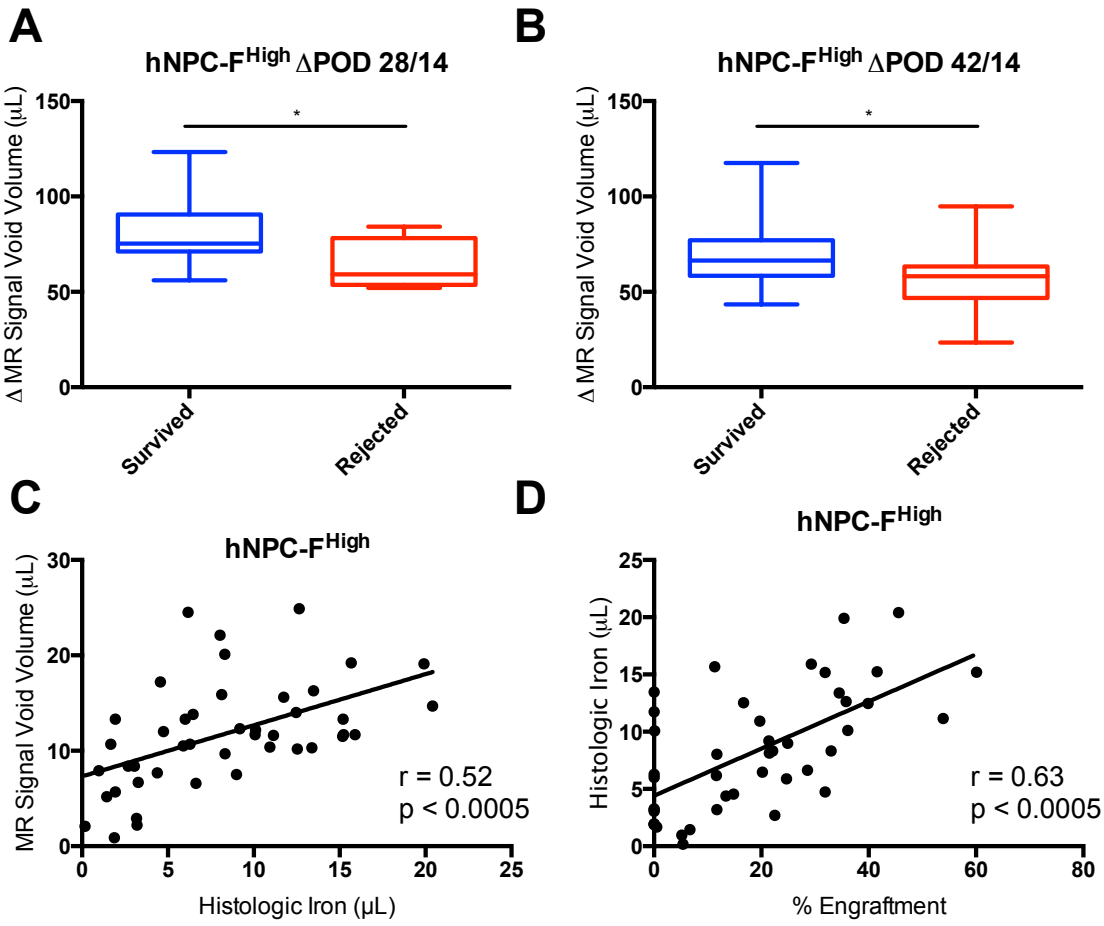

Figure 22. Correlation Analysis of MR Graft Volume, Histological Iron, and Cell Survival of Transplanted Human Neural Progenitor Cells for hNPC-F^{High} Cell Grafts. MR Graft volume is the volume of each transplanted cell graft observed with T2*-weighted MRI. The volume is calculated in μL using a minimum threshold method in ImageJ. Histological Iron is the volume of Iron deposits observed in each transplanted cell graft with Prussian blue staining. The volume is calculated in μL using a minimum threshold method in ImageJ. % Engraftment is the relative percentage of surviving human cells in each graft compared to the original number injected. If 100,000 cells were counted in a graft with stereology, the % engraftment would be 40% because the number of cells transplanted was

250,000 per graft. Linear regression and correlation analysis were performed with one-tailed p tests ($p < 0.05$). The p value and r value are reported. Δ MR signal void volume refers the relative percentage change in MR signal calculated between two time points. "Survived" grafts have engraftment over 5% and "rejected" grafts have engraftment below 5%. Individual t test and one-way linear regression analysis performed. *Significant, $P < 0.05$; **Significant, $P < 0.005$; ***Significant, $P < 0.0005$. hNPC, human neural progenitor cell; F, ferumoxytol. Graphs displayed as mean ± SD.

5.4.7 Differentiation of Ferumoxytol-Labeled Cell Grafts *In Vivo*

A murine monoclonal antibody specific to human glial fibrillary acid protein was used to observe *in vivo* astrocytic differentiation of transplanted human neural progenitor cells of hNPC, hNPC-F^{Low} and hNPC-F^{High} cell grafts (**Figure 23**). Signal was not observed outside of the grafted area in the porcine spinal cord or in completely rejected grafts, confirming the signal is from viable human neural progenitor cells and not from host astrocytes or rejected cells.

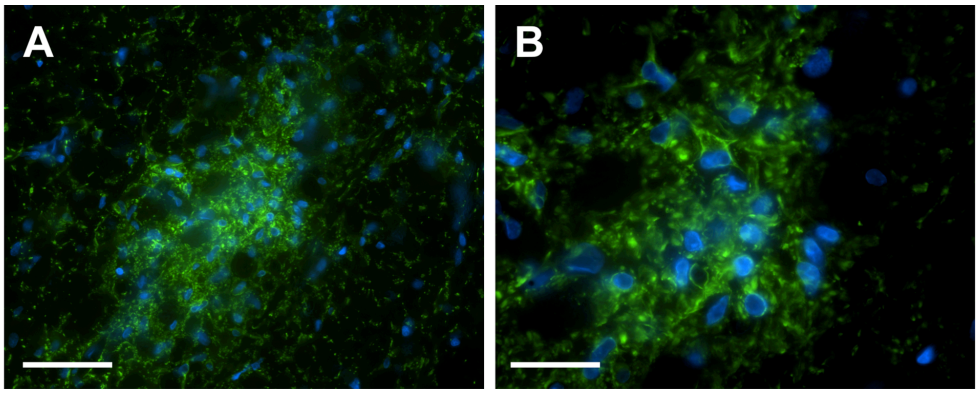

Figure 23. Differentiation of Ferumoxytol-Labeled Human Neural Progenitor Cells in the Porcine Spinal Cord. A fluorescent micrograph of a representative hNPC-F^{High} cell graft is shown at 40X (**A**) and oil-immersion 100X (**B**). A murine monoclonal antibody specifically targeted human glial fibrillary acid protein was used and visualized with a

fluorescent secondary antibody (green). All nuclei are observed with DAPI staining (blue). Scale bars: **A**, 100 µm; **B**, 50 µm.

5.4.8 Ferumoxytol Particles Remain Internalized by Transplanted Human Neural Progenitor Cells

Transmission Electron Microscopy of tissue sections containing hNPC-F^{High} and hNPC-F^{Low} cell grafts stained with DAB-enhanced human nuclear antigen staining revealed numerous DAB positive human nuclei at post-operative day 42. The human cells appeared healthy with numerous mitochondria and proper cytoarchitecture. Furthermore, the cells were observed to be developing neurites (**Figure 24 A**). Importantly, numerous nanoparticle-laden endosomes/lysosomes were observed in the cytoplasm (**Figure 25 B**).

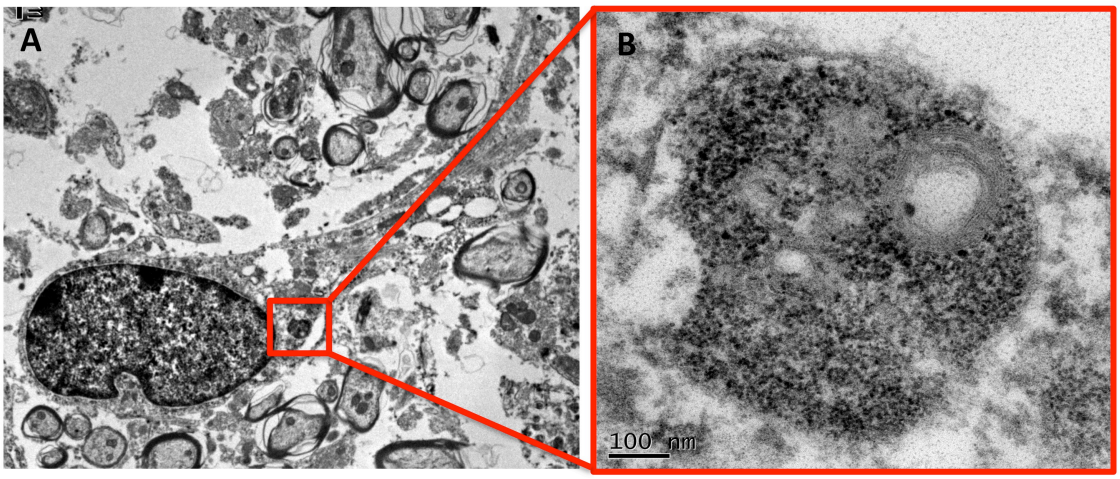

Figure 24: In Vivo Transmission Electron Microscopy. A 50 µm section of a hNPC-F^{High} cell graft containing tissue was stained with DAB-enhanced HuNu. The section was embedded in resin and sectioned at 50 nm. Inspection of tissue at low magnification TEM **(A)** revealed numerous DAB-positive nuclei containing cytoplasmic endosomes/lysosomes containing nanoparticles observed at high magnification **(B).**

5.4.9 Transplantation of Ferumoxytol-Labeled Human Neural Progenitor Cell Grafts into the Spinal Cord Does Not Cause Demyelination of White Mater Tracts

Transplantation of ferumoxytol-labeled cells into the spinal cord does not cause demyelination of local white mater tracts as observed with luxol fast blue staining (**Figure 25**). Both non-rejected and rejected grafts show non-myelinated cells in the graft site, but not demyelination of local white mater tracts.

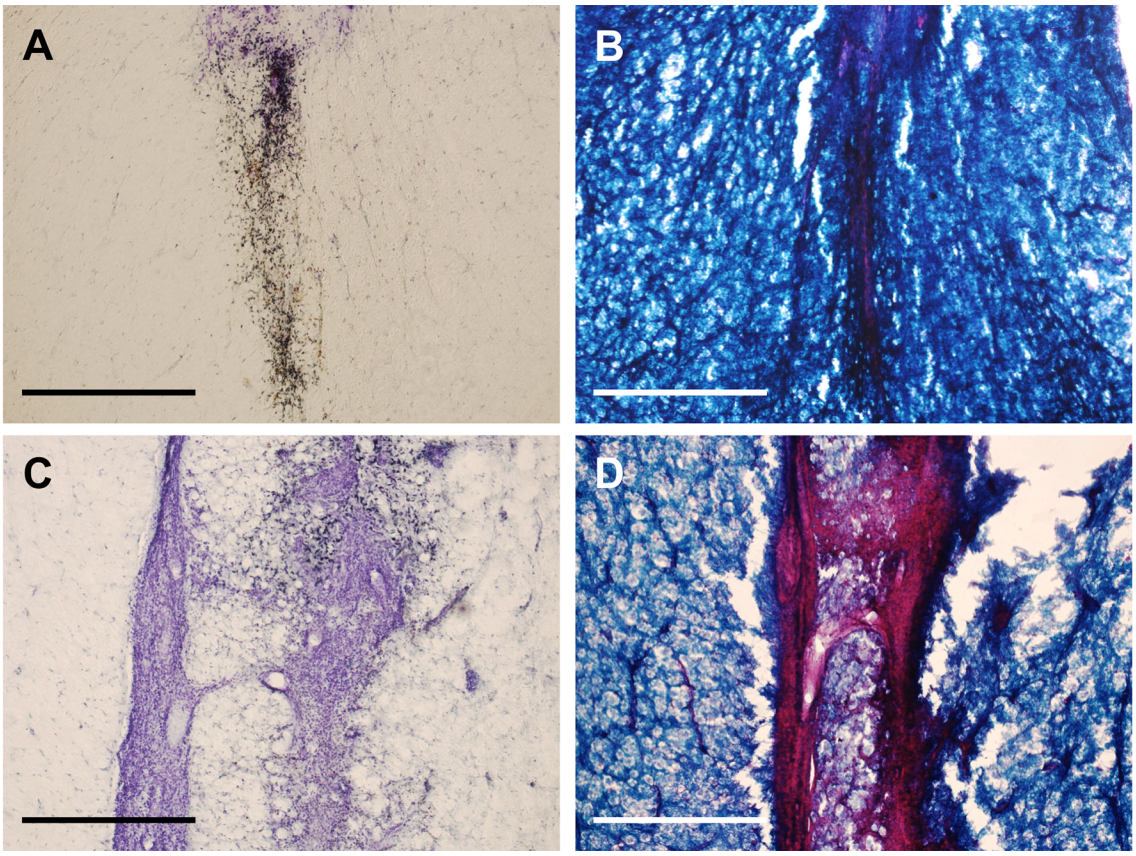

Figure 25. Luxol Fast Blue Staining of Myelination Surrounding Transplanted Ferumoxytol-Labeled Cell Grafts. Human nuclear antigen staining of a well integrated, non rejected hNPC-F^{High} cell graft (**A**) and of a rejected, inflamed hNPC-F^{High} cell graft in the white mater (**C**). Grafts in the white mater were specifically chosen to look for changes in myelination with luxol fast blue staining. Luxol fast blue staining of contiguous sections for the non-rejected (**B**) and rejected graft (**D**) showed non-myelinated cells in the graft (pink),

but no demyelination of surrounding white mater tracts (blue). Light microscopy: 10X. Scale bars: 1 mm.

5.4 CONCLUSIONS

Non-invasive imaging modalities, such as MRI, will play a critical role in the successful, widespread translation of cellular therapeutics to the Central Nervous System. Without imaging, it is impossible to visually observe the transplantation site without an invasive surgical procedure or a reliance on stereotactic methods. Diagnostic monitoring of transplanted cellular therapeutics will most likely be required by future clinical trials to properly assess delivered dose and long-term safety[100]. MRI provides the ability to assess graft location, size, migration, host responses, and investigate potential adverse impacts on host parenchyma. The current study provides framework for investigating the use of MRI to non-invasively track transplanted stem cells in the CNS of a large animal. The current study was not designed to investigate the therapeutic efficacy of the transplanted cell graft, which has been established in previous studies[41,64,149]. The objectives of this study were to: 1) identify the location of transplanted cell grafts *in* vivo with MRI; 2) quantify ferumoxytol-labeled cell graft survival; and 3) correlate MR findings, histological measures of Iron deposits and graft survival.

Transplantation of unlabeled hNPC, and ferumoxytol-labeled low dose hNPC-F^{Low} and high dose hNPC-F^{High} cell grafts directly into the spinal cord of pigs was achieved. The transplantation procedure produced expected transient morbidity and all animals returned to neurological baseline after one week. Permanent behavioral or functional deficits were not observed. The animals were followed for different lengths of time, including a "long-term" group for 105 days after transplantation. The purpose of this study was to visualize

transplanted hNPCs with MRI and identify them post-mortem, not to optimize dose or assess optimal therapeutic benefit. However, the cells were transplanted to the location that would be targeted in a clinical trial for ALS using a clinically approved surgical approach[127,128]. A pilot study was performed and determined 2.5 x 10^5 cells per injection as optimal graft size for visualization with MRI. This graft size is in line with previously published clinical trials[33,70].

The transplanted ferumoxytol-labeled grafts were visualized in the spinal cord of the pig with clinical 3T MRI. The graft size was quantified and corresponded with labeling condition (low vs. high dose). Furthermore, the MRI was predictive of histological graft location. After sacrifice, survival of the cell grafts was quantified with stereology and no difference in survival was observed between ferumoxytol-labeled and unlabeled control grafts. The change in MR signal can be used to predict graft survival or rejection in hNPC-F^{High} cell grafts. Histological iron deposits were located within the transplanted cell grafts. Correlation analysis showed that MR signal correlated with histological iron and that histological iron correlated with graft survival in hNPC-F^{High} cell grafts. It is possible that these correlations were not observed in hNPC-F^{Low} cell grafts because of the relatively small changes in iron due to the lower initial dose. Furthermore, it was demonstrated the ferumoxytol-labeled cell grafts differentiate *in vivo*, ferumoxytol particles remain in the cytoplasm, and that the grafts do not cause damage to local white mater tracts.

This is the first report to document the ability to monitor SPION-labeled cells in the CNS of a large animal model. While SPION-labeled cells have been tracked in the spinal cord of small animal models, these studies were of relatively short duration[39]. To the best of our knowledge, this is longest report published to date in the spinal cord. SPION-labeled

cells have been tracked for over one year in the brain of small animal models[99,107]. The spinal cord presents a challenging environment for MRI due to susceptibility artifacts caused by interactions between the cerebrospinal fluid, bone, fat, and parenchyma. Furthermore, cardioballistic movement of the spinal cord and local gastrointestinal movement further complicate the imaging environment.

The primary objective was to assess the utility of ferumoxytol labeling as a diagnostic marker of transplanted cell graft location and survival. Importantly, the ferumoxytol labeling did not impact cell graft survival. Furthermore, the T2*-weighted MR images were used to predict on and off target grafts with acceptable levels of sensitivity and specificity. The relatively large number of off target grafts could be explained by the use of clinical cannulas with depth settings for the human spinal cord, which is slightly larger than the pig. Most off target grafts were located directly ventral to the ventral horn, which would be explained by the longer cannulas designed for human use. The MR images correlated with the amount of histological iron in the cell grafts. The amount of histological iron co-located well with the transplanted human cells and correlated with the number of surviving cells. With this, ferumoxytol-labeling is capable of predicting on or off target graft delivery with MRI and estimating graft survival with MRI and post-mortem histological analysis in hNPC-F^{High} cell grafts.

Previous groups have reported that transplanted cells do not retain the SPION label[26,73]. Indeed, iron deposits from SPION were observed outside of transplanted labeled cells in rejected grafts. However, numerous cells retained some level of SPION as observed with Transmission Electron Microscopy.

CHAPTER 6

DEVELOPMENT OF A MAGNETIC RESONANCE IMAGING COMPATIBLE SPINAL INJECTION SYSTEM (SPECIFIC AIM 3)

6.1 INTRODUCTION

A minimally invasive system for targeted delivery of therapeutics to the human spinal cord requires an MRI-compatible injection device. MRI is the imaging modality of choice because of its ability to produce high-resolution images of the spinal cord and its ability to visualize cells labeled with SPION. An injection system with a platform that mounts to the spine and contains an injection apparatus that is capable of intra-parenchymal injections was chosen because of our previous experience with this delivery system design for open surgical direct injection studies.

A computer aided design schematic of the current platform used in open surgical procedures shows key features that must be included in the MRI-compatible system (**Figure 1**). Components of the device include:

1. Gray components: Surgical retractors and percutaneous pedicle post blocks. The retractors will be eliminated in the MRI-compatible design.

2. Blue components: Mounting components and rail system which are attached the pedicle post blocks which are fastened to the vertebrae with pedicle screws that will be replaced with an MR-compatible version.

3. Green components: Positioning gondola which adjusts position along and across the spine (x- and y-directions) that will be replaced with an MR-compatible version.

4. Orange components: Catheter guide system and injection drive (which will be replaced by SmartFrame™ system).

5. Figure 2b shows a photo of the device in use during a direct injection surgical procedure.

No system currently exists for minimally invasive, targeted intra-parenchymal delivery of cellular therapeutics to the human spinal cord. The current gold standard is injection based on naked-eye targeting following a major invasive surgical procedure. Additionally, immediate visualization and confirmation of the final cellular graft location *in vivo* is not currently available. The objective of this study is to develop a minimally invasive injection system that allows direct targeting of specific locations within human spinal cord parenchyma for delivery of therapeutics and visual confirmation of their location using MRI. A prototype device will be fabricated and the system will be assessed in an MR phantom spinal cord model.

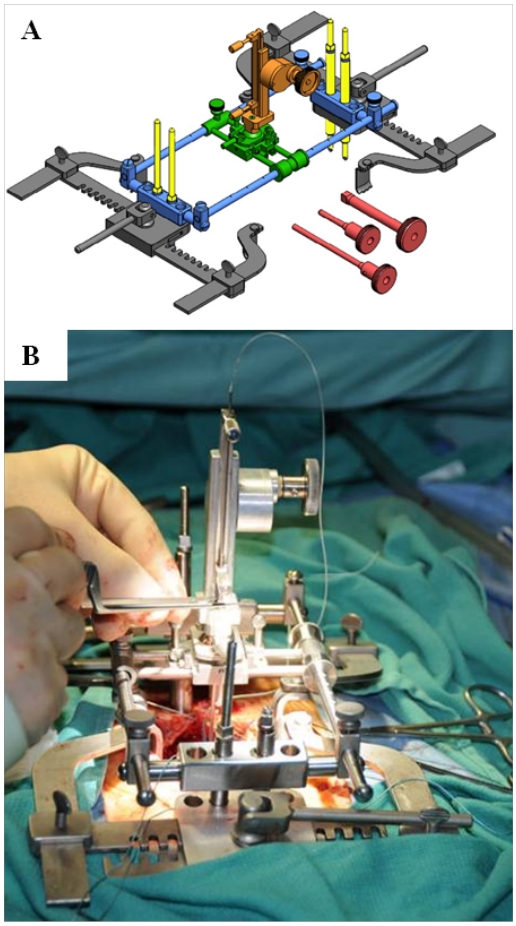

Figure 26. **Surgical Stereotactic Spine-Mounted Injection Platform.** A computer-aid design schematic of the current platform used in open surgical spinal cord transplantation procedures (**A**). A photo of the device in use during a direct injection surgical procedure (**B**).

6.2 METHODS

6.2.1 Design and Fabrication of the MRI-Compatible Platform

The MRI compatible platform (blue and green components in **Figure 14a**) was designed to serve many of the same functions as the previous device developed and used in the open surgical procedure (**Figure 14b**), including the ability to rigidly mount to the

spine, and the ability to move in the x (medial/lateral) and y (rostral/caudal) planes for targeting specific inter-vertebral locations in the spine. In addition, the platform was designed to fasten to the ClearPoint SmartFrame™ injection device developed by MRI Interventions Inc (**Figure 15)**. The platform was designed for fabrication with an MRI-compatible material that was strong but will not cause any artifacts during imaging. For the MR-compatible platform, polyoxymethylene was chosen for the initial prototypes. Polyoxymethylene is a rigid, machineable thermoplastic used in precision parts manufacturing when high stiffness and dimensional stability are required[55]. The platform was designed to maintain a low profile to fit within the bore of the MRI scanner when fastened to the animal's spine, and allow the SmartFrame™ to attach. Construction of the platform occurred at the Emory University Physics machine shop.

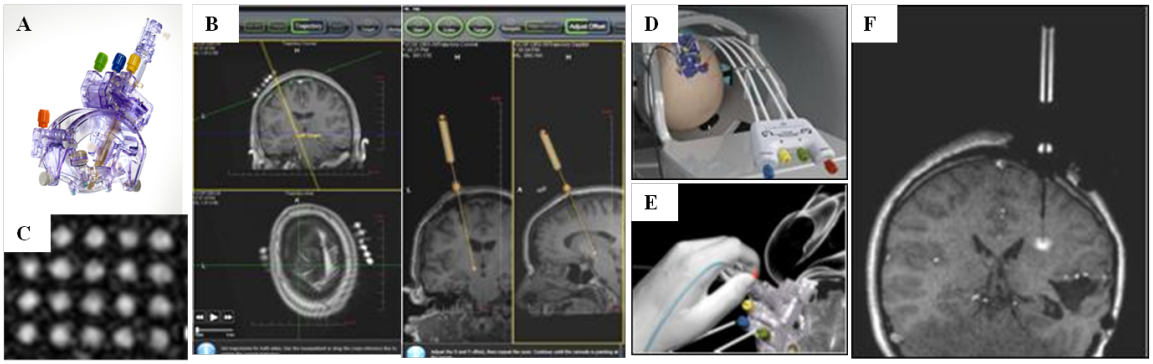

Figure 27. Overview of ClearPoint System from MRI Interventions. The SmartFrame (**A**) mounts to the skull on the cranial DBS lead placement applications, but will be mounted to the MRI-compatible platform we are developing. The frame accepts a cannula and allows for angular adjustments in the sagittal and coronal planes. The Clearpoint software takes high-resolution T1-weighted images that detect the device position in relation to the cranium. The software and device allows for targeting, trajectory planning, and adjustments with near real-time imaging (**B**). The entry position (which aids in targeting and planning) is determined by a fiducial grid (**C**) placed on the

surface of the skull. The hand controller (**D**) allows for regular adjustments while the patient is in the scanner. The device allows a cannula to be passed (**E**) along the planned trajectory and the infusion can be monitored in near real-time (**F**).

6.2.2 Attachment of SmartFrame™ to the MRI-Compatible Platform

The SmartFrame™ cannula targeting system from MRI Interventions replaced the catheter guidance system and injection drive (orange components in F**igure 14a**). The SmartFrame™ rigidly fixates to the MRI-compatible platform. The SmartFrame™ attached to the positioning unit of the MRI-compatible platform with mechanical mounting hardware that allowed the frame to be rigidly mounted but also removed as needed. The SmartFrame™ device allowed for angular adjustments in the coronal and sagittal planes and contained a remote cable drive (SmartFrame™ hand controller) for changing these angles from outside the scanner bore. The ClearPoint SmartFrame™ and targeting software system is shown in **Figure 15**.

The SmartFrame was designed to accommodate a nested dual cannula system consisting of an 18 gauge rigid outer cannula and an inner cannula with a 26 gauge ceramic needle. The system used to penetrate the animal and inject into the cord and was a modified version of this nesting cannula system used for DBS lead placement. The rigid outer cannula can be advanced manually until penetration of the ligamentum flavum then the inner cannula can be connected to the microinjector pump and advanced into the spinal cord and for accurate in delivery small volumes[72].

6.2.3 Construction of the MRI Phantom Spine Model

A human phantom spine model was constructed using Polyvinyl alcohol to mimic spinal cord, gum rubber sheet for the ligamenum, doped water for cerebrospinal fluid, solid foam for bone, foam for intra-laminal disks, and water for the soft tissue. The goal of choosing these materials is to create a model that has the MR image signal properties (T1 and T2) as well as the material properties for developing the injection workflow. This model was used to: 1) evaluate the appearance and potential artifacts of the cannula, needle, platform, and instruments in the MRI, 2) develop and optimize imaging methodology using real-time sequences for visualizing injected cells in the phantom, and 3) establish workflow for image-guided spinal cord injections.

6.2.4 Magnetic Resonance Imaging

Pre-procedure imaging was used to determine the location of relevant anatomy and cannula trajectory planning. MR imaging followed established protocols used for Deep Brain Stimulator lead placement by using a 3D, T1-weighted turbo spin echo (TSE) sequence with 1 x 1 x x 1 mm spatial resolution. The procedure was performed on a 3T, (diameter 50 cm; bore length, 160 cm) clinical MRI scanner (Magnetom Trio Trim, Siemens Medical Solutions). The acquired sequences and the ClearPoint software produced three orthogonal image planes for guidance to inter-actively monitor the delivery needle position. Post-delivery imaging of the labeled cells was done using a T2*-gradient echo sequence (Chapters 4 and 5) designed to maximize susceptibility-induced artifacts from the labeled cells.

6.3 RESULTS

6.3.1 Fabrication of a Prototype MRI-Compatible Spine Injection Platform

The MRI compatible spine injection platform was fabricated form polyoxymethylene at the Emory University Physics Machine Shop. The device was constructed from Computer-Aided Design schematics (**Figure 28**). The device was built to mount to the spine via percutaneous laminar posts that attached to the platform. The center of the platform contains a positioning unit that can be moved 2 cm in the axial plane and 8 cm in the sagittal plane. This flexibility allows the system to access several targets after mounting.

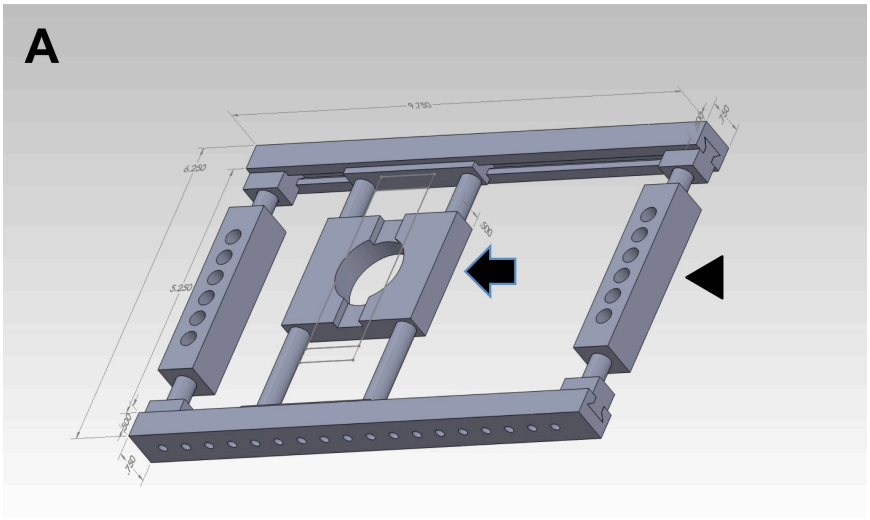

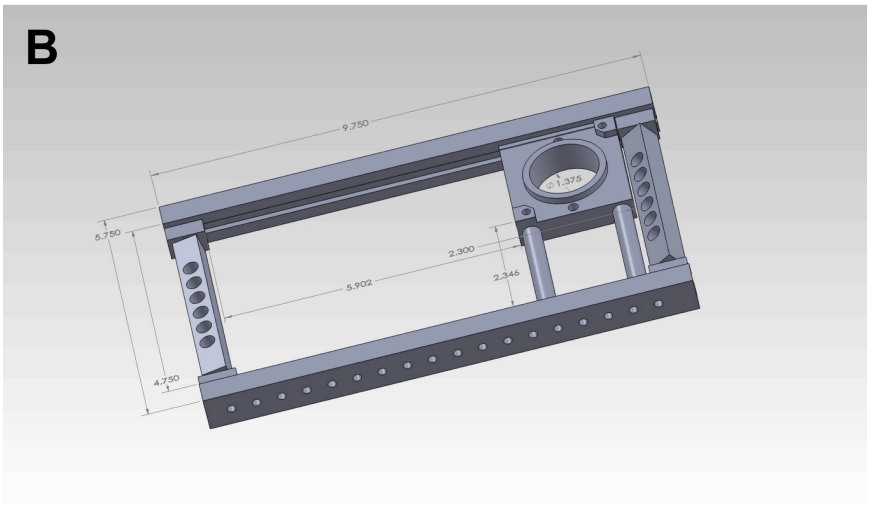

Figure 28. Computed-Aided Design Schematic of Prototype MR-Compatible Injection Platform. The primary features of the platform are shown in the schematic. The injection position unit (black arrow) fixates to the ClearPoint SmartFrame system and the laminar post holders (black arrowhead) fixate to the posts attached to the spine.

MRI Interventions provided a custom-built injection system for this study (**Figure 29**). The system includes a ceramic guide cannula and titanium stylet to pass through the tissue and provide access to the spinal cord. The infusion needle is composed of fused silica with a stepped tip design and contains long flexible tubing for access in the MR scanner.

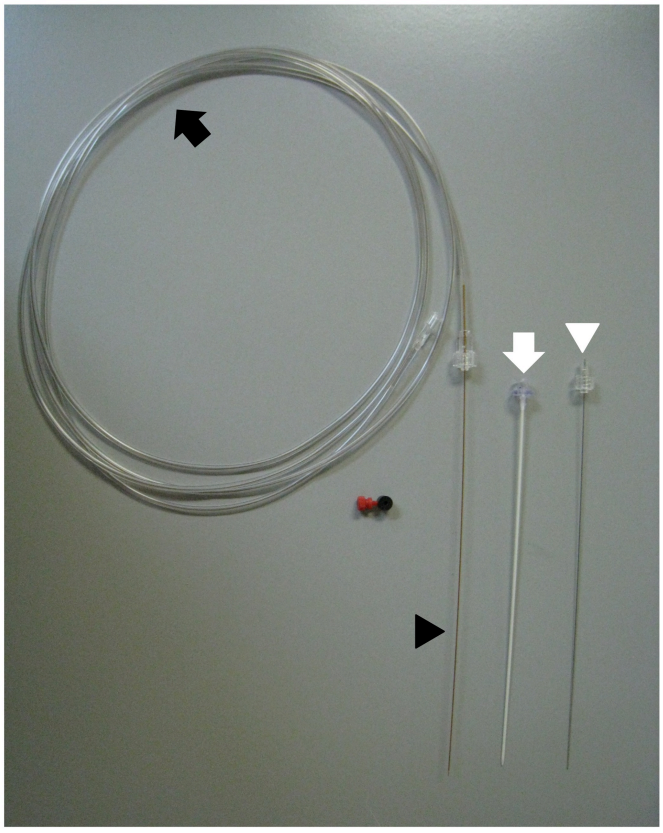

Figure 29. Custom Built Infusion Needle and Guide Cannula. A custom-built system injection cannula system with an infusion needle (black arrowhead) with flexible tubing (black arrow), a guide cannula (white arrow), and a stylet (white arrowhead).

6.3.2 Assessment of the MR-Compatible System in a Spine Phantom Model

To assess the MR-guided injection system and establish procedural workflow, a phantom model of the human spinal cord was employed.

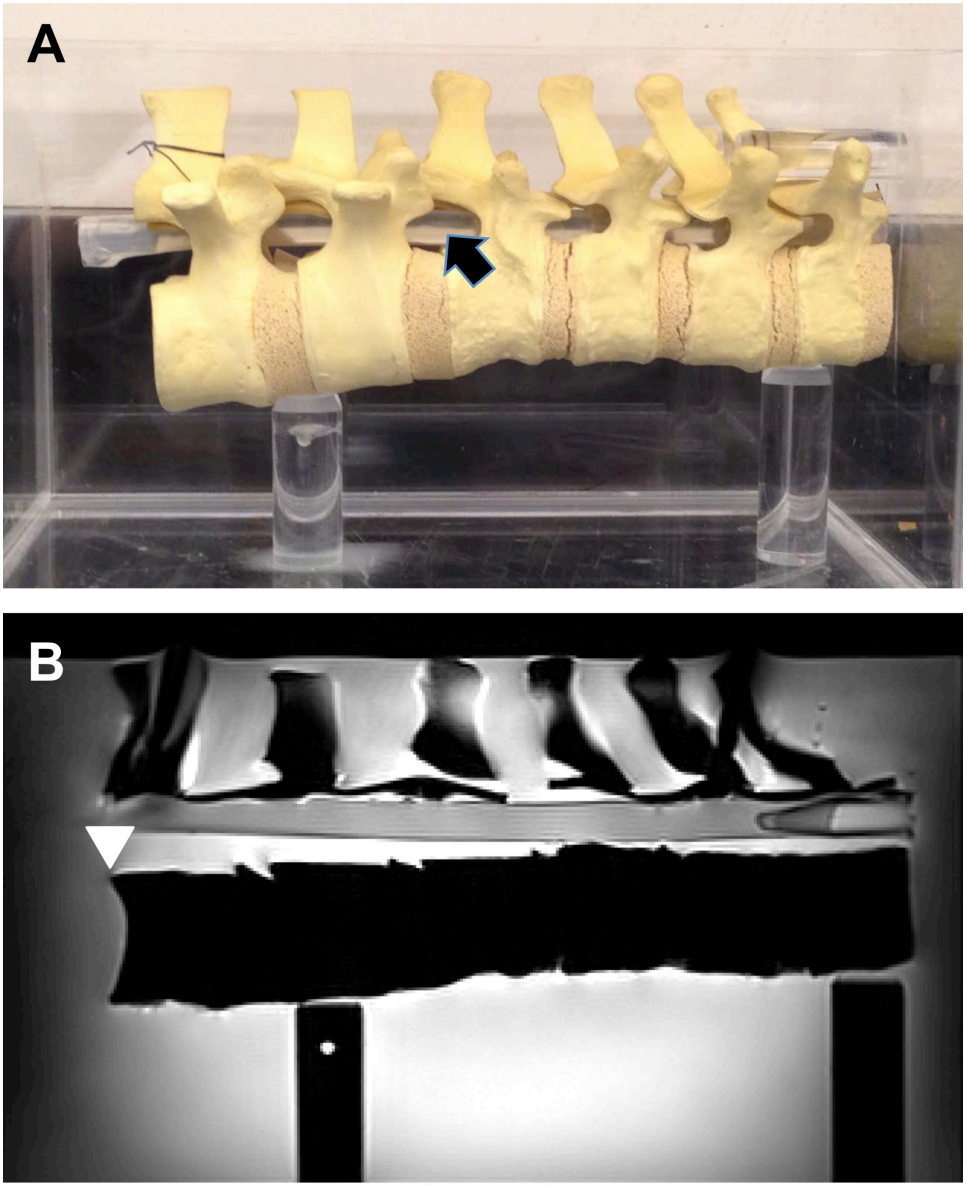

Figure 30. Human Spinal Cord Phantom Model. An image of the spine phantom model showing the spinal cord (black arrow) and a MR image of the spine phantom.

The custom built injection needle system was guided through the MRI Interventions SmartFrame device attached to the spine platform to the surface of the spinal cord using the ClearPoint software. T2*-weighted imaging showed a large artifact from the injection needle and cannula (**Figure 31 A Arrow).** The fine tip of the injection needle was observed in the phantom spinal cord (**Figure 31 A Arrowhead**). An infusion of ferumoxytol nanoparticles into the phantom spinal cord revealed a hypointense foci representative of SPION nanoparticles (**Figure 31 B Arrowhead**).

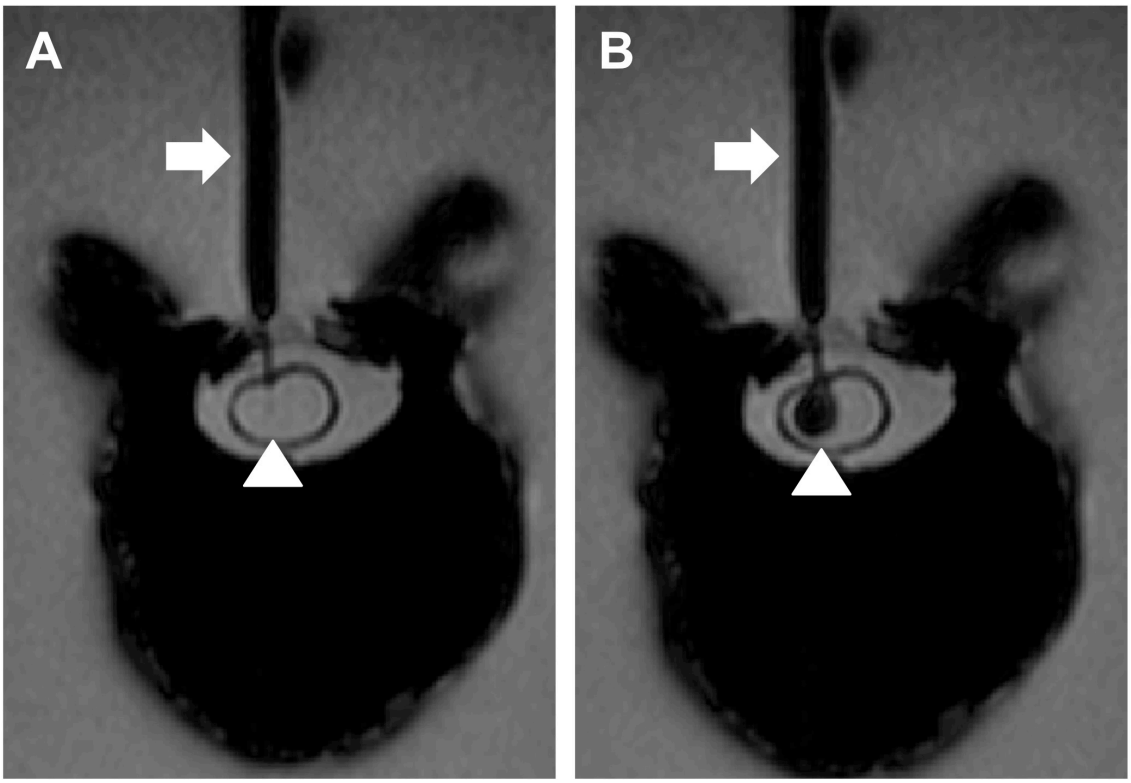

Figure 31. MR-Guided Injection of Ferumoxytol Nanoparticles into the Spinal Cord Phantom. Needle insertion prior to injection showed the cannula artifact (arrow) and needle inserted into the spinal cord (arrowhead) (**A**). After injection, a large hypointense foci was observed in the spinal cord (arrowhead) (**B**).

6.4 CONCLUSIONS

An MRI- compatible injection system was designed with a prototype spine platform, custom-built injection cannulas, and the MRI Interventions ClearPoint system. The prototype spine platform was designed and constructed at Emory University. The system was designed to rigidly attach to the spine of a large animal or human subject and provide access to the spinal cord through MR guidance. The custom system was successfully tested in a custom-built spine phantom. Procedural workflow for animal studies was established.

CHAPTER 7

MAGNETIC RESONANCE IMAGING-GUIDED TRANSPLANTATION OF NEURAL STEM CELLS INTO THE PORCINE SPINAL CORD: A TECHNICAL NOTE*
(SPECIFIC AIM 3)

Purpose: Cell-based therapies are a promising treatment option for traumatic, tumorigenic and degenerative diseases of the spinal cord. Transplantation into the spinal cord is achieved with intravascular, intrathecal or direct intraparenchymal injection. While the current standard, direct injection is limited by surgical invasiveness, difficulty in re-injection, and the inability to directly target anatomic or pathologic landmarks. The objective of this study was to present the proof-of-principle for minimally invasive, percutaneous transplantation of stem cells into the spinal cord parenchyma of live minipigs under MR-guidance.

Methods: A MR-compatible spine injection platform was developed to work with the ClearPoint SmartFrame system (MRI Interventions, Inc.). The system was attached to the spine of live minipigs and a percutaneous injection cannula was advanced into the spinal cord under MR-guidance.

Results: A cell graft of $2.5x10^6$ neural stem cells labeled with ferumoxytol nanoparticles was transplanted into the ventral horn of the spinal cord with MR-guidance. Graft

delivery was visualized with MRI and the grafts were identified in the ventral horn by Prussian blue histochemistry. No post-operative morbidity was observed.

Conclusion: This report supports the proof-of-principle for transplantation of pharmacologic or biological agents into the spinal cord of a large animal under the guidance of MRI.

* **Lamanna JJ**, Urquia LN, Hurtig CV, Gutierrez J, Anderson C, Piferi P, Federici T, Oshinski JN, and Boulis NM. Minimally Invasive Magnetic Resonance Imaging-Guided Transplantation of Magnetic Nanoparticle Labeled Human Neural Stem Cells into the Porcine Spinal Cord. *Magnetic Resonance in Medicine.* In Review.

7.1 INTRODUCTION

Stem cell-based therapies are under clinical evaluation for the treatment of a range of tumorigenic, degenerative and traumatic diseases of the spinal cord, including Amyotrophic Lateral Sclerosis (ALS), Spinal Cord Injury (SCI), and Multiple Sclerosis (MS). Intravascular, intrathecal, and intraparenchymal delivery methods have been employed in these trials[70]. Direct intraparenchymal injection is currently the most straightforward, reliable method for transplanting cell therapies directly into the spinal cord. Furthermore, the safety profile of spine-mounted stereotactic platforms capable of performing multiple direct injections in to the spinal cord parenchyma following laminectomy is established in pre-clinical and clinical studies[10,42,53,65,71,89-91,120,125-128].

Image-guided approaches have been employed in the brain to replace procedures traditionally done with stereotactic systems. The scope and number of MRI-guided interventions has advanced in recent years due to hardware and software developments that exploit the excellent soft tissue contrast, high spatial resolution, and multi-planar imaging capabilities of MRI. Interventional MRI is the method of choice in many centers for guiding implantation of deep brain stimulation (DBS) electrodes[23,88,146].

Moreover, image-guided approaches have been used to access the spine and spinal cord. Computed Tomography (CT) and MRI are used in the clinic to guide percutaneous cordotomy[58,59,94] and other procedures in the spinal cord[30,104]. Pre-clinical studies in canines employed fluoroscopic guidance to percutaneously transplant stem cells into the spinal cord[24,75]. Recently, MRI guidance was used to deliver stem cells to the porcine intervertebral disc[7].

The purpose of this study was to establish the proof-of-principle and feasibility of MR-guided percutaneous injection of cellular therapeutics into the spinal cord. MR-guided direct injection into the spinal cord could allow for transplantation without surgical laminectomy and for direct targeting of anatomic or pathologic landmarks in the spinal cord. Furthermore, the reduced invasiveness could improve procedural recovery time and allow for re-injection into the same spinal cord segments. The current study was not designed to investigate the therapeutic efficacy or biological properties of transplanted cell grafts, which has been established in previous studies[41,64,149]. In this report, we describe a novel method for minimally invasive delivery of cellular therapeutics into the pig spinal cord under the guidance of MRI using a custom-built spine mounted platform and the ClearPoint system (MRI Interventions, Inc.).

7.2 MATERIALS AND METHODS

7.2.1 Ethics Statement

All procedures were conducted at the Division of Animal Resources in accordance with a protocol approved by the Intuitional Animal Care and Use Committee at our University.

7.2.2 Cell Preparation

Human Neural Progenitor cells (hNPCs) isolated from the fetal cortex were provided as frozen stocks (Clive Svendsen at Cedars-Sinai Medical Center[64,149]). The hNPCs were expanded in culture as neurospheres[31] and labeled with ferumoxytol, an ultra-small superparamagnetic iron oxide nanoparticle (SPIO), previously used for

cellular tracking with MRI. Cells were labeled by incubation with 400 μg/mL of ferumoxytol for 7 days[18,153]. Immediately prior to surgery, the neurospheres were washed and chemically dissociated to single cells. Pig Neural Progenitor cells (pNPCs) were provided as dissociated cells prepared for transplantation (Neuralstem, Inc.) and were labeled with SPIO nanoparticles. Cell viability and concentration were assessed with a trypan blue exclusion assay (>80% viable required for transplantation). The hNPCs and pNPCs were maintained on ice in hibernation medium until transplantation.

7.2.3 MR-Compatible Injection System

The prototype injection platform was MRI-compatible and constructed of polyoxymethylene resin. The device was designed to attach to spine laminae rostral and caudal to the region of interest with custom-built percutaneous aluminum posts and titanium lamina screws (4mm anchor). The ClearPoint SmartFrame device (MRI Interventions, Inc.) was rigidly attached to the injection platform and was maneuvered in the rostral/caudal and medial/lateral planes on a rail system (**Figure 32A**). The SmartFrame allowed for targeting and controlled advancement of the custom-built injection needle (MRI Interventions, Inc.) using the ClearPoint targeting software to calculate a trajectory. A ceramic guide cannula with a titanium stylet was used to pass through the soft tissues and provide access to the spinal cord. The infusion needle was composed of fused silica and inserted through the guide cannula after stylet removal. The internal diameter of the needle tip was 200 μm with a stepped tip design. When inserted through the guide cannula, the infusion needle extended 10.5 mm beyond the tip of the cannula, ensuring the guide cannula did not enter the spinal cord parenchyma. A

microprocessor-controlled syringe pump (Tritech Research Inc., Los Angeles, CA) attached to the injection needle was used for cell suspension infusion[32].

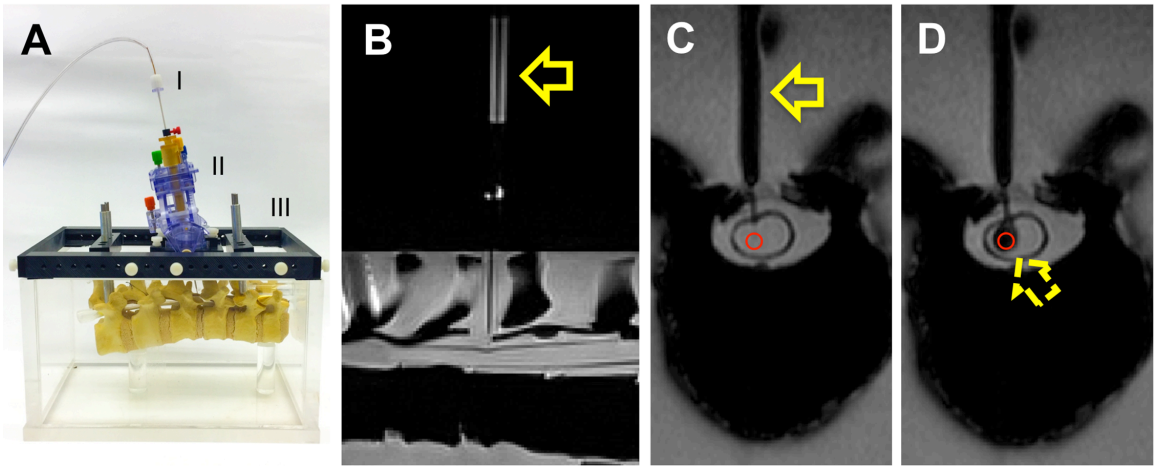

Figure 32. In Vitro Assessment of an MR-Compatible Spinal Injection System with a Phantom Model. The MRI compatible injection system (**A**) utilizes: 1) MR-Compatible SmartFlow catheter (MRI Interventions), 2) Modified ClearPoint device (MRI Interventions), and 3) MR-Compatible spine platform with percutaneous lamina posts for fastening to spine. The system is mounted to a MRI spine phantom model for in vitro assessment. Under the guidance of T1-weighted MRI (3T full-body scanner, Siemens) and the ClearPoint software (MRI Interventions), the catheter (arrow) was advanced to the surface of the spinal cord in the phantom model (**B**). The injection needle was inserted into the spinal cord (**C**) to the planned target (red arrow) and an infusion of ferumoxytol iron oxide nanoparticles was performed (dotted arrow), as seen with gradient echo T2*-weighted MRI (**D**).

7.2.4 In Vitro Assessment

A MR spinal cord phantom model was constructed from a foam spine model and an agar gel spinal cord. The phantom was submerged in water in a clear box (**Figure**

32A). The MR-compatible injection system was attached to the phantom and multiple injections were performed under MR-guidance with the ClearPoint software to establish system workflow and targeting.

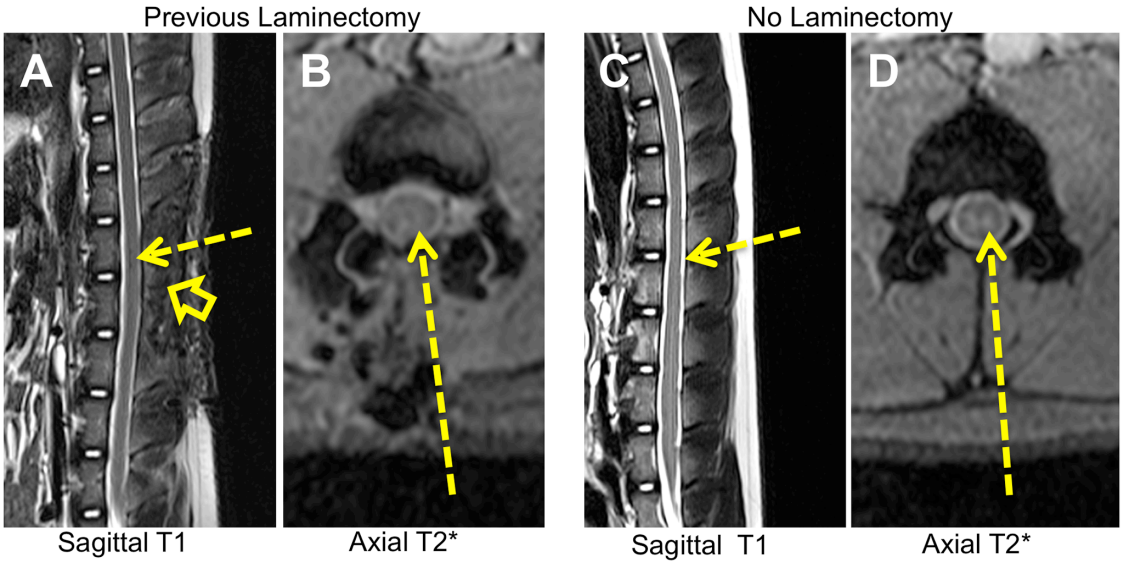

Figure 33. MR-Guided Transplantation Strategy in the Porcine Spinal Cord. Potential cannula trajectories for transplantation of neural stem cells into the spinal cord were designed for an animal with a previous laminectomy (solid arrow) and dural opening (**A, B**). A trajectory (dotted arrow) through the scar tissue (solid arrow) was utilized. A trajectory (dotted arrow) through the interlaminar space was utilized to gain access to the cord in a naïve pig with no previous laminectomy (**C, D**).

7.2.5 Magnetic Resonance Imaging

All images and procedures were done with a clinical 3T MRI scanner (Magnetom TRIO, Siemens Medical, Malvern, PA) with a bore length of 140cm and diameter of 60cm. Structural images were acquired using sagittal T2-weighted turbo spin echo (TSE) and T1-weighted 3D sequences. The T1-weighted images were used for fiducial identification and trajectory planning. For cannula visualization and graft identification,

a gradient echo (GRE) T2*-weighted axial 2D multi-slice sequence was utilized (TE/TR=10/159 msec, Flip Angle=30°, Averages=4, Resolution = 0.9x0.9x1.5 mm).

7.2.6 Anesthesia

The pigs were fasted for 12 hours prior to induction anesthesia with Ketamine (35 mg/kg, IM) and Acepromazine (1.1 mg/kg, IM). The pigs were maintained for the duration of the procedure on Isoflurane (1.5 – 2.5%, Inhaled) mixed with oxygen.

7.2.7 In Vivo MR-Guided Spinal Cord Injection

Two female Göttingen minipigs were enrolled in the study. The pigs were placed in the MRI scanner table in the prone, headfirst position under general anesthesia. Appropriate sterile preparation and draping was done over the thoracolumbar spine. The rostral and caudal portions of the injection platform were fastened to the thoracic vertebra above and below the target site. The aluminum posts were advanced to the surface of the lamina through a 1 cm dermal incision. The titanium lamina screws with a 4mm anchor were advanced through the posts and fastened into the lamina. A fiducial grid was placed over the skin on the target site (SmartGrid, MRI Interventions, Inc.). The SmartFrame was attached to the injection platform. Two phased-array body coils were sterile draped and placed beside the injection platform. Pre-entry sagittal T2 2D TSE, sagittal T1 3D, and axial T2* GRE 2D images covering the fiducial markers and spinal cord region of interest were acquired. The pre-entry images were imported to the ClearPoint software to acquire the target (ventral horn of the spinal cord), plan an initial trajectory, and set the cannula entry point on the skin using the fiducial grid.

The animal was moved out of the scanner bore and the skin was nicked through the fiducial grid to mark the planned entry point and the grid was removed. Due to the thickness of the porcine skin, a 1 cm dermal incision was made over the entry point. Stepwise angular and planar adjustments were made with repeat imaging to align the cannula with the final planned trajectory in near real-time. The ceramic guide and stylet were advanced to depth at the ligamentum flavum. The titanium stylet was removed and imaging was performed to confirm the cannula was on the correct trajectory. Once the final trajectory was determined to be on target, the injection needle was advanced through the cannula and into the spinal cord ventral horn. Final targeting was assessed with T2* GRE imaging. A single injection of $2.5x10^6$ hNPCs or pNPCs in 25 μL was infused into the spinal cord at a rate of 5μL / minute for each animal. The needle remained in the cord for 2 minutes following injection to minimize reflux and repeat GRE imaging was performed to confirm cell graft delivery. The catheter and cannula were removed and post-operative scanning was performed.

7.2.8 Post-Operative Management and Behavioral Assessment

Oral Cyclosporine (10 mg/kg) was administered for immunosuppression from the day of surgery to euthanasia. The pigs underwent general neurological examination/observation before and following the procedure. Sensory evaluation took place in the form of a tactile stimulus to the interdigital space. Behavioral assessment of motor function was performed daily. Gait and motor function were assessed according to the Tarlov scale[125].

7.2.9 Euthanasia, Tissue Processing and Histology

The pigs were euthanized 21 days after transplantation. Transcardiac perfusion with 0.9% NaCl solution followed by 4% paraformaldehyde was performed. The fixed spinal cord was excised and frozen. The cord was sectioned axially at 50 μm intervals and stained with Prussian Blue (PB) reagent for microscopic Iron and counter-stained with Eosin. Images were captured with a digital DS-Qi1 high sensitivity cooled CCD camera using a Nikon E400 microscope supplied with NIS-Elements imaging software (Nikon Instruments, Inc.).

7.3 RESULTS

7.3.1 In Vitro Assessment

A spinal cord phantom model was used to establish workflow of the MR-guided spinal cord injection system. The system was mounted to the phantom and T1-weighted images (**Figure 32B**) were used to plan a trajectory to a target in the spinal cord with the ClearPoint software. The injection needle was inserted along the planned trajectory into the target in the spinal cord and its position was confirmed with T2*-weighted imaging (**Figure 32C**). An infusion of ferumoxytol SPIO nanoparticles in 25 μL saline was performed and a hypointense focus was observed at the targeted injection site (**Figure 32D**). The infusion cloud encompassed the planned target site in 5/5 injections.

7.3.2 Cell transplantation into the spinal cord under MR guidance

Two pigs received MR-guided transplantation of cells into the spinal cord. The first pig had a previous two-level thoracolumbar laminectomy including dural opening

three weeks earlier to simulate previous surgical transplantation (**Figure 33A**). The second pig

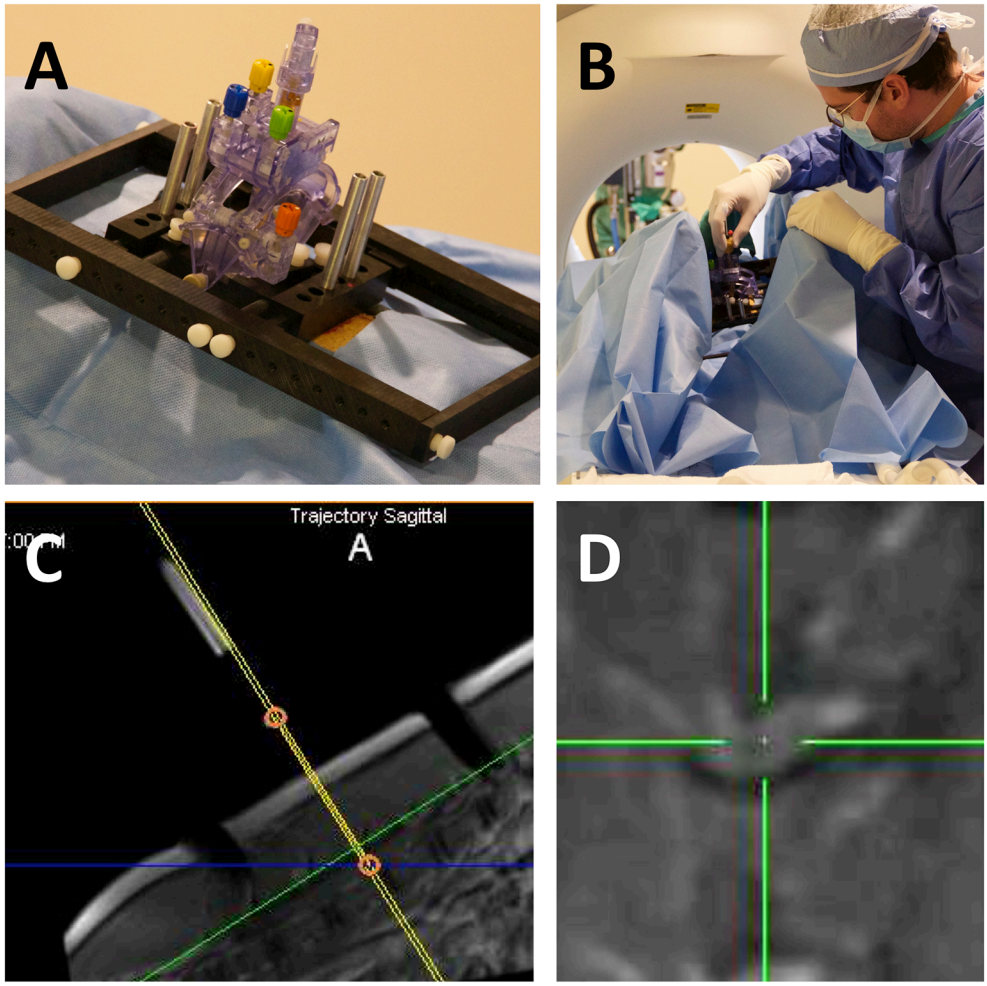

Figure 34. MR-Compatible Spinal Injection System Placement and Targeting/Trajectory Planning In Vivo. The pigs (n = 2) were sterile prepared in the MR scanner and the MRI compatible injection system was securely fastened to the spine with percutaneous lamina posts (**A**). Two body flex radiofrequency coils were placed on either side of the system (**B**). A trajectory through the skin and into the ventral horn of the spinal cord was calculated with T1-weighted MR images (**C**) with the ClearPoint software to go through the interlaminar space (**D**) or through scar tissue on a pig with a previous laminectomy (not shown).

was a naïve pig without previous surgery (**Figure 33B**). Percutaneous stem cell injection into the spinal cord was initiated through placement of the spine-mounted, MR-compatible platform attached to the ClearPoint system while the pig was on the MR scanner table (**Figure 34A**). Two phased-array body coils were placed beside the system (**Figure 34B**). The ventral horn in the spinal cord was targeted using a blend of T2*-weighted GRE and T1-weighted TSE images. A trajectory traversing the soft tissue into the spinal cord target was selected using the ClearPoint software (**Figure 34C)**. In the naïve pig with no laminectomy, a trajectory through the interlaminar space was utilized (**Figure 34D**). Successful alignment of the inserted cannula to the planned trajectory was confirmed with T2*-weighted MRI after the cannula was advanced to the ligamentum flavum (**Figure 35A**). The injection needle was inserted into the spinal cord through the cannula and placement was confirmed with MRI (**Figure 35B, E**). A single graft of $2.5x10^6$ SPIO-labeled pNPCs (previous laminectomy) or hNPCs (no laminectomy) was injected into the cord and a hypointense focus representative of the negative contrast produced by the ferumoxytol-labeled graft was observed at the target site in the spinal cord with T2*-weighted MRI (**Figure 35C, F**). Furthermore, the graft was observed after the needle was removed (**Figure 35D**). The procedure duration was four hours for the pig with laminectomy and six hours in the naïve pig.

7.3.3 Behavioral Assessment

Pre- and post-operative behavioral assessment was completed. Following recovery from anesthesia, the pigs showed no signs of distress and ambulated within two hours. No deficits were observed in the general neurological exam, sensory evaluation,

or motor assessment from the day after surgery. Post-recovery from anesthesia, both pigs received a 4/4 for motor function on the Tarlov scale and withdrew all limbs adequately to tactile stimulus. No deficits were observed over the course of the experiment (21 days).

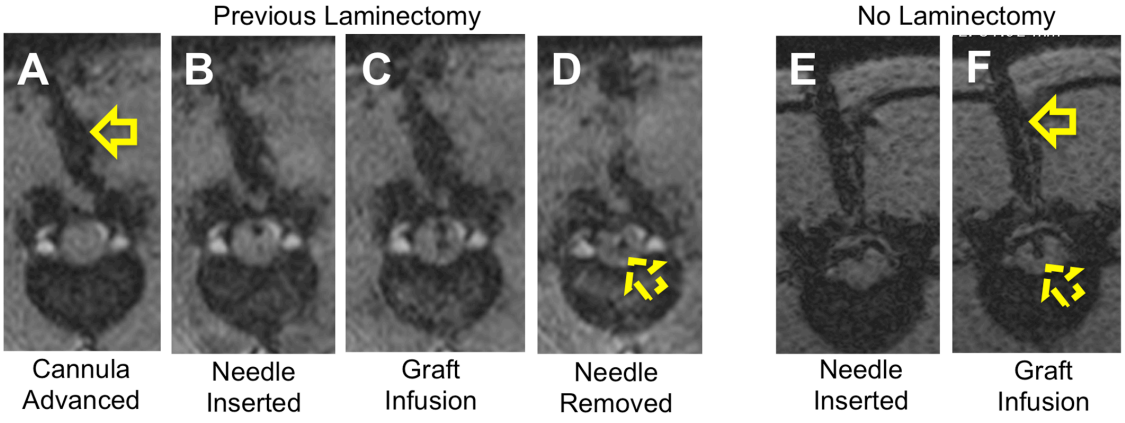

Figure 35. MR-Guided Spinal Cord Transplantation In Vivo. Representative T2*-weighted images from MR-guided spinal cord injection show the SmartFlow catheter (arrow) advanced to the surface of the spinal cord (**A**) in the pig with previous laminectomy. The titanium stylet was removed from the ceramic guide cannula and the injection needle was inserted into the spinal cord (**B**). A graft of 2.5 x 10^5 pig neural stem cells with ferumoxytol nanoparticles was injected into the cord (**C**). The needle was removed and a hypointense focus (dotted arrow) representative of the graft was observed in the cord at the target site (**D**). In the animal without laminectomy, the cannula (arrow) was guided through the interlaminar space and the injection needle inserted into the cord (**E**). Once in the cord, a graft of 2.5 x 10^5 human neural stem cells labeled with ferumoxytol nanoparticles was injected. The graft was observed as a hypointense focus on T2*-weighted MRI (**F**).

7.3.4 Histological Targeting Confirmation

To validate the MR results and confirm the intraspinal location of SPIO-labeled cell grafts, the spinal cord was excised and stained for the presence of microscopic iron using the Prussian blue reagent. Characteristic blue precipitates representative of the SPIO-labeled cell grafts were located in the ventral horn of the spinal cord in both pigs, confirming the MRI findings and delivery of cells into the spinal cord (**Figure 36**).

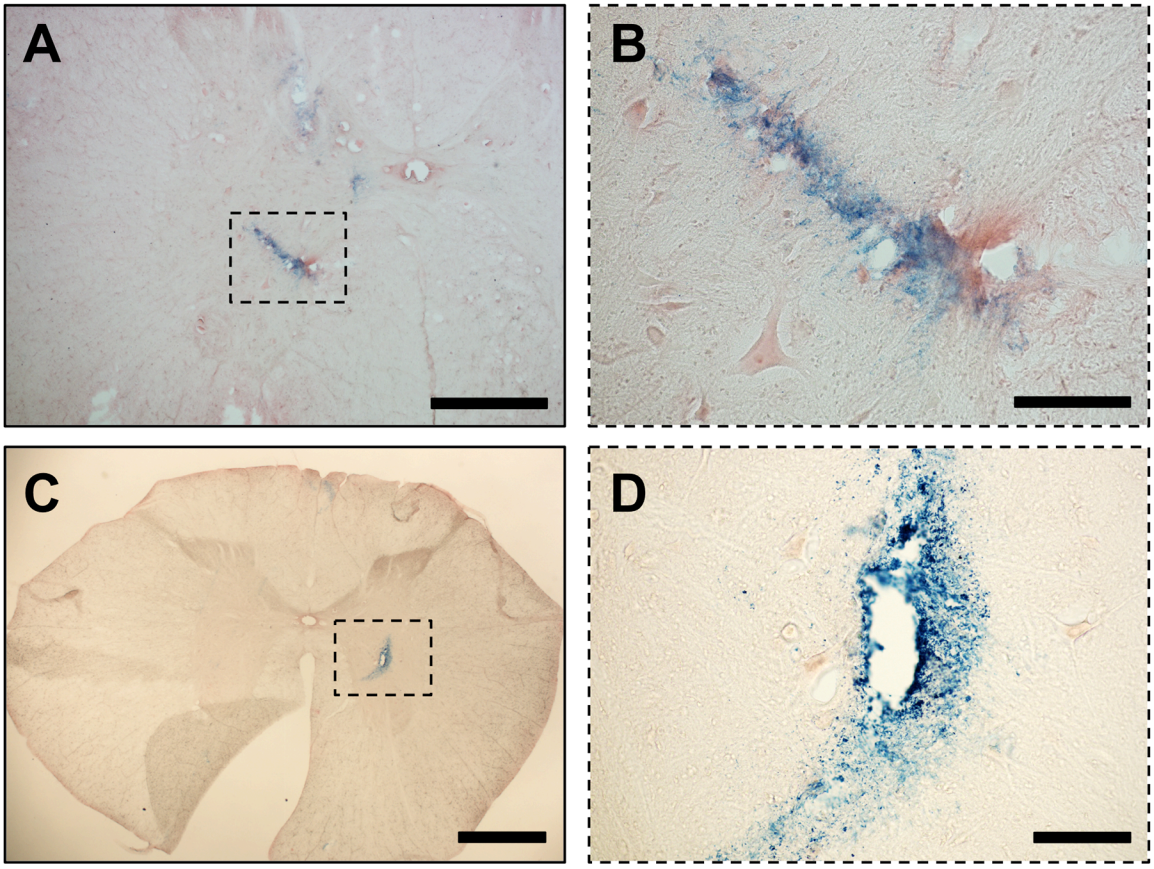

Figure 36. Histological Confirmation of Graft Delivery into the Spinal Cord. Representative light microscopy images of histochemical staining for iron deposits with prussian blue reagent. Characteristic blue precipitates indicative of the ferumoxytol-labeled cell graft were observed in the ventral horn of the pig with previous laminectomy (**A, B**) and in the central grey mater/ventral horn of the pig with no laminectomy (**C, D**). Scale bars: (**A, C**) 1 mm; (**B, D**) 50 µm.

7.4 DISCUSSION

The results of this study provide preliminary evidence for a novel, minimally invasive approach aimed at achieving delivery of pharmacologic or biological agents directly into spinal cord parenchyma under MRI guidance. This is the first published report of MRI-guided intraspinal stem cell transplantation in a live animal. Most importantly, the use of a large animal model and clinical MRI scanner make this procedure directly applicable to clinical translation. Intraoperative MR targeting, trajectory planning and cannula guidance are well established in the brain for the implantation of DBS electrodes using the ClearPoint system and sub-millimeter accuracy has been achieved[72].

Successful translation of stem cell-based therapies for spinal cord disease requires optimization of many parameters, including the delivery method. The method that delivers the most cells to the target site with the least invasive approach would be ideal. Ongoing and completed clinical trials have employed intravascular, intrathecal, and intraparenchymal delivery approaches to transplant cell therapies to the spinal cord. Minimal adverse events, mostly transient sensory deficits, have been observed in these trials[70]. However, limited evidence exists confirming successful graft delivery, engraftment, or survival. For intrathecal and intravascular approaches, questions remain as to how many cells reach the target site. In comparative studies in rodents, intraparenchymal approaches have been superior to both intrathecal and intravascular approaches in delivering and engrafting cells to the target site[111,151]. Intravascular approaches require cells to traverse the blood-brain barrier and reach target sites through homing mechanisms. Intrathecal infusion requires cells to traverse the pia mater and

penetrate several millimeters of white mater tracts to reach deep grey structures such as the ventral horn. Thus, direct intraparenchymal delivery represents the most straightforward approach for delivering cells to the target site. Optimizing the intraparenchymal approach with MR-guidance could allow for increased accuracy with direct visualization and targeting of anatomic or pathologic sites in the spinal cord while concurrently reducing procedural morbidity.

The safety profile for intraparenchymal transplantation of cellular therapeutics is established in large animal models and clinical trials[89-91,120,125-128] _ENREF_2. While MR-guidance could reduce the need for an open surgical procedure and allow for percutaneous delivery, it raises other concerns, including: cerebrospinal fluid leakage or hemorrhage of vasculature from incidental needle puncture; inaccurate targeting due to displacement of the cord from the resistance of the dura mater to needle puncture; and limited range of transplantation sites due to the vertebra. However, the advantages of this approach are: direct targeting to pathology (e.g. SCI lesion), confirmation of needle location at target site with MRI, and decreased invasiveness compared to the current intraparenchymal delivery procedure. Furthermore, this approach could allow for repeat injection in areas of spinal cord that have been operatively exposed and injected previously. Repeat surgical exposure is challenging due to scar tissue formation, loss of tissue planes, and potential adhesion of spinal cord to dura mater. Extensive preclinical studies in large animal models must be conducted to evaluate the safety and accuracy of percutaneous, MR-guided spinal cord cell graft transplantation. The purpose of this study was not to investigate the survival, engraftment, or function of the transplanted therapeutic product. A limitation of this report is the use of only two animals for

injection. However, the main objective was to provide proof-of-principle for this procedure.

7.5 CONCLUSIONS

We describe the first successful MRI-guided, percutaneous stem cell transplant into the spinal cord. This supports the proof-of-principle for transplantation of stem cells into the spinal cord of a large animal under the guidance of MRI. Additional studies are underway to assess the safety and accuracy of the procedure in repeated experiments. This MRI-guided, minimally invasive approach could be used clinically to directly deliver pharmacologic or biological therapeutics to the spinal cords of patients with ALS, SCI lesions, intraspinal tumors, or MS plaques.

CHAPTER 8

CONCLUSIONS

In this thesis, I have described the current state of spinal cord stem cell transplantation, with particular regard to delivery methodology and the limited techniques available for identifying transplanted cell grafts. I have also shown how most clinical trials transplanting cellular therapeutics to the spinal cord do not have a method for identifying/monitoring the transplanted therapy. Furthermore, these trials rely on surgical methods for transplantation. I described our motivation for developing a diagnostic marker for tracking transplanted cell grafts *in vivo* and post-mortem. I also described our motivation for developing an image-guided, minimally invasive method for spinal cord stem cell transplantation. I discussed the utility of using a clinical grade cell line, an FDA approved diagnostic marker, clinical MRI scanner, and a clinically relevant large animal (porcine) model in the translation of this approach.

From these experiments, I developed a method for labeling human neural progenitor cells cultured as neurospheres with ferumoxytol nanoparticle for diagnostic tracking with Magnetic Resonance Imaging. I confirmed the cells internalized the ferumoxytol nanoparticles, characterized the labeling efficiency and showed the method has limited biological effects.

The ferumoxytol-labeled human neural progenitor cells were transplanted into the spinal cord of live pigs to assess the utility of ferumoxytol as a diagnostic marker. The

transplantation to did not produce any permanent neurological deficits in the pigs. The transplanted cell grafts were visualized *in vivo* with MRI and was predictive of graft location. Importantly, the ferumoxytol labeling does not impact cell survival *in vivo* as measured by stereological quantification of cell engraftment. Correlation analysis showed the MR signal correlated with histological iron from ferumoxytol nanoparticles and the histological iron correlates with cell survival. The ferumoxytol labeled cells differentiate *in vivo.* Together, this suggests the utility of ferumoxytol as a diagnostic marker for transplanted human neural progenitor cell grafts in a large animal model.

Improving on current delivery systems, I developed a novel method for MRI-guided spinal cord stem cell transplantation. I fabricated a MR-compatible spine injection platform and worked in collaboration with MRI Interventions Inc. to adapt their ClearPoint SmartFrame system to our application. I developed a workflow and method for conducting MRI-guided transplantation and assessed our ability to do so in a phantom spinal cord model. Next, I assessed the utility of our system in a live pig where I successfully transplanted ferumoxytol-labeled cells into the spinal cord of a live pig through a small dermal incision. No post-operative deficits were observed and the graft was identified in the spinal cord post-mortem. This was the first MR-guided spinal cord injection performed.

8.1 FUTURE DIRECTIONS

The next step in utilizing ferumoxytol as a cellular therapeutic diagnostic marker in the clinic is to assess efficacy, biodistribution and toxicity in two animal models with large cohorts under Good Laboratory Practice conditions.

Developing the MR-guided spinal cord injection system in to a clinical product will require additional large animal studies to further refine the procedure and assess safety. A study of five consecutive animals transplanted under the same conditions is planned.

REFERENCES

1. Aguado BA, Mulyasasmita W, Su J, Lampe KJ, Heilshorn SC: Improving viability of stem cells during syringe needle flow through the design of hydrogel cell carriers. **Tissue Eng Part A 18:**806-815, 2012
2. Akiyama Y, Radtke C, Honmou O, Kocsis JD: Remyelination of the spinal cord following intravenous delivery of bone marrow cells. **Glia 39:**229-236, 2002
3. Attar A, Ayten M, Ozdemir M, Ozgencil E, Bozkurt M, Kaptanoglu E, et al: An attempt to treat patients who have injured spinal cords with intralesional implantation of concentrated autologous bone marrow cells. **Cytotherapy 13:**54-60, 2011
4. Bak TH, Chandran S: What wires together dies together: verbs, actions and neurodegeneration in motor neuron disease. **Cortex 48:**936-944, 2012
5. Bakshi A, Barshinger AL, Swanger SA, Madhavani V, Shumsky JS, Neuhuber B, et al: Lumbar puncture delivery of bone marrow stromal cells in spinal cord contusion: a novel method for minimally invasive cell transplantation. **J Neurotrauma 23:**55-65, 2006
6. Bakshi A, Hunter C, Swanger S, Lepore A, Fischer I: Minimally invasive delivery of stem cells for spinal cord injury: advantages of the lumbar puncture technique. **J Neurosurg Spine 1:**330-337, 2004
7. Barczewska M, Wojtkiewicz J, Habich A, Janowski M, Adamiak Z, Holak P, et al: MR monitoring of minimally invasive delivery of mesenchymal stem cells into the porcine intervertebral disc. **PLoS One 8:**e74658, 2013
8. Barczewska M, Wojtkiewicz J, Habich A, Janowski M, Adamiak Z, Holak P, et al: MR Monitoring of Minimally Invasive Delivery of Mesenchymal Stem Cells into the Porcine Intervertebral Disc. **PLoS ONE 8:**e74658, 2013
9. Berman SC, Galpoththawela C, Gilad AA, Bulte JW, Walczak P: Long-term MR cell tracking of neural stem cells grafted in immunocompetent versus immunodeficient mice reveals distinct differences in contrast between live and dead cells. **Magn Reson Med 65:**564-574, 2011
10. Blanquer M, Moraleda JM, Iniesta F, Gomez-Espuch J, Meca-Lallana J, Villaverde R, et al: Neurotrophic bone marrow cellular nests prevent spinal motoneuron degeneration in amyotrophic lateral sclerosis patients: a pilot safety study. **Stem Cells 30:**1277-1285, 2012
11. Boddington SE, Henning TD, Jha P, Schlieve CR, Mandrussow L, DeNardo D, et al: Labeling human embryonic stem cell-derived cardiomyocytes with indocyanine green for noninvasive tracking with optical imaging: an FDA-compatible alternative to firefly luciferase. **Cell transplantation 19:**55-65, 2010
12. Bonner JF, Blesch A, Neuhuber B, Fischer I: Promoting directional axon growth from neural progenitors grafted into the injured spinal cord. **J Neurosci Res 88:**1182-1192, 2010

13. Boutry S, Brunin S, Mahieu I, Laurent S, Vander Elst L, Muller RN: Magnetic labeling of non-phagocytic adherent cells with iron oxide nanoparticles: a comprehensive study. **Contrast Media Mol Imaging 3:**223-232, 2008
14. Boutry S, Forge D, Burtea C, Mahieu I, Murariu O, Laurent S, et al: How to quantify iron in an aqueous or biological matrix: a technical note. **Contrast Media Mol Imaging 4:**299-304, 2009
15. Callera F, de Melo CM: Magnetic resonance tracking of magnetically labeled autologous bone marrow CD34+ cells transplanted into the spinal cord via lumbar puncture technique in patients with chronic spinal cord injury: CD34+ cells' migration into the injured site. **Stem Cells Dev 16:**461-466, 2007
16. Callera F, do Nascimento RX: Delivery of autologous bone marrow precursor cells into the spinal cord via lumbar puncture technique in patients with spinal cord injury: a preliminary safety study. **Exp Hematol 34:**130-131, 2006
17. Cao Q, He Q, Wang Y, Cheng X, Howard RM, Zhang Y, et al: Transplantation of ciliary neurotrophic factor-expressing adult oligodendrocyte precursor cells promotes remyelination and functional recovery after spinal cord injury. **J Neurosci 30:**2989-3001, 2010
18. Castaneda RT, Khurana A, Khan R, Daldrup-Link HE: Labeling stem cells with ferumoxytol, an FDA-approved iron oxide nanoparticle. **J Vis Exp:**e3482, 2011
19. Chen C-CV, Ku M-C, D. M J, Lai J-S, Hueng D-Y, Chang C: Simple SPION Incubation as an Efficient Intracellular Labeling Method for Tracking Neural Progenitor Cells Using MRI. **PLoS ONE 8:**e56125, 2013
20. Chen CC, Ku MC, D MJ, Lai JS, Hueng DY, Chang C: Simple SPION incubation as an efficient intracellular labeling method for tracking neural progenitor cells using MRI. **PLoS One 8:**e56125, 2013
21. Cheng I, Mayle RE, Cox CA, Park DY, Smith RL, Corcoran-Schwartz I, et al: Functional assessment of the acute local and distal transplantation of human neural stem cells after spinal cord injury. **Spine J 12:**1040-1044, 2012
22. Chernykh ER, Stupak VV, Muradov GM, Sizikov MY, Shevela EY, Leplina OY, et al: Application of autologous bone marrow stem cells in the therapy of spinal cord injury patients. **Bull Exp Biol Med 143:**543-547, 2007
23. Chhabra V, Sung E, Mewes K, Bakay RA, Abosch A, Gross RE: Safety of magnetic resonance imaging of deep brain stimulator systems: a serial imaging and clinical retrospective study. **J Neurosurg 112:**497-502, 2010
24. Chung WH, Park SA, Lee JH, Chung DJ, Yang WJ, Kang EH, et al: Percutaneous transplantation of human umbilical cord-derived mesenchymal stem cells in a dog suspected to have fibrocartilaginous embolic myelopathy. **J Vet Sci 14:**495-497, 2013
25. Cristante AF, Barros-Filho TE, Tatsui N, Mendrone A, Caldas JG, Camargo A, et al: Stem cells in the treatment of chronic spinal cord injury: evaluation of somatosensitive evoked potentials in 39 patients. **Spinal Cord 47:**733-738, 2009

26. Cromer Berman SM, Kshitiz, Wang CJ, Orukari I, Levchenko A, Bulte JW, et al: Cell motility of neural stem cells is reduced after SPIO-labeling, which is mitigated after exocytosis. **Magn Reson Med 69:**255-262, 2013
27. de Vries IJ, Lesterhuis WJ, Barentsz JO, Verdijk P, van Krieken JH, Boerman OC, et al: Magnetic resonance tracking of dendritic cells in melanoma patients for monitoring of cellular therapy. **Nat Biotechnol 23:**1407-1413, 2005
28. Deda H, Inci MC, Kurekci AE, Sav A, Kayihan K, Ozgun E, et al: Treatment of amyotrophic lateral sclerosis patients by autologous bone marrow-derived hematopoietic stem cell transplantation: a 1-year follow-up. **Cytotherapy 11:**18-25, 2009
29. DeJesus-Hernandez M, Mackenzie IR, Boeve BF, Boxer AL, Baker M, Rutherford NJ, et al: Expanded GGGGCC hexanucleotide repeat in noncoding region of C9ORF72 causes chromosome 9p-linked FTD and ALS. **Neuron 72:**245-256, 2011
30. Duprez TP, Jankovski A, Grandin C, Hermoye L, Cosnard G, Raftopoulos C: Intraoperative 3T MR imaging for spinal cord tumor resection: feasibility, timing, and image quality using a "twin" MR-operating room suite. **AJNR Am J Neuroradiol 29:**1991-1994, 2008
31. Ebert AD, McMillan EL, Svendsen CN: Isolating, expanding, and infecting human and rodent fetal neural progenitor cells. **Curr Protoc Stem Cell Biol Chapter 2:**Unit 2D 2, 2008
32. Federici T, Hurtig CV, Burks KL, Riley JP, Krishna V, Miller BA, et al: Surgical technique for spinal cord delivery of therapies: demonstration of procedure in gottingen minipigs. **J Vis Exp:**e4371, 2012
33. Feldman EL, Boulis NM, Hur J, Johe K, Rutkove SB, Federici T, et al: Intraspinal neural stem cell transplantation in amyotrophic lateral sclerosis: phase 1 trial outcomes. **Ann Neurol 75:**363-373, 2014
34. Feron F, Perry C, Cochrane J, Licina P, Nowitzke A, Urquhart S, et al: Autologous olfactory ensheathing cell transplantation in human spinal cord injury. **Brain 128:**2951-2960, 2005
35. Fischer LR, Glass JD: Axonal degeneration in motor neuron disease. **Neurodegener Dis 4:**431-442, 2007
36. Frolov AA, Bryukhovetskiy AS: Effects of hematopoietic autologous stem cell transplantation to the chronically injured human spinal cord evaluated by motor and somatosensory evoked potentials methods. **Cell Transplant 21 Suppl 1:**S49-55, 2012
37. Furlani D, Ugurlucan M, Ong L, Bieback K, Pittermann E, Westien I, et al: Is the intravascular administration of mesenchymal stem cells safe? Mesenchymal stem cells and intravital microscopy. **Microvasc Res 77:**370-376, 2009
38. Glass JD, Boulis NM, Johe K, Rutkove SB, Federici T, Polak M, et al: Lumbar intraspinal injection of neural stem cells in patients with amyotrophic lateral sclerosis: results of a phase I trial in 12 patients. **Stem Cells 30:**1144-1151, 2012
39. Gonzalez-Lara LE, Xu X, Hofstetrova K, Pniak A, Chen Y, McFadden CD, et al: The use of cellular magnetic resonance imaging to track the fate of iron-

labeled multipotent stromal cells after direct transplantation in a mouse model of spinal cord injury. **Mol Imaging Biol 13:**702-711, 2011
40. Gordon PH: Amyotrophic Lateral Sclerosis: An update for 2013 Clinical Features, Pathophysiology, Management and Therapeutic Trials. **Aging Dis 4:**295-310, 2013
41. Gowing G, Shelley B, Staggenborg K, Hurley A, Avalos P, Victoroff J, et al: Glial cell line-derived neurotrophic factor-secreting human neural progenitors show long-term survival, maturation into astrocytes, and no tumor formation following transplantation into the spinal cord of immunocompromised rats. **Neuroreport 25:**367-372, 2014
42. Guest J, Benavides F, Padgett K, Mendez E, Tovar D: Technical aspects of spinal cord injections for cell transplantation. Clinical and translational considerations. **Brain Res Bull 84:**267-279, 2011
43. Gundersen HJ, Jensen EB: The efficiency of systematic sampling in stereology and its prediction. **J Microsc 147:**229-263, 1987
44. Gutierrez J, Lamanna JJ, Grin N, Hurtig CV, Miller JH, Riley J, et al: Preclinical Validation of Multilevel Intraparenchymal Stem Cell Therapy in the Porcine Spinal Cord. **Neurosurgery**, 2015
45. Gutova M, Frank JA, D'Apuzzo M, Khankaldyyan V, Gilchrist MM, Annala AJ, et al: Magnetic resonance imaging tracking of ferumoxytol-labeled human neural stem cells: studies leading to clinical use. **Stem Cells Transl Med 2:**766-775, 2013
46. Guzman R, Uchida N, Bliss TM, He D, Christopherson KK, Stellwagen D, et al: Long-term monitoring of transplanted human neural stem cells in developmental and pathological contexts with MRI. **Proc Natl Acad Sci U S A 104:**10211-10216, 2007
47. Habisch HJ, Janowski M, Binder D, Kuzma-Kozakiewicz M, Widmann A, Habich A, et al: Intrathecal application of neuroectodermally converted stem cells into a mouse model of ALS: limited intraparenchymal migration and survival narrows therapeutic effects. **J Neural Transm 114:**1395-1406, 2007
48. Horwitz EM, Prockop DJ, Gordon PL, Koo WW, Fitzpatrick LA, Neel MD, et al: Clinical responses to bone marrow transplantation in children with severe osteogenesis imperfecta. **Blood 97:**1227-1231, 2001
49. Hurlbert RJ, Hadley MN, Walters BC, Aarabi B, Dhall SS, Gelb DE, et al: Pharmacological therapy for acute spinal cord injury. **Neurosurgery 72 Suppl 2:**93-105, 2013
50. Inoue M, Honmou O, Oka S, Houkin K, Hashi K, Kocsis JD: Comparative analysis of remyelinating potential of focal and intravenous administration of autologous bone marrow cells into the rat demyelinated spinal cord. **Glia 44:**111-118, 2003
51. Janowski M, Engels C, Gorelik M, Lyczek A, Bernard S, Bulte JW, et al: Survival of neural progenitors allografted into the CNS of immunocompetent recipients is highly dependent on transplantation site. **Cell Transplant 23:**253-262, 2014

52. Janson C, McPhee S, Bilaniuk L, Haselgrove J, Testaiuti M, Freese A, et al: Clinical protocol. Gene therapy of Canavan disease: AAV-2 vector for neurosurgical delivery of aspartoacylase gene (ASPA) to the human brain. **Hum Gene Ther 13:**1391-1412, 2002
53. Jones LA, Lammertse DP, Charlifue SB, Kirshblum SC, Apple DF, Ragnarsson KT, et al: A phase 2 autologous cellular therapy trial in patients with acute, complete spinal cord injury: pragmatics, recruitment, and demographics. **Spinal Cord 48:**798-807, 2010
54. Jung DI, Ha J, Kang BT, Kim JW, Quan FS, Lee JH, et al: A comparison of autologous and allogenic bone marrow-derived mesenchymal stem cell transplantation in canine spinal cord injury. **J Neurol Sci 285:**67-77, 2009
55. Kanematsu N, Koba Y, Ogata R: Evaluation of plastic materials for range shifting, range compensation, and solid-phantom dosimetry in carbon-ion radiotherapy. **Med Phys 40:**041724, 2013
56. Kang JH, Lee DS, Paeng JC, Lee JS, Kim YH, Lee YJ, et al: Development of a sodium/iodide symporter (NIS)-transgenic mouse for imaging of cardiomyocyte-specific reporter gene expression. **J Nucl Med 46:**479-483, 2005
57. Kanpolat Y: Percutaneous destructive pain procedures on the upper spinal cord and brain stem in cancer pain: CT-guided techniques, indications and results. **Adv Tech Stand Neurosurg 32:**147-173, 2007
58. Kanpolat Y, Akyar S, Caglar S, Unlu A, Bilgic S: CT-guided percutaneous selective cordotomy. **Acta Neurochir (Wien) 123:**92-96, 1993
59. Kanpolat Y, Savas A, Ucar T, Torun F: CT-guided percutaneous selective cordotomy for treatment of intractable pain in patients with malignant pleural mesothelioma. **Acta Neurochir (Wien) 144:**595-599; discussion 599, 2002
60. Kaplitt MG, Feigin A, Tang C, Fitzsimons HL, Mattis P, Lawlor PA, et al: Safety and tolerability of gene therapy with an adeno-associated virus (AAV) borne GAD gene for Parkinson's disease: an open label, phase I trial. **Lancet 369:**2097-2105, 2007
61. Karamouzian S, Nematollahi-Mahani SN, Nakhaee N, Eskandary H: Clinical safety and primary efficacy of bone marrow mesenchymal cell transplantation in subacute spinal cord injured patients. **Clin Neurol Neurosurg 114:**935-939, 2012
62. Karussis D, Karageorgiou C, Vaknin-Dembinsky A, Gowda-Kurkalli B, Gomori JM, Kassis I, et al: Safety and immunological effects of mesenchymal stem cell transplantation in patients with multiple sclerosis and amyotrophic lateral sclerosis. **Arch Neurol 67:**1187-1194, 2010
63. Kim C, Lee HC, Sung JJ: Amyotrophic lateral sclerosis - cell based therapy and novel therapeutic development. **Exp Neurobiol 23:**207-214, 2014
64. Klein SM, Behrstock S, McHugh J, Hoffmann K, Wallace K, Suzuki M, et al: GDNF delivery using human neural progenitor cells in a rat model of ALS. **Hum Gene Ther 16:**509-521, 2005
65. Knoller N, Auerbach G, Fulga V, Zelig G, Attias J, Bakimer R, et al: Clinical experience using incubated autologous macrophages as a treatment for

complete spinal cord injury: phase I study results. **J Neurosurg Spine 3:**173-181, 2005
66. Krauze MT, Saito R, Noble C, Bringas J, Forsayeth J, McKnight TR, et al: Effects of the perivascular space on convection-enhanced delivery of liposomes in primate putamen. **Experimental neurology 196:**104-111, 2005
67. Krestel HE, Mihaljevic AL, Hoffman DA, Schneider A: Neuronal co-expression of EGFP and beta-galactosidase in mice causes neuropathology and premature death. **Neurobiology of disease 17:**310-318, 2004
68. Kumar AA, Kumar SR, Narayanan R, Arul K, Baskaran M: Autologous bone marrow derived mononuclear cell therapy for spinal cord injury: A phase I/II clinical safety and primary efficacy data. **Exp Clin Transplant 7:**241-248, 2009
69. Kwon BK, Soril LJ, Bacon M, Beattie MS, Blesch A, Bresnahan JC, et al: Demonstrating efficacy in preclinical studies of cellular therapies for spinal cord injury - How much is enough? **Exp Neurol 248C:**30-44, 2013
70. Lamanna JJ, Miller JH, Riley JP, Hurtig CV, Boulis NM: Cellular therapeutics delivery to the spinal cord: technical considerations for clinical application. **Ther Deliv 4:**1397-1410, 2013
71. Lammertse DP, Jones LA, Charlifue SB, Kirshblum SC, Apple DF, Ragnarsson KT, et al: Autologous incubated macrophage therapy in acute, complete spinal cord injury: results of the phase 2 randomized controlled multicenter trial. **Spinal Cord 50:**661-671, 2012
72. Larson PS, Starr PA, Bates G, Tansey L, Richardson RM, Martin AJ: An optimized system for interventional magnetic resonance imaging-guided stereotactic surgery: preliminary evaluation of targeting accuracy. **Neurosurgery 70:**95-103; discussion 103, 2012
73. Lee ES, Chan J, Shuter B, Tan LG, Chong MS, Ramachandra DL, et al: Microgel iron oxide nanoparticles for tracking human fetal mesenchymal stem cells through magnetic resonance imaging. **Stem Cells 27:**1921-1931, 2009
74. Lee JH, Chang HS, Kang EH, Chung DJ, Choi CB, Hwang SH, et al: Percutaneous transplantation of human umbilical cord blood-derived multipotent stem cells in a canine model of spinal cord injury. **J Neurosurg Spine 11:**749-757, 2009
75. Lee JH, Chang HS, Kang EH, Chung DJ, Choi CB, Lee JH, et al: Percutaneous transplantation of human umbilical cord blood-derived multipotent stem cells in a canine model of spinal cord injury. **J Neurosurg Spine 11:**749-757, 2009
76. Lee JH, Jung MJ, Hwang YH, Lee YJ, Lee S, Lee DY, et al: Heparin-coated superparamagnetic iron oxide for in vivo MR imaging of human MSCs. **Biomaterials 33:**4861-4871, 2012
77. Lepore AC, Bakshi A, Swanger SA, Rao MS, Fischer I: Neural precursor cells can be delivered into the injured cervical spinal cord by intrathecal injection at the lumbar cord. **Brain Res 1045:**206-216, 2005
78. Li Z, Suzuki Y, Huang M, Cao F, Xie X, Connolly AJ, et al: Comparison of reporter gene and iron particle labeling for tracking fate of human embryonic

stem cells and differentiated endothelial cells in living subjects. **Stem Cells 26:**864-873, 2008
79. Liang Q, Satyamurthy N, Barrio JR, Toyokuni T, Phelps MP, Gambhir SS, et al: Noninvasive, quantitative imaging in living animals of a mutant dopamine D2 receptor reporter gene in which ligand binding is uncoupled from signal transduction. **Gene therapy 8:**1490-1498, 2001
80. Lima C, Escada P, Pratas-Vital J, Branco C, Arcangeli CA, Lazzeri G, et al: Olfactory mucosal autografts and rehabilitation for chronic traumatic spinal cord injury. **Neurorehabil Neural Repair 24:**10-22, 2010
81. Lima C, Pratas-Vital J, Escada P, Hasse-Ferreira A, Capucho C, Peduzzi JD: Olfactory mucosa autografts in human spinal cord injury: a pilot clinical study. **J Spinal Cord Med 29:**191-203; discussion 204-196, 2006
82. Liu H, Honmou O, Harada K, Nakamura K, Houkin K, Hamada H, et al: Neuroprotection by PlGF gene-modified human mesenchymal stem cells after cerebral ischaemia. **Brain 129:**2734-2745, 2006
83. Liu HS, Jan MS, Chou CK, Chen PH, Ke NJ: Is green fluorescent protein toxic to the living cells? **Biochem Biophys Res Commun 260:**712-717, 1999
84. Liu J, Cheng EC, Long RC, Yang SH, Wang L, Cheng PH, et al: Noninvasive monitoring of embryonic stem cells in vivo with MRI transgene reporter. **Tissue Eng Part C Methods 15:**739-747, 2009
85. Liu J, Han D, Wang Z, Xue M, Zhu L, Yan H, et al: Clinical analysis of the treatment of spinal cord injury with umbilical cord mesenchymal stem cells. **Cytotherapy 15:**185-191, 2013
86. Logroscino G, Traynor BJ, Hardiman O, Chio A, Couratier P, Mitchell JD, et al: Descriptive epidemiology of amyotrophic lateral sclerosis: new evidence and unsolved issues. **J Neurol Neurosurg Psychiatry 79:**6-11, 2008
87. Mackay-Sim A, Feron F, Cochrane J, Bassingthwaighte L, Bayliss C, Davies W, et al: Autologous olfactory ensheathing cell transplantation in human paraplegia: a 3-year clinical trial. **Brain 131:**2376-2386, 2008
88. Martin AJ, Larson PS, Ostrem JL, Keith Sootsman W, Talke P, Weber OM, et al: Placement of deep brain stimulator electrodes using real-time high-field interventional magnetic resonance imaging. **Magn Reson Med 54:**1107-1114, 2005
89. Mazzini L, Fagioli F, Boccaletti R, Mareschi K, Oliveri G, Olivieri C, et al: Stem cell therapy in amyotrophic lateral sclerosis: a methodological approach in humans. **Amyotroph Lateral Scler Other Motor Neuron Disord 4:**158-161, 2003
90. Mazzini L, Ferrero I, Luparello V, Rustichelli D, Gunetti M, Mareschi K, et al: Mesenchymal stem cell transplantation in amyotrophic lateral sclerosis: A Phase I clinical trial. **Exp Neurol 223:**229-237, 2010
91. Mazzini L, Mareschi K, Ferrero I, Miglioretti M, Stecco A, Servo S, et al: Mesenchymal stromal cell transplantation in amyotrophic lateral sclerosis: a long-term safety study. **Cytotherapy 14:**56-60, 2012
92. Mazzini L, Vercelli A, Mareschi K, Ferrero I, Testa L, Fagioli F: Mesenchymal stem cells for ALS patients. **Amyotroph Lateral Scler 10:**123-124, 2009

93. McCormack E, Silden E, West RM, Pavlin T, Micklem DR, Lorens JB, et al: Nitroreductase, a near-infrared reporter platform for in vivo time-domain optical imaging of metastatic cancer. **Cancer Res 73:**1276-1286, 2013
94. McGirt MJ, Villavicencio AT, Bulsara KR, Gorecki J: MRI-guided frameless stereotactic percutaneous cordotomy. **Stereotact Funct Neurosurg 78:**53-63, 2002
95. McKay SM, Brooks DJ, Hu P, McLachlan EM: Distinct types of microglial activation in white and grey matter of rat lumbosacral cord after mid-thoracic spinal transection. **J Neuropathol Exp Neurol 66:**698-710, 2007
96. McLaren FH, Svendsen CN, Van der Meide P, Joly E: Analysis of neural stem cells by flow cytometry: cellular differentiation modifies patterns of MHC expression. **J Neuroimmunol 112:**35-46, 2001
97. Mendonca MV, Larocca TF, Souza BS, Villarreal CF, Silva LF, Matos AC, et al: Safety and neurological assessments after autologous transplantation of bone marrow mesenchymal stem cells in subjects with chronic spinal cord injury. **Stem Cell Res Ther 5:**126, 2014
98. Mitsumoto H, Brooks BR, Silani V: Clinical trials in amyotrophic lateral sclerosis: why so many negative trials and how can trials be improved? **The Lancet Neurology 13:**1127-1138, 2014
99. Modo M, Beech JS, Meade TJ, Williams SC, Price J: A chronic 1 year assessment of MRI contrast agent-labelled neural stem cell transplants in stroke. **Neuroimage 47 Suppl 2:**T133-142, 2009
100. Modo M, Kolosnjaj-Tabi J, Nicholls F, Ling W, Wilhelm C, Debarge O, et al: Considerations for the clinical use of contrast agents for cellular MRI in regenerative medicine. **Contrast Media Mol Imaging 8:**439-455, 2013
101. Mothe AJ, Bozkurt G, Catapano J, Zabojova J, Wang X, Keating A, et al: Intrathecal transplantation of stem cells by lumbar puncture for thoracic spinal cord injury in the rat. **Spinal Cord 49:**967-973, 2011
102. Moviglia GA, Fernandez Vina R, Brizuela JA, Saslavsky J, Vrsalovic F, Varela G, et al: Combined protocol of cell therapy for chronic spinal cord injury. Report on the electrical and functional recovery of two patients. **Cytotherapy 8:**202-209, 2006
103. Naumova AV, Modo M, Moore A, Murry CE, Frank JA: Clinical imaging in regenerative medicine. **Nat Biotech 32:**804-818, 2014
104. Netuka D, Ostry S, Belsan T, Kramar F, Benes V: Intraoperative MR imaging in a case of a cervical spinal cord lesion. **J Neurosurg Spine 14:**754-757, 2011
105. Neuhuber B, Barshinger AL, Paul C, Shumsky JS, Mitsui T, Fischer I: Stem cell delivery by lumbar puncture as a therapeutic alternative to direct injection into injured spinal cord. **J Neurosurg Spine 9:**390-399, 2008
106. Neumann M, Sampathu DM, Kwong LK, Truax AC, Micsenyi MC, Chou TT, et al: Ubiquitinated TDP-43 in frontotemporal lobar degeneration and amyotrophic lateral sclerosis. **Science 314:**130-133, 2006
107. Obenaus A, Dilmac N, Tone B, Tian HR, Hartman R, Digicaylioglu M, et al: Long-term magnetic resonance imaging of stem cells in neonatal ischemic injury. **Ann Neurol 69:**282-291, 2011

108. Pal R, Venkataramana NK, Bansal A, Balaraju S, Jan M, Chandra R, et al: Ex vivo-expanded autologous bone marrow-derived mesenchymal stromal cells in human spinal cord injury/paraplegia: a pilot clinical study. **Cytotherapy 11:**897-911, 2009
109. Park JH, Kim DY, Sung IY, Choi GH, Jeon MH, Kim KK, et al: Long-term results of spinal cord injury therapy using mesenchymal stem cells derived from bone marrow in humans. **Neurosurgery 70:**1238-1247; discussion 1247, 2012
110. Park S, Kim HT, Yun S, Kim IS, Lee J, Lee IS, et al: Growth factor-expressing human neural progenitor cell grafts protect motor neurons but do not ameliorate motor performance and survival in ALS mice. **Experimental & molecular medicine 41:**487-500, 2009
111. Paul C, Samdani AF, Betz RR, Fischer I, Neuhuber B: Grafting of human bone marrow stromal cells into spinal cord injury: a comparison of delivery methods. **Spine (Phila Pa 1976) 34:**328-334, 2009
112. Paul C, Samdani AF, Betz RR, Fischer I, Neuhuber B: Grafting of human bone marrow stromal cells into spinal cord injury: a comparison of delivery methods. **Spine 34:**328-334, 2009
113. Perin EC, Dohmann HF, Borojevic R, Silva SA, Sousa AL, Mesquita CT, et al: Transendocardial, autologous bone marrow cell transplantation for severe, chronic ischemic heart failure. **Circulation 107:**2294-2302, 2003
114. Pickard MR, Barraud P, Chari DM: The transfection of multipotent neural precursor/stem cell transplant populations with magnetic nanoparticles. **Biomaterials 32:**2274-2284, 2011
115. Potts MB, Silvestrini MT, Lim DA: Devices for cell transplantation into the central nervous system: Design considerations and emerging technologies. **Surg Neurol Int 4:**S22-30, 2013
116. Prabhakar S, Marwaha N, Lal V, Sharma RR, Rajan R, Khandelwal N: Autologous bone marrow-derived stem cells in amyotrophic lateral sclerosis: a pilot study. **Neurol India 60:**465-469, 2012
117. Purandare C, Shitole DG, Belle V, Kedari A, Bora N, Joshi M: Therapeutic potential of autologous stem cell transplantation for cerebral palsy. **Case Rep Transplant 2012:**825289, 2012
118. Ra JC, Shin IS, Kim SH, Kang SK, Kang BC, Lee HY, et al: Safety of intravenous infusion of human adipose tissue-derived mesenchymal stem cells in animals and humans. **Stem Cells Dev 20:**1297-1308, 2011
119. Rademakers R, Neumann M, Mackenzie IR: Advances in understanding the molecular basis of frontotemporal dementia. **Nat Rev Neurol 8:**423-434, 2012
120. Raore B, Federici T, Taub J, Wu MC, Riley J, Franz CK, et al: Cervical multilevel intraspinal stem cell therapy: assessment of surgical risks in Gottingen minipigs. **Spine (Phila Pa 1976) 36:**E164-171, 2011
121. Renton AE, Chio A, Traynor BJ: State of play in amyotrophic lateral sclerosis genetics. **Nat Neurosci 17:**17-23, 2014

122. Renton AE, Majounie E, Waite A, Simon-Sanchez J, Rollinson S, Gibbs JR, et al: A hexanucleotide repeat expansion in C9ORF72 is the cause of chromosome 9p21-linked ALS-FTD. **Neuron 72:**257-268, 2011
123. Richards JM, Shaw CA, Lang NN, Williams MC, Semple SI, MacGillivray TJ, et al: In vivo mononuclear cell tracking using superparamagnetic particles of iron oxide: feasibility and safety in humans. **Circ Cardiovasc Imaging 5:**509-517, 2012
124. Richardson PM, McGuinness UM, Aguayo AJ: Axons from CNS neurons regenerate into PNS grafts. **Nature 284:**264-265, 1980
125. Riley J, Butler J, Baker KB, McClelland S, 3rd, Teng Q, Yang J, et al: Targeted spinal cord therapeutics delivery: stabilized platform and microelectrode recording guidance validation. **Stereotact Funct Neurosurg 86:**67-74, 2008
126. Riley J, Federici T, Park J, Suzuki M, Franz CK, Tork C, et al: Cervical spinal cord therapeutics delivery: preclinical safety validation of a stabilized microinjection platform. **Neurosurgery 65:**754-761; discussion 761-752, 2009
127. Riley J, Federici T, Polak M, Kelly C, Glass J, Raore B, et al: Intraspinal stem cell transplantation in amyotrophic lateral sclerosis: a phase I safety trial, technical note, and lumbar safety outcomes. **Neurosurgery 71:**405-416; discussion 416, 2012
128. Riley J, Glass J, Feldman EL, Polak M, Bordeau J, Federici T, et al: Intraspinal stem cell transplantation in amyotrophic lateral sclerosis: a phase I trial, cervical microinjection, and final surgical safety outcomes. **Neurosurgery 74:**77-87, 2014
129. Riley J, Taub J, Raore B, Boulis NM: An overview of domestic and international clinical trials for delivery of cellular therapies to the spinal cord. **Clin Neurosurg 59:**98-104, 2012
130. Riley JP, Raore B, Taub JS, Federici T, Boulis NM: Platform and cannula design improvements for spinal cord therapeutics delivery. **Neurosurgery 69:**ons147-154; discussion ons155, 2011
131. Ryken TC, Hurlbert RJ, Hadley MN, Aarabi B, Dhall SS, Gelb DE, et al: The acute cardiopulmonary management of patients with cervical spinal cord injuries. **Neurosurgery 72 Suppl 2:**84-92, 2013
132. Saberi H, Moshayedi P, Aghayan HR, Arjmand B, Hosseini SK, Emami-Razavi SH, et al: Treatment of chronic thoracic spinal cord injury patients with autologous Schwann cell transplantation: an interim report on safety considerations and possible outcomes. **Neurosci Lett 443:**46-50, 2008
133. Saito F, Nakatani T, Iwase M, Maeda Y, Hirakawa A, Murao Y, et al: Spinal cord injury treatment with intrathecal autologous bone marrow stromal cell transplantation: the first clinical trial case report. **J Trauma 64:**53-59, 2008
134. Saito F, Nakatani T, Iwase M, Maeda Y, Murao Y, Suzuki Y, et al: Administration of cultured autologous bone marrow stromal cells into cerebrospinal fluid in spinal injury patients: a pilot study. **Restor Neurol Neurosci 30:**127-136, 2012

135. Sakowski SA, Heavener SB, Lunn JS, Fung K, Oh SS, Spratt SK, et al: Neuroprotection using gene therapy to induce vascular endothelial growth factor-A expression. **Gene Ther 16:**1292-1299, 2009
136. Sakowski SA, Schuyler AD, Feldman EL: Insulin-like growth factor-I for the treatment of amyotrophic lateral sclerosis. **Amyotroph Lateral Scler 10:**63-73, 2009
137. Satake K, Lou J, Lenke LG: Migration of mesenchymal stem cells through cerebrospinal fluid into injured spinal cord tissue. **Spine 29:**1971-1979, 2004
138. Schmitz C, Hof PR: Design-based stereology in neuroscience. **Neuroscience 130:**813-831, 2005
139. Sharma A, Gokulchandran N, Chopra G, Kulkarni P, Lohia M, Badhe P, et al: Administration of autologous bone marrow-derived mononuclear cells in children with incurable neurological disorders and injury is safe and improves their quality of life. **Cell Transplant 21 Suppl 1:**S79-90, 2012
140. Shen WB, Plachez C, Chan A, Yarnell D, Puche AC, Fishman PS, et al: Human neural progenitor cells retain viability, phenotype, proliferation, and lineage differentiation when labeled with a novel iron oxide nanoparticle, Molday ION Rhodamine B. **Int J Nanomedicine 8:**4593-4600, 2013
141. Shin DA, Kim JM, Kim HI, Yi S, Ha Y, Yoon DH, et al: Comparison of functional and histological outcomes after intralesional, intracisternal, and intravenous transplantation of human bone marrow-derived mesenchymal stromal cells in a rat model of spinal cord injury. **Acta Neurochir (Wien)**, 2013
142. Silani V, Calzarossa C, Cova L, Ticozzi N: Stem cells in amyotrophic lateral sclerosis: motor neuron protection or replacement? **CNS Neurol Disord Drug Targets 9:**314-324, 2010
143. Skuk D, Paradis M, Goulet M, Tremblay JP: Ischemic central necrosis in pockets of transplanted myoblasts in nonhuman primates: implications for cell-transplantation strategies. **Transplantation 84:**1307-1315, 2007
144. Soenen SJ, De Cuyper M: Assessing cytotoxicity of (iron oxide-based) nanoparticles: an overview of different methods exemplified with cationic magnetoliposomes. **Contrast Media Mol Imaging 4:**207-219, 2009
145. Soenen SJ, De Cuyper M: How to assess cytotoxicity of (iron oxide-based) nanoparticles: a technical note using cationic magnetoliposomes. **Contrast Media Mol Imaging 6:**153-164, 2011
146. Starr PA, Martin AJ, Ostrem JL, Talke P, Levesque N, Larson PS: Subthalamic nucleus deep brain stimulator placement using high-field interventional magnetic resonance imaging and a skull-mounted aiming device: technique and application accuracy. **J Neurosurg 112:**479-490, 2010
147. Sun N, Lee A, Wu JC: Long term non-invasive imaging of embryonic stem cells using reporter genes. **Nat Protoc 4:**1192-1201, 2009
148. Suzuki M, McHugh J, Tork C, Shelley B, Klein S, Aebischer P, et al: GDNF secreting human neural progenitor cells protect dying motor neurons, but not their projection to muscle, in a rat model of familial ALS. . **PLoS ONE 2:**e689, 2007

149. Suzuki M, McHugh J, Tork C, Shelley B, Klein SM, Aebischer P, et al: GDNF secreting human neural progenitor cells protect dying motor neurons, but not their projection to muscle, in a rat model of familial ALS. **PLoS One 2:**e689, 2007
150. Tadesse T, Gearing M, Senitzer D, Saxe D, Brat DJ, Bray R, et al: Analysis of graft survival in a trial of stem cell transplant in ALS. **Ann Clin Transl Neurol 1:**900-908, 2014
151. Takahashi Y, Tsuji O, Kumagai G, Hara CM, Okano HJ, Miyawaki A, et al: Comparative study of methods for administering neural stem/progenitor cells to treat spinal cord injury in mice. **Cell Transplant 20:**727-739, 2011
152. Takahashi Y, Tsuji O, Kumagai G, Hara CM, Okano HJ, Miyawaki A, et al: Comparative study of methods for administering neural stem/progenitor cells to treat spinal cord injury in mice. **Cell transplantation 20:**727-739, 2011
153. Thu MS, Bryant LH, Coppola T, Jordan EK, Budde MD, Lewis BK, et al: Self-assembling nanocomplexes by combining ferumoxytol, heparin and protamine for cell tracking by magnetic resonance imaging. **Nat Med 18:**463-467, 2012
154. Tol M, Akar AR, Durdu S, Ayyildiz E, Ilhan O: Comparison of different needle diameters and flow rates on bone marrow mononuclear stem cell viability: an ex vivo experimental study. **Cytotherapy 10:**98-99, 2008
155. Toso C, Vallee JP, Morel P, Ris F, Demuylder-Mischler S, Lepetit-Coiffe M, et al: Clinical magnetic resonance imaging of pancreatic islet grafts after iron nanoparticle labeling. **Am J Transplant 8:**701-706, 2008
156. Traxinger K, Kelly C, Johnson BA, Lyles RH, Glass JD: Prognosis and epidemiology of amyotrophic lateral sclerosis: Analysis of a clinic population, 1997-2011. **Neurol Clin Pract 3:**313-320, 2013
157. Turner MR, Hardiman O, Benatar M, Brooks BR, Chio A, de Carvalho M, et al: Controversies and priorities in amyotrophic lateral sclerosis. **Lancet Neurol 12:**310-322, 2013
158. Vaquero J, Zurita M, Oya S, Santos M: Cell therapy using bone marrow stromal cells in chronic paraplegic rats: systemic or local administration? **Neuroscience letters 398:**129-134, 2006
159. Wang L, Ji H, Zhou J, Xie J, Zhong Z, Li M, et al: Therapeutic potential of umbilical cord mesenchymal stromal cells transplantation for cerebral palsy: a case report. **Case Rep Transplant 2013:**146347, 2013
160. Wollert KC, Meyer GP, Lotz J, Ringes-Lichtenberg S, Lippolt P, Breidenbach C, et al: Intracoronary autologous bone-marrow cell transfer after myocardial infarction: the BOOST randomised controlled clinical trial. **Lancet 364:**141-148, 2004
161. Xu J, Ji BX, Su L, Dong HQ, Sun WL, Wan SG, et al: Clinical outcome of autologous peripheral blood stem cell transplantation in opticospinal and conventional forms of secondary progressive multiple sclerosis in a Chinese population. **Ann Hematol 90:**343-348, 2011
162. Xu L, Ryugo DK, Pongstaporn T, Johe K, Koliatsos VE: Human neural stem cell grafts in the spinal cord of SOD1 transgenic rats: differentiation and

structural integration into the segmental motor circuitry. **J Comp Neurol 514:**297-309, 2009
163. Yaghoubi SS, Jensen MC, Satyamurthy N, Budhiraja S, Paik D, Czernin J, et al: Noninvasive detection of therapeutic cytolytic T cells with 18F-FHBG PET in a patient with glioma. **Nat Clin Pract Oncol 6:**53-58, 2009
164. Yan J, Xu L, Welsh AM, Hatfield G, Hazel T, Johe K, et al: Extensive neuronal differentiation of human neural stem cell grafts in adult rat spinal cord. **PLoS Med 4:**e39, 2007
165. Yoon SH, Shim YS, Park YH, Chung JK, Nam JH, Kim MO, et al: Complete spinal cord injury treatment using autologous bone marrow cell transplantation and bone marrow stimulation with granulocyte macrophage-colony stimulating factor: Phase I/II clinical trial. **Stem Cells 25:**2066-2073, 2007
166. Zhu J, Zhou L, XingWu F: Tracking neural stem cells in patients with brain trauma. **N Engl J Med 355:**2376-2378, 2006
167. Zurkiya O, Chan AW, Hu X: MagA is sufficient for producing magnetic nanoparticles in mammalian cells, making it an MRI reporter. **Magn Reson Med 59:**1225-1231, 2008

VITA

JASON J. LAMANNA

LAMANNA was born in Winter Park, Florida. He attended public schools in Winter Park and received a B.S. in Chemistry from the University of Florida, Gainesville, Florida, in 2009. He was class valedictorian and graduated summa cum laude. He came to Atlanta, Georgia in 2009 to pursue doctorates in Medicine and Biomedical Engineering at Emory University and Georgia Institute of Technology. When he is not working on his research or practicing medicine, Jason enjoys traveling, scuba diving, playing sports, and spending time with his family and friends.